PREDICTIVE MODELING OF FREEZING AND THAWING OF FROST-SUSCEPTIBLE SOILS

Final Report

Report Number: RC-1619

Michigan Department of Transportation
Office of Research Administration
8885 Ricks Road
Lansing, MI 48909

By

Gilbert Baladi and Pegah Rajaei

Michigan State University
Department of Civil & Environmental Engineering
3546 Engineering Building
East Lansing, MI 48824

September 2015

Technical Report Documentation Page

1. Report No. RC-1619	**2. Government Accession No.** N/A	**3. MDOT Project Manager** Richard Endres
4. Title and Subtitle Predictive Modeling of Freezing and Thawing of Frost-Susceptible Soils		**5. Report Date** September 2015 **6. Performing Organization Code** N/A
7. Author(s) Gilbert Baladi and Pegah Rajaei Michigan State University Department of Civil and Environmental Engineering		**8. Performing Org. Report No.** N/A
9. Performing Organization Name and Address Michigan State University Department of Civil and Environmental Engineering 3546 Engineering East Lansing, Michigan 48824		**10. Work Unit No. (TRAIS)** N/A **11. Contract No.** 2010-0294 **11(a). Authorization No.** Z9
12. Sponsoring Agency Name and Address Michigan Department of Transportation Research Administration 8885 Ricks Rd. P.O. Box 30049 Lansing MI 48909		**13. Type of Report & Period Covered** Final Report 10/01/12 to 9/30/15 **14. Sponsoring Agency Code** N/A
15. Supplementary Notes		

16. Abstract

Frost depth is an essential factor in design of various transportation infrastructures. In frost susceptible soils, as soils freezes, water migrates through the soil voids below the freezing line towards the freezing front and causes excessive heave. The excessive heave can cause instability issues in the structure, therefore predicting the frost depth and resulting frost heave accurately can play a major role in the design. The objectives of this study are to develop accurate and reliable models for predicting frost depths and frost heave and to estimate the resulting heave pressure. The frost depth model was developed and verified using data from MDOT and Minnesota DOT. The frost heave model was also developed and verified using the available MDOT data.

17. Key Words Heat Transfer, Thermal Conductivity, Cumulative Freezing Index, Frost Depth, Analytical Models, Empirical Models, Frost Heave, , Heave Pressure, Frost Heave and Frost Depth Field Data	**18. Distribution Statement** No restrictions. This document is available to the public through the Michigan Department of Transportation.

19. Security Classification - report Unclassified	**20. Security Classification - page** Unclassified	**21. No. of Pages**	**22. Price** N/A

Acknowledgement

The authors like to thank the Michigan Department of Transportation (MDOT) for the financial support and the MDOT staff for their cooperation and for providing soil samples and the soil temperature data. In addition the authors gratefully acknowledge the Minnesota Department of Transportation (MNDOT) for providing the soil temperature data and for its assistance.

Research Report Disclaimer

Table of Contents

List of Tables

List of Figures

Executive Summary

Frost depth is an important factor that affects the design of various transportation infrastructures including pavements, retaining structures, bridge foundations, utility lines, and so forth. Soil freezing can lead to frost heave and heave pressure, which may cause serious stability issues. The objectives of this study are to develop accurate and reliable frost depth prediction model and frost heave model and estimate heave pressure.

After extensive literature review various existing frost depth models were identified and tested. These include the finite difference UNSAT-H, the Stefan, the Modified Berggren, and the Chisholm and Phang models. Unfortunately, some of these models require substantial input data that are not available at MDOT and all models yielded inaccurate results. Therefore, statistical frost depth models were developed; one for clay soils and one for sand. The two models were then combined using the thermal conductivity of soil samples supplied by MDOT and the measured subsurface temperatures. The combined statistical model was then verified using frost depth data collected by MDOT and the Minnesota DOT. The input data to the statistical model include the thermal conductivity of the soil and the cumulative freezing degree day (CFDD).

Moreover, the calculated cumulative thaw degree day (CTDD) and the thaw depth data measured in the state of Michigan were used to assess existing thaw depth predictions models. They did not produce accurate and acceptable results.

Additionally, The Gilpin's mechanistic-empirical model was employed to predict frost heave. The model produced inaccurate and counterintuitive results in some cases. Therefore, the model was modified and the empirical frost depth model developed in this study was incorporated into the model. The resulting model was then simplified to replace some of the required of input data that are not available at MDOT by data elements that are available at MDOT or can be easily obtained. The modified and simplified model's inputs are soil type, winter duration, surface temperature, ground water table (GWT) depth and temperature, the effective size of soil, the soil thermal conductivity, the soil dry unit weight and water content, and the soil void ratio and hydraulic conductivity. The modified model accuracy was assessed using the frost heave data measured at 5 sites in Oakland County, Michigan. Further, the relationship between frost heave and heave pressures were established for four soil types.

Finally, based on the heat balance in the soil layers and the developed statistical frost depth equation, a model was developed to estimate the required insulation thickness to reduce the frost depth to the desired one. Unfortunately, field data were not available to verify the accuracy of the model.

Chapter 1

Introduction

1.1 Problem Statement

In cold regions such as Michigan, where air temperature drops below 32°F for extended periods of time, frost depth is an important factor that affects the design of all infrastructures including pavements, building and bridge foundations and/or utility lines. During freezing, soils containing substantial amount of water undergo heave due to the formation and growth of ice lenses. The heave could result in significant vertical and lateral stresses and movements which could lift foundations or apply substantial additional stresses to retaining structures. In addition, frost heave is typically followed by thaw consolidation and settlement. Therefore, spread footings located on soils subjected to frost-thaw cycles would experience up and down vertical movements. For bridges, such movements may create unsafe driving conditions at the boundaries between the bridge and the adjacent pavement structure.

Frost heave is a function of many variables including soil type and its water holding capacity and thermal conductivity, air temperature, and frost depth. The prediction of frost depth in soils is fairly well established and not complex for a single layered system. However, it is a challenging task for multi-layered systems subjected to various surface boundary conditions where the air temperature fluctuates. The other complex aspect of freeze-thaw cycles is the estimation of the frost heave of multi layered system due to ground freezing. Perhaps complex and sophisticated models to predict the propagation of freezing and thawing fronts and to estimate frost heave can be developed. However, such models require a large amount of data that are expensive to obtain and hence, they cannot be easily implemented. It is assumed herein that simplified analytical and numerical methods can be developed and customized to predict freezing and thawing of soils. The input data to these methods must be readily available or can be obtained at a minimum cost.

1.2 Study Objectives

The objectives of this study are:

1. Develop accurate and reliable models for predicting the frost depth during freezing period in Michigan.
2. Develop a model to predict heave and the resulting pressure under the pavement or behind existing retaining structures due to freezing of frost-susceptible soils in Michigan.

1.3 Research Plan

To accomplish the objectives of the study, a research plan consisting of 5 tasks was drawn and approved by MDOT. The five tasks are summarized below.

Task 1 - Conduct Comprehensive Literature Review – The literature review includes:

1. The state of the art of modeling freeze and thaw in soils and their applicability to this study.
2. The state of the practice of State Highway Agencies (SHAs) for forecasting frost depth, frost heave, and the time at which to post and remove seasonal load restriction (SLR).
3. The state of art of modeling of frost heave and the resulting pressure behind retaining walls.

Task 2 - Development of Heat Transfer Predictive Model – After reviewing available models to predict the propagation of the freezing front in non-uniform and multilayered soils; the ones that simulate the MDOT data the most will be further scrutinized and perhaps modified. Further, the thawing front will be modeled using a modified version of Nixon and McRoberts (1973) equation to fit the MDOT measured field data.

Task 3 - Couple Heat Transfer Models with Prediction of Frost heave and Frost Pressure - The initiation and growth of ice lenses in a soil deposit in cold environment exert uplift pressure against the foundation and lateral pressures against a retaining structure and the soil behind it. Both pressures could be calculated using approximate analytical techniques based on heat transfer models and can be simulated using existing theory of consolidation coupled with unsaturated flow and heat transfer for estimating the rate of ice growth. The efforts in this task consist of the three steps listed below.

1. Estimate the freezing depth (Task 2).
2. Estimate the rate of flow of water to the frozen depth from a water supply (ground water table, surface water source, etc.) to calculate the rate of growth of ice lenses during the critical time period and at the most critical location of the site. The estimation of the rate of flow of water to the frozen depth could be based on several parameters including unsaturated/saturated hydraulic conductivity of the subsoil,

soil-water retention properties, and the depth to the water table or the distance to the closest free supply of water.

3. Estimate the amount of frost heave and earth pressures due to heave based on compressibility and consolidation theory.

Task 4 - Validate the Models Using the Measured MDOT Field Data from Selected Sites - The models developed in Tasks 2 and 3 will be validated and calibrated using the data provided by MDOT from selective field sites that represent typical conditions. The validation will be performed using a two-tiered approach:

1. Model the freezing, thawing and stress generation due to heaving ground using the models developed in Tasks 2 and 3.
2. Based on the results, calibrate the models to fit the measured MDOT data.

Task 5 - Professional training/workshop for MDOT Staff on Application of the model

Task 6 - Final Report - The final report will include documentations of the modeling approaches and how to apply the models. In addition, PowerPoint slides and handout explaining the assumptions and the use of the models with example problems will be prepared. A one-day professional training/workshop session will be organized for the MDOT staff in Lansing.

1.4 Organization of this Report

This report is organized in 5 chapters and appendices. The contents of each chapter are detailed in the table of contents. The title of each chapter is listed below.

Chapter 1 - Introduction

Chapter 2 - Literature Review

Chapter 3 - Data Mining

Chapter 4 - Analyses and Discussion of Frost Depth and Frost Heave

Chapter 5 - Conclusions

Appendices - Additional data, figures and drawings are presented in the appendices.

Chapter 2

Literature Review

2.1 Frost Depth

One of the important aspects of infrastructure design such as pavement, foundations or utility line is frost depth prediction. Frost depth is a function of the material type, soil thermal properties, soil water content, and climatic conditions such as temperature, wind speed, precipitation, and solar radiation. In order to neutralize the effects of frost, foundations are usually built below the frost line. For pavements, most State Highway Agencies (SHAs) use non-frost susceptible soils (granular materials). However, over time, fine aggregates migrate from the lower soil layers and soil becomes frost susceptible. In general, any soil might be considered frost susceptible when the percent fine (passing sieve number 200) exceeds about seven percent. Since silt has high water holding capacity and relatively low permeability, it is the most frost susceptible soil. Depending on the availability of the input data and the required accuracy, frost depth can be estimated by numerical, empirical, and/or mechanistic-empirical models.

2.1.1 Numerical Models

Different numerical techniques (finite element and finite difference) have been used for modeling complex transient heat flow in pavement layers. Hsieh et al (Hsieh et al., 1989) developed a three-dimensional finite difference computer program for predicting temperature profile in concrete pavements and rainfall infiltration into the layered system. The program inputs consist of typical meteorological year (TMY) data and typical physical soil and concrete properties. They reported that their results were in a good agreement with the test results provided by the Florida DOT. Thompson et al. (Thompson et al., 1987) established a climate database for pavements in the state of Illinois. He used a transient one-dimensional finite difference model (Climatic-Materials-Structural) and the climate database to predict the pavement temperature profile. The other required inputs for his model are thermal properties of materials, air temperature, solar radiation data, and wind velocity. Yavuzturk et al (Yavuzturk et al., 2005) proposed a transient two-dimensional finite difference model to assess the thermal behavior and temperature distribution in asphalt pavement. TMY weather data were used and sensitivity analyses were conducted to determine the influence of different thermal properties of the materials on the predicted asphalt temperature. They reported that the temperature predictions were most effected by variation of the absorptivity, volumetric heat capacity,

emissivity and thermal conductivity of the materials. Chapin et al (Chapin et al., 2012) utilized finite element program TEMP/W (GEO-SLOPE 2007) to simulate freezing and thawing front in the pavement. They applied the program to two sites in northern Ontario with considerably different pavement structures. First, a steady state analysis was conducted to establish the initial conditions within the model and second, a transient analysis was conducted. By using adiabatic* conditions on the lateral boundaries they induced one-dimensional heat flow. They reported that the predicted frost front was several days behind the measured frost front.

- **UNSAT-H Modeling**

UNSAT-H is a one dimensional, finite difference computer program developed at Pacific Northwest Laboratory (Fayer and Jones, 2000). UNSAT-H can simulate the water and heat balance in a layered cross section simultaneously. The input properties for the models are listed below:

1. Hydraulic Properties

To solve the water balance equations, relationships for both water content and hydraulic conductivity as a function of suction head are required.

To describe soil water retention from measured data the van Genuchten function has been used:

$$\theta = \theta_r + (\theta_s - \theta_r)[1 + (\beta h)^n]^{-m} \qquad Equation\ 2-1$$

Where θ_r= residual water content (cm^3/cm^3);

θ_s = saturated water content (cm^3/cm^3);

h = suction (cm); and β, n, m = fitting parameters

2. Thermal Properties

UNSAT-H model use **C**ass et al. equation to express thermal conductivity (k_h) as a function of water content (Stormont,J., and Zhou, S. 2001):

$$k_h = A + B\frac{\theta}{\theta_s} - (A - D)\exp^{-\left[C\frac{\theta}{\theta_s}\right]^E} \qquad Equation\ 2-2$$

* An ADIABATIC process is the changing temperature of air due to its movement. Rising air will cool adiabatically, whereas sinking air warms adiabatically. The DIABATIC process, on the other hand, is any change in air temperature not associated with adiabatic vertical displacement of air. The prime source of heating in the DIABATIC process is the sun, while the main cause of cooling is evaporation and the emission of long wave energy from the ground surface.

Where k_h= thermal conductivity (J/ (s.cm.^{o}K));

θ = the water content corresponding to the measured k_h (cm^3/cm^3);

A, B ,C ,D, E = the fitting parameters; and

All other parameters are as before.

2.1.2 Mechanistic Empirical Models

Neumann proposed the first solution to the heat transfer phase-change problem in his lectures in the 1860's; he then published his work in 1912(Jiji, 2009). In his solution, one-dimensional heat transfer in a semi-infinite region was assumed. The above freezing initial surface temperature (T_i) drops to T_0 (a temperature below the freezing point) and freezing starts to propagate through the liquid phase as shown in Figure 2-1(Jiji, 2009).

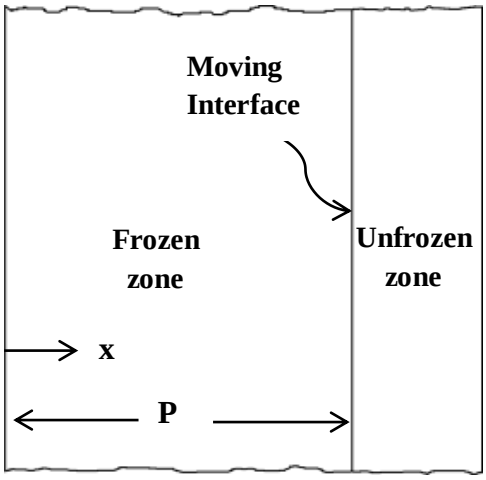

Figure 2-1 A schematic representation of two phase heat conduction

The governing heat conduction equations for solid and liquid phases are stated in Equations 2-3 and 2-4, respectively.

$$\frac{\partial^2 T_f}{\partial x^2} = \frac{1}{\alpha_f}\frac{\partial T_f}{\partial t} \qquad 0 < x < P \qquad \text{Equation } 2-3$$

$$\frac{\partial^2 T_u}{\partial x^2} = \frac{1}{\alpha_u}\frac{\partial T_u}{\partial t} \qquad x > P \qquad \text{Equation } 2-4$$

Where the subscripts u and f refer to unfrozen and frozen, respectively;

t = time since the freezing starts (s);

x_i = frost depth (m);

T = temperature (^{o}C); and

α = thermal diffusivity (m^2/s) calculated using Equation 2-5.

$$c = \frac{k}{\rho c_p} \qquad \text{Equation } 2-5$$

Where k = thermal conductivity of the soil (W/ (m·^{o}K);

c_p = specific heat at constant pressure (J/(Kg.^{o}C));

ρ = density (Kg/m^{3}).

The interface energy equation is stated in Equation 2-6:

$$k_f \frac{\partial^2 T_f(x_i,t)}{\partial x^2} - k_u \frac{\partial^2 T_u(x_i,t)}{\partial x^2} = \rho_f l \frac{dx_i}{dt} \qquad \text{Equation } 2-6$$

The boundary conditions are

$$T_f(0,t) = T_0$$

$$T_f(x_i,t) = T_m$$

$$T_u(x_i,t) = T_m$$

$$T_u(\infty,t) = T_i$$

And the initial conditions are

$$T_u(x,t) = T_i$$

$$x_i(0) = 0$$

Where l = latent heat of fusion (J/Kg);

T_m= bulk freezing temperature (^{o}C); and

All parameters are as before.

The frost depth can be estimated using Equation 2-7

$$P = \mu\sqrt{4\alpha_f t} \qquad \text{Equation } 2-7$$

Where P = frost depth (m);

μ = constant obtained from Equation 2-8; and

All parameters are as before.

The parameters μ can be calculated using Equations 2-8

$$\frac{\exp(-\mu^2)}{erf\mu} - \sqrt{\frac{\alpha_f}{\alpha_u}}\frac{k_u}{k_f}\frac{T_i - T_m}{T_m - T_0}\frac{\exp\left(-\frac{\mu^2\alpha_f}{\alpha_u}\right)}{1-\mathrm{erf}\left(\sqrt{\frac{\alpha_f}{\alpha_u}}\mu\right)} = \frac{\sqrt{\pi}\mu l}{c_{pf}(T_m - T_0)} \qquad \text{Equation } 2-8$$

Where the subscripts u and f refer to unfrozen and frozen, respectively;

erf = Gauss error function;

T_i = initial surface temperature (^oC);

T_0 = surface temperature at t≠0 (^oC); and

All parameters are as before.

Further, Stefan solved Neumann's equation for a special case of no heat transfer in liquid layer in 1891, (Jiji, 2009) as follow:

$$P = \sqrt{\frac{2k_f(T_m - T_0)}{\rho l}t} \qquad \text{Equation } 2-9$$

It was assumed that the applied constant surface temperature ($T_m - T_0$) multiplied by the time (t) is equivalent to the freezing index (*FI*) at that time. He further introduced a dimensionless multiplication parameter (n) to converts air temperature to surface temperature. After converting metric units to English system Equation 2-9 became

$$P = \sqrt{\frac{48k_f * n * FI}{L}} \qquad \text{Equation } 2-10$$

$$L = 144w\gamma_d \qquad \text{Equation } 2-11$$

Where P = depth of freeze or thaw (ft);

k_f = thermal conductivity of soil (Btu/(ft hr °F));

n = dimensionless parameter which converts air index to surface index;

FI = freezing index (^{o}F-day); note that the freezing index in Stefan equation is similar to the cumulative degree day at time t, it is not the conventionally defined freezing index for a winter season.

L = volumetric latent heat of fusion (Btu/ft^3);

w = water content; and

γ_d = dry density (pcf).

Since Stefan's equation does not consider the volumetric heat capacity of the soil and water the accuracy of the results are debatable. Consequently, several studies have been conducted to improve the prediction of frost depth, including the Modified Berggren equation (Aldrich et al., 1953). Berggren Equation is very much similar to the early work of Neumann; therefore it is not explained here. Aldrich et al applied a correction factor to Berggren Equation which is a function of two dimensionless parameters, the thermal ratio (α) and the fusion parameter (μ) (see Figure 2-2).

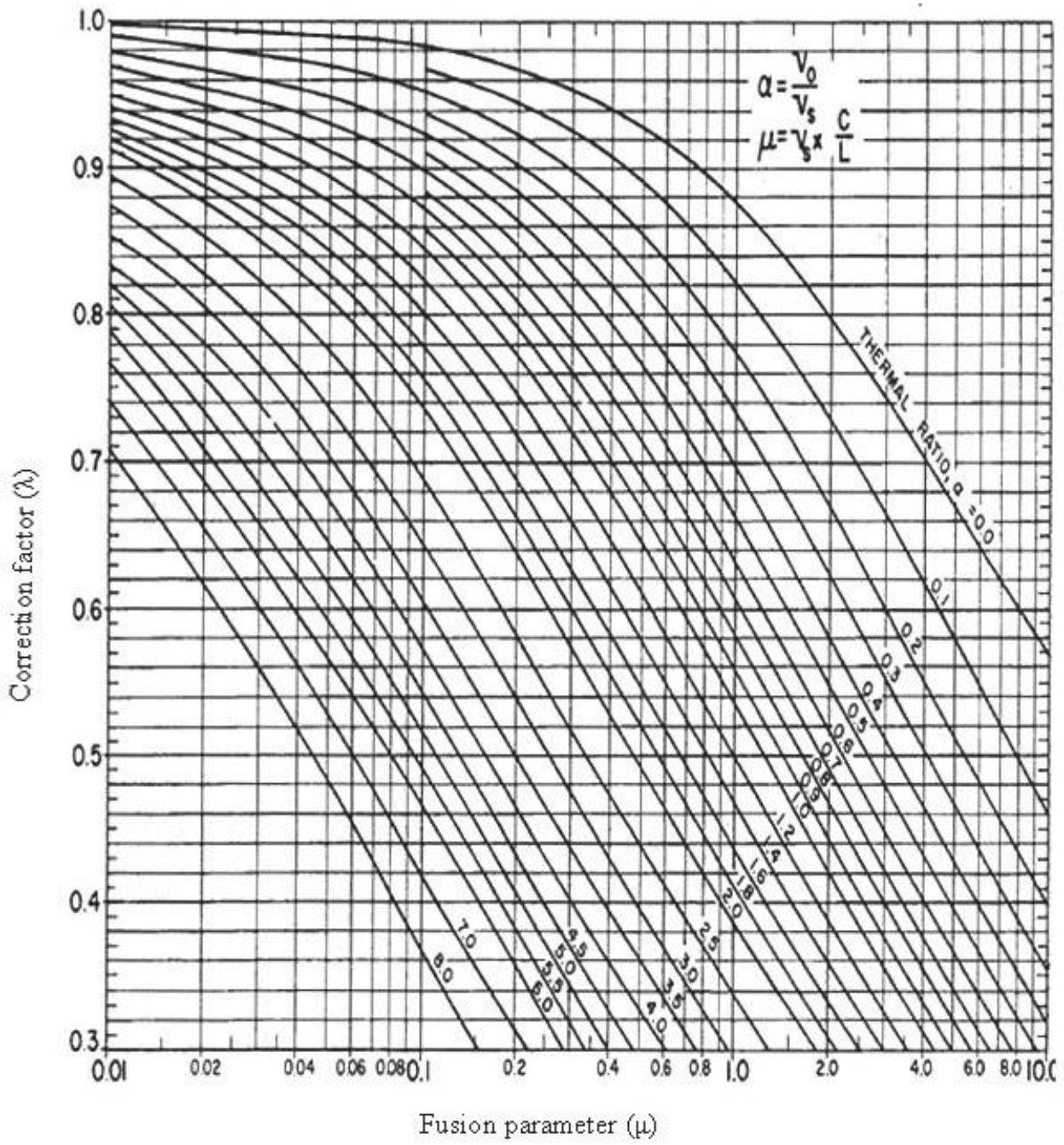

Figure 2-2 Fusion parameter (μ) versus correction factor (λ). In this figure V_0 is initial temperature differential (mean annual temperature -32 ^{0}F), V_s is average temperature differential (nFI/t), C in average volumetric heat capacity, L is volumetric heat of fusion.

These parameters take the effect of temperature changes in the soil mass into account and depend on the freezing index, the annual average temperature in the site and the thermal properties of the soil (USACE, 1988). The Modified Berggren equation can be written as follow:

$$P = \lambda \sqrt{\frac{48k * n * FI}{L}} \qquad \text{Equation } 2-12$$

Where $\lambda =$ correction factor; and

All other factors are as before.

A multilayer solution to the Modified Berggren equation can be applied to nonhomogeneous soils by calculating the required cumulative freezing degree day (CFDD) for frost to penetrate each layer. The maximum summation of the CFDDs must be equal to or less than the regional and seasonal freezing index. The frost depth can be estimated as the sum of the thicknesses of all the frozen layers (USACE,1988). The CFDD required to penetrate the nth layer is defined as:

$$CFDD_n = \frac{L_n d_n}{24\lambda_n^2}\left[\left(\sum_1^{n-1} R_n\right) + \frac{R_n}{2}\right] \qquad \text{Equation } 2-13$$

Where L_n= volumetric latent heat of fusion of the nth layer (Btu/ft^3);

R_n= thermal diffusivity of the nth layer= d_n/k_n (hr-°F/ Btu);

d_n = depth of the nth layer (ft);

λ_n = correction factor of the nth layer;

k_n = thermal conductivity of the nth layer (Btu/ft-hr-°F); and

$CFDD_n$ = cumulative freezing degree day required for frost to penetrate the nth layer (°F-days).

The Pavement-Transportation Computer Assisted Structural Engineering (PCASE) software provided a more accurate numerical solution of the Modified Berggren equation, (Bianchini et al. 2012).

Berg (Berg,1996) applied Modified Berggren equation to 40 sites in the state of Minnesota for 3 years to assess the accuracy of the results. He reported that predicted frost depths were within ±15 percent of the measured frost depth. He also conducted different sensitivity analysis to assess the dependence of the predicted frost depths to the n-factor (defined on page 2-5), water content, dry density, thermal conductivity, and each layer thickness. Berg concluded that small variation in thickness, water content and dry density of each layer would have a small effect on the predicted frost depths. On the other hand he found that increases in the n-factor values would result in deeper frost depths prediction. Whereas increasing the measured thermal conductivity by 25 percent would lead to better frost depths prediction. Stated

differently, Berg found that the Modified Berggren equation produces more accurate estimates of the frost depth when the measured thermal conductivity is artificially increased by 25 percent.

2.1.3 Empirical Models

Chisholm and Phang used the data from different stations throughout Ontario and developed an empirical equation to correlate the calculated cumulative freezing degree day (CFDD) and the measured frost depths (Chisholm and Phang, 1983).

$$P = 1.6968\ \sqrt{CFDD} - 12.91 \qquad \text{Equation } 2-14$$

Where P = depth of freeze or thaw (in); and

All parameters are as before.

Many State Highway Agencies (SHAs) used similar approach to generate their own equations or simply calibrated Equation 2-14 using local frost depth data and CFDD.

Dore (Tighe et al, 2007) conducted a research to develop an empirical model for frost depth in Quebec, Canada. First, he developed Equation 2-15 to estimate pavement surface temperatures (PST) based on the measured air temperatures. Second, he calculated the cumulative freezing degree day (CFDD) based on the estimated pavement surface temperature (PST of Equation 2-15) and estimated the frost depth using Equation 2-16. Third, he correlated the estimated frost depths from Equation 2-16 to the measured frost depth and obtained statistical Equation 2-17.

$$PST = T_{MEAN} + [0.178(T_{MAX} - T_{MIN})] + 1.628 \qquad \text{Equation } 2-15$$

$$P = C\sqrt{CFDD} \qquad \text{Equation } 2-16$$

$$P_{corr} = P + \left[CI(S_e)\left(1 + \frac{1}{398}\right) + \left(\frac{\left(\sqrt{CFDD} - X_{MEAN}\right)^2}{\sum (X_i - X_{MEAN})^2} \right)^{0.5} \right] \qquad \text{Equation } 2-17$$

Where; T_{MEAN} = (T_{MAX}+T_{MIN})/2;

T_{MAX} = maximum daily air temperature (^oC);

T_{MIN} = minimum daily air temperature (^oC) and; and

PST = estimated pavement surface temperature (^oC).

P = frost depth (cm);

C = regression constant; and

CFDD = cumulative freezing degree days based on the estimated pavement surface temperature (PST) (^{o}C-day).

P_{corr} = corrected frost depth;

CI = confidence interval for a population mean, a function of significance level, alpha=0.4, one standard deviation and a sample size of one;

S_e = sum of squared errors;

X_i = measured frost depth (cm); and

X_{MEAN} = Average measured frost depth (cm)

Tighe et.al (Tighe et.al, 2007) used data from one study site along Highway 569 in Northern Ontario and calibrated the Chisholm and Phang model. Furthermore, they used CFDD and cumulative thawing degree day (CTDD) and developed a modified model for estimating the frost depths as follow:

For $0 \leq i \leq i_0$ $$P_i = a + b\sqrt{CFDD_i} + c\sqrt{CTDD_i}$$ Equation $2-18$

For $i \geq i_0$ $$P_i = d + e\sqrt{CFDD_i} + f\sqrt{CTDD_i}$$ Equation $2-19$

Where i = number of days after the day indexed as day i=0 (i= 0 day on which air temperature first falls below 0 ^{o}C);

i_0 = day after which the CTDD consistently increases;

P_i = depth of frost on day i;

$CFDD_i$ = cumulative freezing degree day on day i (in ^{o}C-days);

$CTDD_i$ = cumulative thawing degree day on day i (in ^{o}C-days); and

a,b,c,d,e,f = calibration coefficients.

Moreover, they used Road Weather Information Systems (RWIS) in three sites close to the study site to estimate the frost depths and compare them with the study site data. They estimated the calibration coefficients and calculated the frost depth. Although, the coefficient of determination was 91%, the reliability of the model is questionable since only one year of data was used.

2.2 Frost Heave

In seasonally frozen regions, soil freezing causes frost heave, which may cause extensive damage to various civil engineering structures, such as pavements and utility lines (Liu et.al, 2013).

Frost heave refers to the uplifting of ground surface caused by freezing of water within the layers of soil. Taber (Taber, 1930) was the first one that demonstrated experimentally the features of frost heave. Before Taber frost heaving was explained based on experiments with closed systems. Taber showed that under normal conditions, the freezing occurs in an open system. Therefore in the freezing process water migrates through the soil voids below the freezing zone, causes excessive heaving by creating segregated ice layers. Tendency of a soil to heave under the freezing conditions is known to be influenced by parameters such as soil type, freezing rate, availability of water and the applied load or overburden pressure.

The magnitude and the rate of frost heave can be predicted in terms of certain characteristics of the freezing system and some boundary conditions by use of a practical theory explaining the frost heave of a specific soil (Konrad and Morgenstren, 1980). In general the theories toward this matter can be classified into two categories, capillary theory and frozen-fringe theory.

2.2.1 Capillary Theory

Capillary theory, also known as primary frost heave, is characterized by a frozen and an unfrozen zone within the soil strata. Consider pure water to be at equilibrium with ice, when a differential amount of water freezes at constant temperature and pressure:

$$dG = VdP - SdT = 0 \qquad \text{Equation } 2-20$$

For two phases of ice and water;

$$dG_i = dG_w \qquad \text{Equation } 2-21$$

$$V_i dP - S_i dT = V_w dP - S_w dT \qquad \text{Equation } 2-22$$

By rearrangement the equation becomes

$$\frac{dP}{dT} = \frac{S_i - S_w}{V_i - V_w} = \frac{\Delta S_{wi}}{\Delta V_{wi}} \qquad \text{Equation } 2-23$$

Where the subscripts “i” and “w” stand for ice and water, respectively (Takagi, 1978).

G = Gibbs free energy (J/mol);

S = entropy (J/^{o}K);

V = volume (m^3);

P = pressure (Pa) ; and

T= temperature (^{o}K).

The entropy change ΔS_{wi} and the volume change ΔV_{wi} are the changes which occur when a unit amount of water is transferred from phase w to phase i at the equilibrium temperature and pressure.

Clapeyron substituted the latent heat of phase transition as $\Delta H_{wi} = T_m \Delta S_{wi}$ in Equation 2-23 and obtained Equation 2-24 (Smith et, al. 2001):

$$\frac{dP}{dT} = \frac{\Delta H_{wi} * \gamma_w}{T_m(\frac{\gamma_w}{\gamma_i} - 1)} \qquad \text{Equation } 2-24$$

Where ΔH_{wi} = the enthalpy change when a unit amount of water is transferred from water to ice (J);

γ_i = specific volume of ice (1/ m^3)

γ_w = specific volume of water (1/ m^3); and

All parameters are as before.

Since $\gamma_w \approx \gamma_i$, by neglecting the term $(\frac{\gamma_w}{\gamma_i} - 1)$ Equation 2-24 can be rewrite as (Peppin and Style, 2012)

$$P_i - P_w = \frac{\rho_w L}{T_m}(T_m - T) \qquad \text{Equation } 2-25$$

Where T = the thermodynamic equilibrium temperature of the system (^{o}K);

T_m = the bulk freezing temperature, 273 (^{o}K);

L = latent heat of fusion (J/Kg);

P_i = ice pressure (Pa);

P_w = water pressure (Pa); and

ρ_w = density of water (Kg/m^3).

The Clapeyron equation explains thermodynamically why lowering the temperature below freezing temperature causes water to move (be sucked) toward the ice.

Black (Black, 1995) solved Clapeyron equation for different scenarios.

1. If the pressure difference in ice and water are the same, by increasing the confining pressure of 1 MPa the melting temperature decreases by 0.074^{o}C.
2. If the change in confining pressure in water is 1.09 times greater than the change in ice pressure then the melting temperature remains constant.
3. If water pressure is constant by increasing the ice confining pressure of 1 MPa the melting temperature decreases by 0.893^{o}C.

4. If ice pressure is constant by decreasing the water confining pressure of 1 MPa the melting temperature decreases by 0.810^{o}C.

Everret (Everret ,1960) constructed a simple model for explaining the capillary theory. He considered two cylinders each closed up by a piston and joined by a capillary tube as shown in Figure 2-3-b. By lowering the temperature water starts to freeze in the upper cylinder. When the upper cylinder is completely filled up with ice, further decreases in temperature results in water flow from the lower cylinder to the upper one.

According to Laplas Equation if the radius of the capillary tube is r, ice can only penetrate to the capillary tube when

$$P_i - P_w = \frac{2\sigma_{iw}}{r} \qquad \text{Equation } 2-26$$

Where σ_{iw} = ice-water surface energy (dyne) ;

All other parameters are as before.

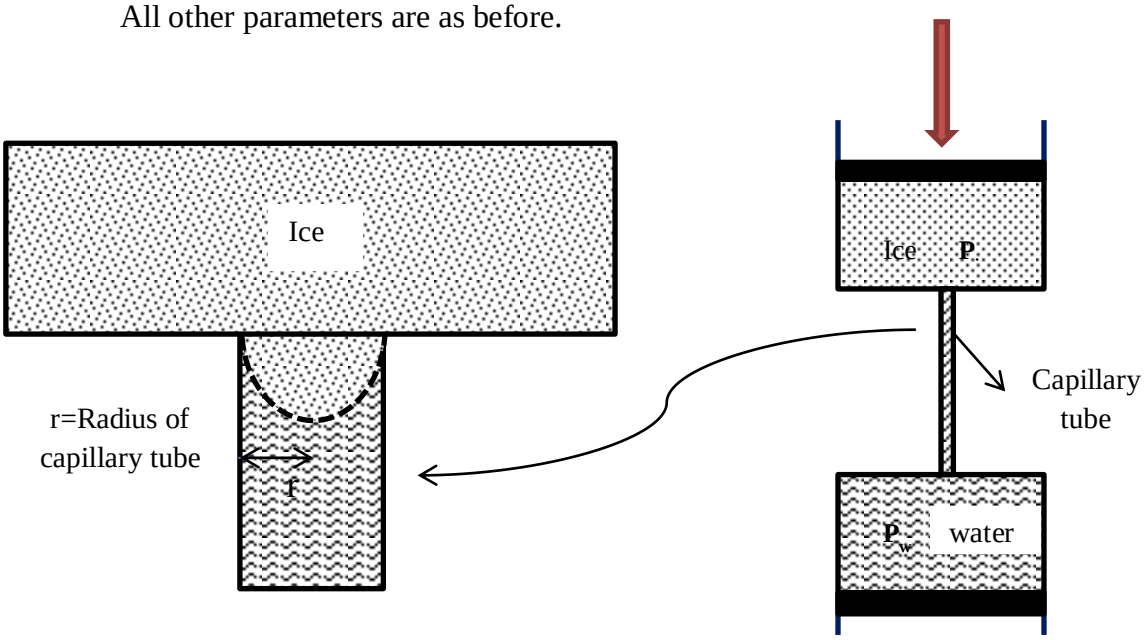

Figure 2-3 (a) **Figure 2-3 (b)**

Figure 2-3 Equilibrium interface between ice and water (a), and simple ice-water model (b)

Since the capillary tube represents the soil pores, it implies that segregated ice forms when

$$P_i < P_w + \frac{2\sigma_{iw}}{r} \qquad \text{Equation } 2-27$$

And pore ice forms when

$$P_i > P_w + \frac{2\sigma_{iw}}{r} \qquad \text{Equation } 2-28$$

This implies that the growth of ice lenses will stop as the ice invades the soil at the maximum heaving pressure given in Equation 2-29 (Loch and Miller, 1975):

$$p_{max} = P_w + \frac{2\sigma_{iw}}{r} \qquad \text{Equation } 2-29$$

The temperature T_l at which ice invades the pores can be found by combining 2-25 and 2-26 into Equation 2-30 (Peppin and Style, 2012):

$$T_l = T_m\left(1 - \frac{2\sigma_{iw}}{\rho_w L_f r}\right) \qquad \text{Equation } 2-30$$

Where

T_l= The temperature at which ice invades the pores (^{o}K); and

All other parameters are as before.

The capillary theory has various limitations including:

1. Predictions of the maximum frost-heave pressure works well with idealized soils composed of particles with one size. But in soils with different particle sizes the heaving pressures are considerably larger (Peppin and Style, 2013).

2. Basically, capillary theory can be used to predict the flow rate towards the ice lenses in the frozen region. By assuming that the porous medium is incompressible, Darcy's law can be used to determine the flow rate of water towards the lenses by Equation 2-31. But the equation tends to over predict the measured values of flow rate (Peppin and Style, 2012)

$$V = \frac{k}{\mu}\frac{P_R - P_f}{Z_h} \qquad \text{Equation } 2-31$$

Where V=flow rate (m/s);

k = permeability of the soil (m/s);

μ = the dynamic viscosity of water (m.Pa.s);

Z_h = the distance between the ice lens and the water reservoir (m);

P_R = the ground water pressure (Pa); and

P_f = the pressure of the water directly below the warmest lens (Pa).

3. No mechanism for initiation of new lenses has been explained by this method.

2.2.2 Frozen Fringe Theory

Since the capillary theory has limitations, some researchers explained the propagation of frost heave phenomenon by another theory, Frozen Fringe. Frozen Fringe theory, also termed as secondary frost heave, is characterized by three zones: a frozen zone, a partially frozen thin zone and unfrozen zone. According to this theory frost heave can continue to occur at ice-lens temperatures above T_l (the temperature at the bottom of the frozen zone) when a frozen fringe is shaped by formation of ice in the soil pores, see Figure 2-4.

Stated differently, if the rate of extracting heat is too large or the soil column is too tall, or too impervious to prevent ice entry the frozen fringe is created beneath ice lenses at the top. Therefore ice pressure could rise above the maximum (P_{max}).This process is called secondary heaving (Loch and Miller, 1972).

At the interface of ice lens and soil particles, there are repulsive intermolecular forces (surface tension). These forces act like a disjointing pressure that separate ice and soil particles and initiating a microscopically thin layer of water between the ice lenses and the soil particles below the freezing temperature, T_m , (Dash et al. 2006), see Figure 2.5. Because of the repulsive forces between the ice lenses and the soil particles, the pressure in the thin water film is reduced causing suction and upward water movement toward the growing ice lenses (Peppin and Style, 2012).

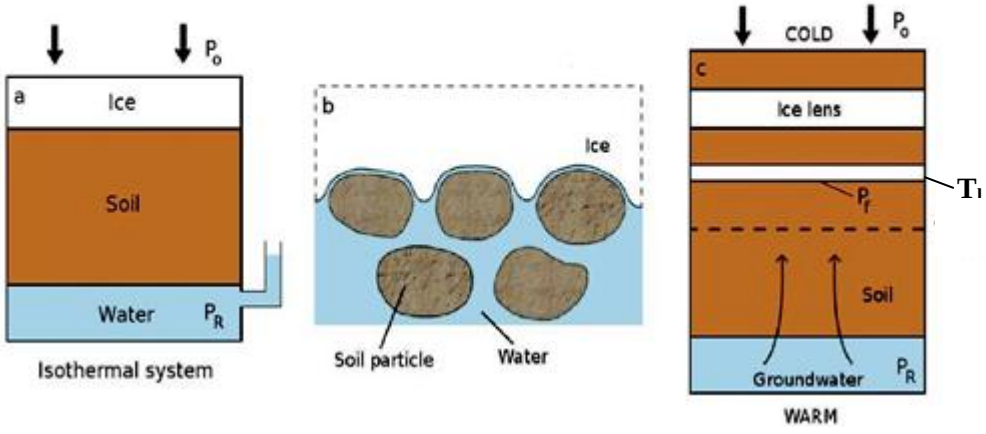

Figure 2-4 Schematic diagrams for the frost heave process (Peppin and Style, 2012)

Secondary frost heave can be affected by the suction pressure. The specific characteristics of the soil determine the practical relation between the suction and the unfrozen

water content. As the ice-water interface curvature is increasing, the unfrozen water content decreases which consequently yields an increase in suction.

According to the Clapeyron formula, an increase in load results into a decrease in the amount of unfrozen water, which consequently increases the suction. However, increase in load makes the onset of new ice lens formation more difficult. Therefore higher suction is required to separate the soil grains. These dual effects of increase in load make the ice lenses initiation in clays more easily. The secondary frost heave occurs mostly under any load condition in clays, while rarely takes place in sands (Fowler and Krantz, 1994).

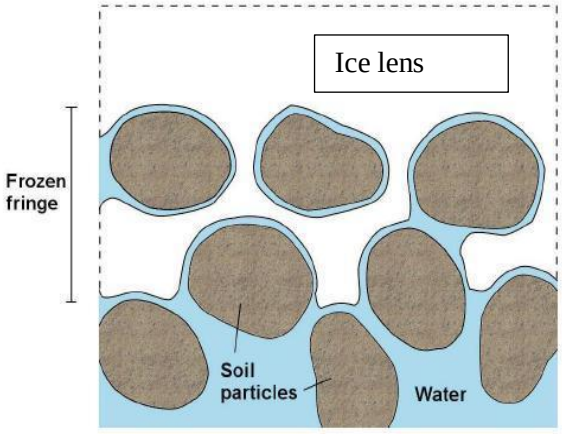

Figure 2-5 Schematic diagram of a freezing soil with frozen fringe (Peppin and Style, 2012)

When the freezing front penetrates into the soil, it absorbs the moisture in the soil, which stands for a process of both heat and mass transfer (Harlen1973). The complexity in the frost heave theory arose from this coupled effect of heat and mass transfer. The first model which considers heat and mass flow in the soil was proposed by Harlan (Harlan, 1973). He proposed that the generalized one-dimensional mass flow for steady or unsteady flow in a saturated or partially saturated soil media can be modeled by Equation 2-32 and the one-dimensional transient heat transfer can be modeled by Equation 2-33

$$\frac{\partial}{\partial x}\left[\rho_w K(x,T,\psi)\frac{\partial H}{\partial x}\right] = \frac{\partial(\rho_w \theta_l)}{\partial t} + \Delta M \qquad \text{Equation } 2-32$$

$$\frac{\partial}{\partial x}[k(x,T,t)\frac{\partial T}{\partial x} - c_l \rho_w \frac{\partial(\vartheta_x T)}{\partial x} = \frac{\partial(CT)}{\partial t} \qquad \text{Equation } 2-33$$

Where t = time (minutes);

ρ_w = density of water fraction (gr/cm^3);

θ_l = volumetric water content = volume of water/ total volume (cm^3/cm^3) ;

K = hydraulic conductivity (cm/ min);

T = temperature (C^o);

H = total head (cm);

ψ = capillary pressure head (cm); and

ΔM =change in mass of ice per unit volume, unit time (gr/ (cm^3. min)).

c_l = bulk specific heat of water (cal /gm / C^o);

ϑ_x =water flow velocity in x direction (cm/ min);

C= 'apparent' volumetric specific heat (cal /cm^2/ C^o); and

All other parameters are as before.

Gilpin (Gilpin 1979, 1980a, 1980b) studied water flow towards the ice layer and proposed a physical model for prediction of ice lensing and heave rate, he suggested that frost heave is a function of basic soil properties and boundary conditions. He assumed that the free energy of water in the pores is lowered by the surface effect of the solid. Figure 2-6 shows the pressures in the water near the solid soil surface in the case of the existence of tension between the water meniscus and the soil. The effect of the tensile surface force on free energy could be described as follow:

$$G_w = G_{wO} + \nu_w P_w - S_w T_w - g(y) \qquad \text{Equation } 2-34$$

Where the subscripts w stand for water;

g(y)= is a dummy variable expressing the effect of the particle surfaces on the free energy of water (KJ/mol), g(y) is estimated using Equation 2.38 by setting y equal to h (the distance between the soil particle surface and the ice lenses);

G_w = the free energy of water near the surface (KJ/mol);

G_{wO} = the free energy at bulk conditions T_0 and P_0 (KJ/mol) ;

ν_w = specific volumes of water (m^3/Kg); and

All other parameters are as before.

In the case of thermodynamic equilibrium G_w should be constant in the water layer and also the temperature could be considered constant because the layer is thin. Therefore the effect of surface can be obtained as:

$$P_{wy} = \frac{1}{\nu_w} g(y) \qquad \text{Equation } 2-35$$

Where P_{wy} = pressure at the distance y from the surface (Pa);

All other parameters are as before.

On the other hand the free energy in the ice G_i can be obtained as:

$$G_i = G_{iO} + \nu_i P_i - S_i T_i \qquad \text{Equation } 2-36$$

Where the subscripts i stand for ice

G_i = the free energy of ice (KJ/mol);

G_{io} = the free energy at bulk conditions T_0 and P_0 (KJ/mol);

ν_i = specific volumes of ice (m^3/Kg); and

All other parameters are as before.

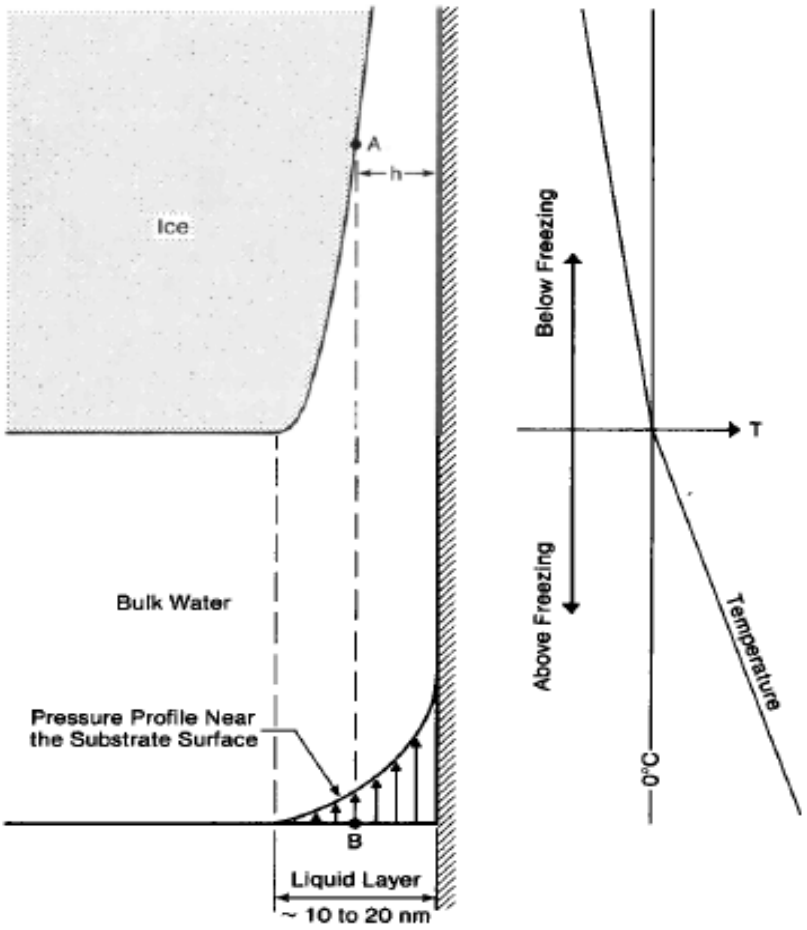

Figure 2-6 A schematic representations of equilibrium conditions for ice and water near a substrate (Gilpin, 1980)

The temperature cannot be different across the phase boundary, but the pressure difference can be gained as:

$$P_i - P_{wh} = \sigma_{iw}\overline{K} \qquad \text{Equation } 2-37$$

Where $\overline{K}$= the mean curvature of the interface (m),

P_{wh} = pressure at the distance h from the surface (Pa),

All other parameters are as before.

Equating Equations 2-34 and 2-36 and using Equation 2-37, $g(h)$ can be calculated as

$$g(h) = -\Delta\nu P_{wh} - \nu_i\sigma_{iw}\overline{K} - \frac{LT}{T_m} \qquad \text{Equation } 2-38$$

Using Equation 2-37 and Equation 2-38, the pressure gradient can be obtained as

$$\frac{dP_{wy}}{dx} = \frac{\nu_i}{\nu_w}\frac{d}{dx}\left[P_{wh} + \sigma_{iw}\overline{K} + \frac{LT}{\nu_i T_m}\right] = \frac{\nu_i}{\nu_w}\frac{d}{dx}\left[P_i + \frac{LT}{\nu_i T_m}\right] \qquad \text{Equation } 2-39$$

Therefore the flow rate through water layer can be calculated as

$$q = -k\frac{\nu_i}{\nu_w}\frac{d}{dx}\left[P_i + \frac{LT}{\nu_i T_m}\right] \qquad \text{Equation } 2-40$$

The above equation can be modified to obtain the water velocity in the frozen fringe as

$$V_{ff} = K_f\frac{\nu_i}{g}\frac{d}{dx}\left[P_i + \frac{LT}{\nu_i T_m}\right] \qquad \text{Equation } 2-41$$

Where K_f = the permeability in the frozen fringe (m/s),

V_{ff} = the velocity of water flow in the frozen fringe (m/s).

Figure 2-7 illustrates schematically the frost heave simulation. A linear temperature profile is assumed in each layer and the heat balance equation can be written as:

$$-\frac{k_f(T_{TOP} - T_l)}{H} - \frac{k_{ff}(T_{ff} - T_l)}{a} = \frac{L}{\nu_i}V_H \qquad \text{Equation } 2-42$$

$$\frac{k_{ff}(T_{ff} - T_l)}{a} - \frac{k_{uf}(T_{BOT} - T_{ff})}{Z} = \rho_{si}L\frac{dz}{dt} \qquad \text{Equation } 2-43$$

Where a = thickness of the frozen fringe (m);

H = thickness of frozen zone (m);

k_f = thermal conductivity of the frozen zone (W/(^{o}C.m));

k_{ff}= thermal conductivity of the partially frozen zone (W/(^{o}C.m));

k_{uf}= thermal conductivity of the unfrozen zone (W/(^{o}C.m));

L = latent heat of fusion of water (J/Kg);

T_{TOP}, T_{BOT} = temperatures at the top and bottom of the soil column (^{o}C);

V_H= frost heave rate (m/s);

Z= distance between bottom of soil column and position of ice penetration (m);

T_l= temperature at the base of the active ice lens (^{o}C);

T_{ff}= temperature at the base of the frozen fringe (^{o}C);

$\frac{dz}{dt}$= frost depth propagation rate (m/s); and

ρ_{si}= mass of ice per unit volume of soil.

The water pressure at the T_f boundary is:

$$P_{wf} = -g\frac{z}{\nu_L}\left(1 + \frac{V_{uf}}{K_{uf}}\right) \qquad \text{Equation } 2-44$$

$$P_{wf} = -g\frac{z}{\nu_w}\left(1 + \frac{\nu_w}{\nu_i}\frac{\left(V_H + \rho_{st}\Delta\nu\frac{dz}{dt}\right)}{K_{uf}}\right) \qquad \text{Equation } 2-45$$

And finally the velocity in the active frozen zone can be obtained as:

$$V_H = \frac{\nu_i^2}{g\nu_w}\frac{1}{\left[\frac{aI_{fl}}{T_{ff}-T_l}\right] + (\frac{1}{K_L})}\left[\frac{L(-T_l)}{\nu_w T_m} - P_{OB} + P_{Lf}\right] \qquad \text{Equation } 2-46$$

$$I_{fl} = \int_{T_f}^{T_l}\frac{1}{K_{ff}}dT \qquad \text{Equation } 2-47$$

Where g = acceleration of gravity (m/s^2);

P_{wf} = water pressure at the edge of the frozen fringe (Pa);

$\Delta\nu$= specific volume difference ($\nu_i - \nu_w$);

P_{OB}= overburden pressure (KPa);

K_L= permeability of ice lenses (m/s);

K_{uf} = permeability of unfrozen zone (m/s); and

All other parameters are the same as before.

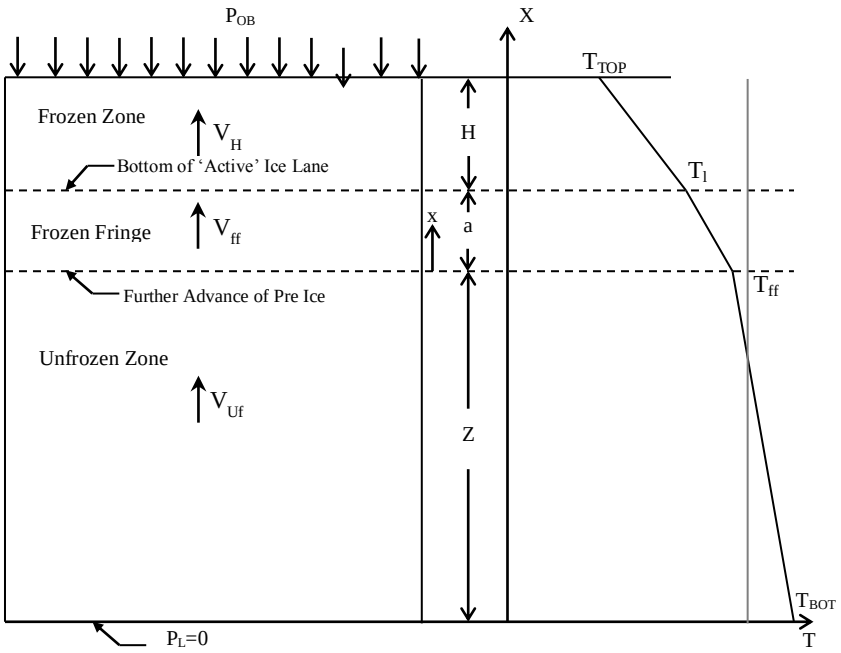

Figure 2-7 The frost heave simulation model (Gilpin, 1980)

Using different boundary conditions and solving equation 2-42, 2-43, 2-45 and 2-46 simultaneously, the water pressure at the bottom of the frozen fringe and the heave rate can be obtained. Also Gilpin proposed an approximate analytical solution.

Nixon (Nixon, 1991) modified the approximate analytical solution of Gilpin. In this approach a relationship between the frozen hydraulic conductivity and temperature is needed to predict the distinct location of each ice lens within the frozen zone. As shown in Figure 2-8, a linear temperature distribution (see Equation 2-48) and permeability distribution (see Equation 2-49) across the frozen fringe were assumed.

$$T = \left(T_l - T_{ff}\right)\left(1 - \frac{x}{a}\right) + T_{ff} \qquad \text{Equation } 2-48$$

$$k = \frac{k_{uf}}{\left[-\left(T_l - T_{ff}\right)\left(1 - \frac{x}{a}\right) - T_{ff}\right]^{\alpha}} \qquad \text{Equation } 2-49$$

Where x = the depth from the face of the active ice lens (m);

All other parameters are as before.

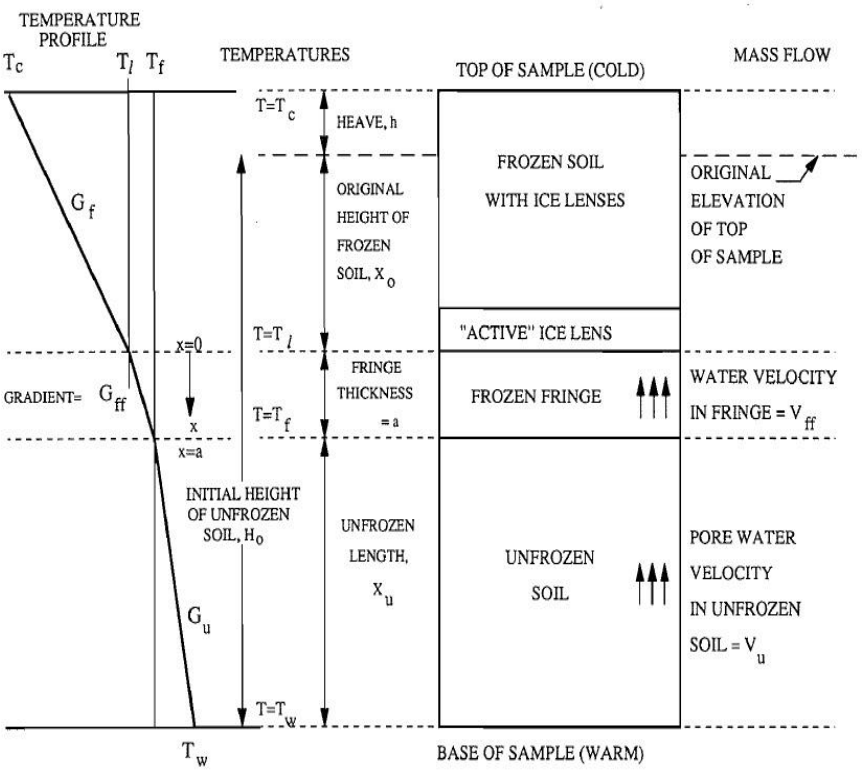

Figure 2-8 A zone of frozen soil, a freezing fringe, and an underlying zone of unfrozen soil (Nixon ,1991)

If the assumptions of no pore-water phase expansion and incompressible soil are made, the continuity of water flow indicates that

$$\frac{d}{dx}\left\{\frac{dP_w}{dx}\right\} = 0 \qquad \text{Equation } 2-50$$

So the velocity of water flow should be constant in the frozen fringe. At any temperature the unfrozen water content can be characterized by

$$W_u = \frac{w_u}{w_{tot}} = \frac{A(-T)^B}{w_{tot}} \qquad \text{Equation } 2-51$$

Where T = the temperature (^{o}C);

w_u = the gravimetric unfrozen water content;

W_u = the fraction of the unfrozen water content;

w_{tot} = the total gravimetric moisture content; and

A , B = constants.

The frost heave can then be calculated as

$$H_f = n\int_0^a (1 - W_u)dx \qquad \text{Equation } 2-52$$

Where n = porosity of soil;

H_f = frost heave (m); and

All other parameters are as before.

The unfrozen water content parameter is redefined as follow: $A_l = A/w_{tot}$, and the distribution of W_u with depth in the frozen fringe x is

$$W_u = A(-T)^B = A[-(T_l - T_{ff})(1 - x/a) - T_f]^B \qquad \text{Equation } 2-53$$

After integration, the frost heave can be calculated using Equation 2-54

$$H_f = n\,a\,\frac{1 + A\{(-T_f)^{1+B} - (-T_l)^{1+B}\}}{(1+B)(T_{ff} - T_l)} \qquad \text{Equation } 2-54$$

The frost heave rate can be obtained from Equation 2-55.

$$\frac{LdH_f}{dt} = L\left(\frac{dH_f}{da}da\frac{da}{dt} + \frac{\frac{dH_f}{dT_l}dT_l}{dt}\right) = (Q_{ff} - Q_u) \qquad \text{Equation } 2-55$$

Where Q_{ff} = heat flux through frozen fringe (W/m^2);

Q_u = heat flux through unfrozen zones (W/m^2); and

All other parameters are the same.

By comparison with a numerical solution, the assumptions of linearity of the temperature profile can be checked. The results of the finite difference calculation and the comparison with the approximate analytical solution are displayed in Figure 2-9. Also the model was used for different kinds of soil and the comparison between the predicted and observed laboratory results was made as shown in Figure 2-10 for one of the cases.

Fowler and Krantz (Fowler and Krantz ,1994) developed a generalized model for the secondary frost heave. In order to simplify the governing model's equations, dimensional analysis techniques (i.e. normalization and scaling) were used and a new dimensionless parameter was introduced. The model could predict the thickness of ice lenses. It was also shown that the thickness of the frozen fringe initially starts to increase then it reaches a steady state. The results were in good agreement with experimental data based on a step freezing process. The model is also capable of being extended to incorporate the solute effects on the freezing temperature and the unsaturated soils effects in the secondary frost heave.

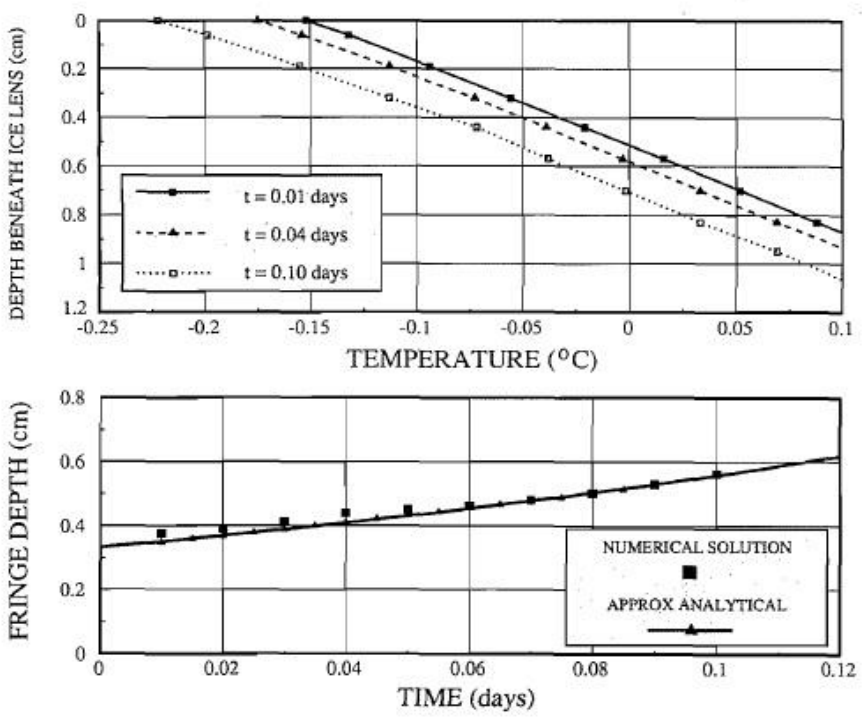

Figure 2-9 Numerical verification of linear temperature profile assumption. T = + 2.7^{O}C at sample base, cooling rate = 0.84^{O}C/day, sample height = 10 cm, initial lens temperature = - 0.14"C, A = 0.05, B = 0.5, W = 20%, and initial freezing point = - 0.04^{O}C, (Nixon,1991)

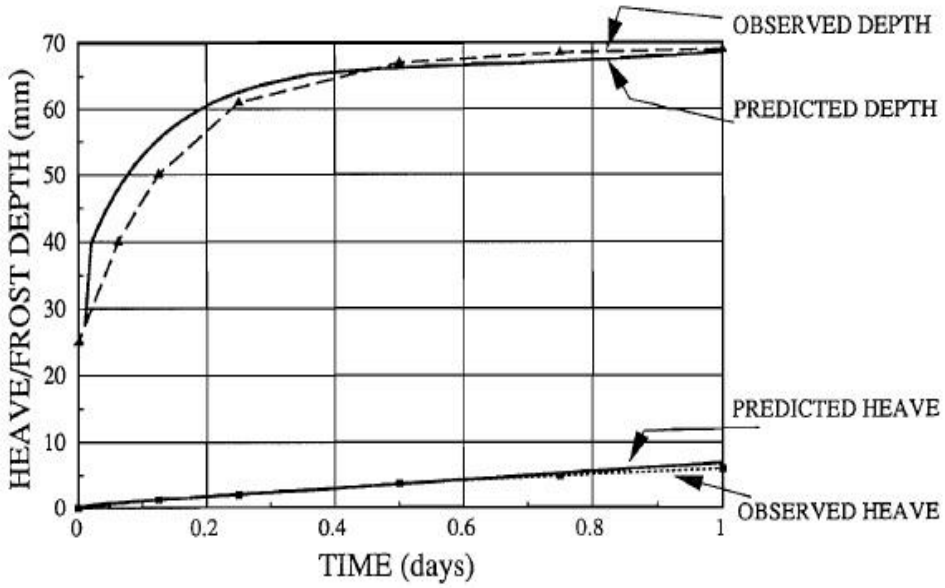

Figure 2-10 Predicted and observed heave for Konrad test No. 4 (Nixon, 1991)

Konrad and Morgenstern (Konrad and Morgenstern, 1980) proposed a semi empirical model to solve the mass and heat transfer. The model is based on two assumptions. The first is zero overburden pressure, which implies that the weight of the overlying soil can be ignored and the second, Clapeyron equation at the base of the ice lens is valid.

$$P_w = \frac{\rho_w L}{T_m}(T - T_m) = MT_l^* \qquad \text{Equation } 2-56$$

$$In\ term\ of\ total\ head;\ H_w = \left(\frac{P_w}{\gamma_w}\right) + h_e \qquad \text{Equation } 2-57$$

$$Neglecting\ the\ elevation\ head\ yields;\ H_w = \left(\frac{P_w}{\gamma_w}\right) = \left(\frac{M}{\gamma_w}\right) T_l \qquad \text{Equation } 2-58$$

Where $T_l^* = T - T_m$(^{o}C);

M= constant;

h_e = elevation head (m);

H_w= total head (m);

T_l = is the temperature at the bottom of the frozen zone (the top of the frozen fringe) which depends on the soil type (^{o}C); and

All other parameters are as before.

Assuming Darcy law is valid and considering a two layered system consisting of unfrozen soil of thickness $l_u(t)$ having hydraulic conductivity k_u and a frozen fringe thickness d(t) with the overall hydraulic conductivity $\overline{K_f}(t)$, the velocity of water movement can be attained using Equation 2-59.

$$v(t) = \frac{|H_w(t)|}{\frac{l_u}{K_u} + \frac{d(t)}{\overline{K_f}(t)}} \qquad \text{Equation } 2-59$$

Where $l_u(t)$ = unfrozen soil of thickness (m);

k_u= hydraulic conductivity in unfrozen zone (m/s);

$\overline{K_f}(t)$= overall hydraulic conductivity of frozen fringe (m/s);

$d(t)$ = frozen fringe thickness (m);

$v(t)$= water flow velocity (m/s); and

All other parameters are as before.

At last, the integration of heave rate over the duration of freezing yields the total heave $h_s(t)$ as stated in Equation 2-60.

$$h_s(t) = \int_0^t \frac{dh_s}{dt} dt = 1.09 \int_0^t v(t) dt \qquad \text{Equation } 2-60$$

For one dimensional heat flow the above Fourier equation can be written as

$$\frac{\partial}{\partial z}\left(k \frac{dT}{dz}\right) + Q = C \frac{\partial T}{\partial t} \qquad \text{Equation } 2-61$$

where C = volumetric heat capacity (J/m^3^{o}C);

k = thermal conductivity (W/ (m.^{o}C);

Q = internal heat generation term per unit area and per unit time (W/m^2); and

All other parameters are as before.

By solving the coupled heat and mass flow, heave can be calculated. The T_l and $\overline{K_f}(t)$ are physical parameters of the soil that can be determined in the laboratory and must be known in order to use equations 2-56 to 2-61.

In another development, Konrad and Morgenstern introduced the concept of segregation potential (SP). They conducted a simple linear analysis based on the following three assumptions

1- Clapeyron equation is valid at the ice lens base.
2- Water flows continuously with an overall hydraulic conductivity in frozen fringe.
3- The temperature (T_l) at the top of the frozen fringe measured in the laboratory for certain soil type is the same as that in the field. This temperature is called segregation temperature.

The results of their analysis indicate that when the temperature of the warm-side of a soil sample is held constant and the other side freezes under various freezing temperatures, the water intake flow toward the ice lenses (heave rate) increases linearly as the temperature gradient increases. The slope of such linear line is called segregation potential (SP) which can be expressed as:

$$V_H = SP\ \Delta T \qquad Equation$$

Where ΔT = the temperature gradient in the frozen fringe (^{o}F/in);

SP = segregation potential (in^2/(day. ^{o}F)); and

All other parameters are the same.

They also conducted laboratory test in order to evaluate the theory. Their laboratory results were consistent with the theory (Konrad and Morgenstern, 1981).

Nixon 1991, stated that the segregation potential theory published by Konrad and Morgenstern (Konrad and Morgenstern, 1981) address the velocity of the migrating water toward the freezing front and temperature gradient in the frozen fringe. He stated that "the velocity of water arriving at an advancing frost front is related to the temperature gradient in the frozen soil just behind the frost front".

However this theory is fully empirical therefore laboratory test are needed to be done to find the segregation potential in each soil type under different field conditions. Also, since laboratory and field conditions are not necessarily based on the same physical conditions, the predictions might not be fully reliable (Gilpin, 1982).

Additionally, Konrad and Morgenstern investigated the effect of the overburden pressure on the frost heave rate. They concluded that

1- As the overburden pressure increases, the segregation temperature decreases.
2- Increasing the overburden pressure causes decreases in the unfrozen water content and consequently decreases in permeability. They reported that 400kPa overburden pressure causes 25 percent decrease in the permeability relative to zero overburden pressure.
3- Decreases in segregation temperature lead to lager frozen fringe.
4- Increasing overburden pressure causes decreases in the heave rate. The reason is that increases in the overburden pressure cause decreases in the overall permeability and decreases in the suction pressure to move water toward the frozen front.

They also, investigated the concept of "shut-off pressure" at which no water will flow into or out of the soil. This concept is controversial, some researchers showed that such pressure can be found in different soil in laboratory conditions and water is drawn to the freezing front in pressures less than the shut-off pressure and expelled from the frost front as the pressure exceeded the shut-off pressure. Others believe that given a sufficient freezing time, the water expulsion could be followed by water intake again.

Konrad and Morgenstern also pointed out that because frozen fringe is relatively large in the field and frost penetration rate is small it is reasonable to assume that the T_f/dt is zero. Applying this condition in laboratory, they developed an equation for SP and for different overburden pressure (P_{OB}) as follows:

$$SP = a\exp(-bP_{OB}) \qquad Equation\ 2-62$$

Where a and b = statistical constants that can be obtained by modeling the data obtained from laboratory tests; and

All other parameters are the same as before.

Gilpin (Gilpin, 1982) tried to relate the SP approach to his model (Gilpin, 1980). This model gave a physical foundation to the empirical model. He introduced a dimensionless segregation potential (DSP) as follows:

$$DSP = \frac{L\, V_H}{\vartheta_i K_{ff}(T_l - T_f)} \qquad \text{Equation } 2-63$$

Where *DSP*= dimensionless segregation potential; and

All other parameters are the same as before

Then, he used Equation 2-63 and d laboratory data to obtain the constant values in the following two equation forms

$$DSP = C_1(P_{OB} + P_{sep} - P_{Lf})^{-\alpha} \qquad \text{Equation } 2-64$$

$$DSP = C_2 \exp\left[\frac{-\left(P_{OB} - P_{Lf}\right)}{P_{sep}}\right] \qquad \text{Equation } 2-65$$

Where all parameters are the same as before

The results indicated that the correlation coefficients are approximately the same (0.97) for both forms, so either one of them could be used for the calculation of DSP.

The segregation potential applicability was investigated by some researchers (Nixon, 1982; Hayhoe and Balchin, 1990). Nixon installed two circular frost heave test plates at Foothills Pipe Lines test facility in Calgary, Canada and compared the measured data to the calculated ones. The SP values were obtained from laboratory data. The water intake at the bottom of ice lens was calculated using the following equation

$$V_{ff} = SP\ grad\ T \qquad \text{Equation } 2-66$$

Where V_{ff}= the velocity of water flow in the frozen fringe (mm/s);

SP= segregation potential ($mm^2/(s.^oC)$) and;

grad T= the temperature gradient in the frozen fringe ($^oC/mm$).

The total heave was then estimated the following three equations:

$$\Delta h_{total} = \Delta h_s + \Delta h_i \qquad \text{Equation } 2-67$$

$$\Delta h_s = 1.09 * V_{ff} * \Delta t \qquad \text{Equation } 2-68$$

$$\Delta h_i = 0.09 * n * H \qquad \text{Equation } 2-69$$

Where Δh_{total}= total frost heave (mm);

Δh_s= frost heave due to water intake (mm);

Δh_s= frost heave due to in-situ pore water freezing (mm);

Δt= time interval (s);

n= soil porosity; and

H= frost depth (mm).

The results were in relatively good agreement with the measured data in the field (Nixon, 1982). Hayhoe and Balchin (Hayhoe and Balchin, 1990) used field data in Ottawa, Canada and segregation potential approach to calculate the frost heave. Their data showed that SP could depend on time because of the change in soil properties with depth. However assuming a fixed value for SP, the estimated heave values were in relatively good agreements with the field data.

Han and Goodings (Han and Goodings, 2006) investigated the differences between clay and silt freezing behavior due to lower hydraulic conductivity and higher water content of the saturated clay. They used a geotechnical centrifuge in order to observe the behavior of the soil. They found that in the unfrozen zone, consolidation occurs due to water migration toward the frozen zone. This consolidation reduced the total heave. The results of their tests indicated that, as for other soil type, the heave in clay decreases with increasing overburden pressure. They also found that due to the low hydraulic conductivity of the clay, its low the water content effect heave more than the ground water level (GWL). In other words, due to low hydraulic conductivity, it requires long time for water to migrate from the GWL toward the frozen zone. Therefore freezing in clay appears to be a close system and the immediate accessible supply of water has more effect than the GWL. Further, they developed a simple analytical model (see Equation 2-70) based on using consolidation concept for 100% saturated soils.

$$\Delta H = \left(\frac{0.09 e_f}{1 + 1.09 e_f}\right) * H_f \qquad \text{Equation } 2-70$$

Where ΔH= heave (mm);

H_f= frost depth including heave (mm); and

e_f= final void ratio in the frozen fringe.

For the case where saturation falls below 100% during the freezing the heave can be estimated as follows

$$\Delta H = \left[\left(\frac{1.09e_f - S_{rf}e_i}{S_{rf} + 1.09e_f}\right) - \left(\frac{e_f - e_i}{1 + 1.09e_f}\right)\right] * H_f \qquad \text{Equation } 2-71$$

Where S_{rf}= degree of saturation in the frozen zone,

e_i= initial void ratio.

2.2.3 Frost Pressure

The magnitudes of heave pressure and heave caused by frost action vary from one scenario to another and they are function of water availability, soil type, overburden pressure, below freezing temperatures and the duration of cold season (Loch and Miller, 1972; Nixon, 1991; Konrad and Morgenstern, 1981). The magnitude of frost pressure highly depends on the particle sizes. In fine sand the pressure is low, whereas it is intermediate for silt and high for clay. In fact, the pressure could vary between 420 psf in sand to 6300 psf in clay (Hoekstra, 1969).

For certain design scenario where the frost potential cannot be eliminated, the heave pressure and heave should be accounted for in the design phase of the structure. Therefore, accurate estimation of the magnitudes of frost pressure and frost heave are essential part of the design process. The direction of frost heave and frost pressure is parallel to the heat flow direction (Penner and Irwin, 1969). For example under the pavement and bridge foundations, the frozen front advances vertically downward whereas for retaining wall, frost heave progresses vertically and horizontally behind the wall (Andersland and Anderson, 1978). In order to eliminate or decrease frost heave potential, building foundations are typically placed below the frost line. Otherwise, frost will cause upward pressure against the foundation. When the upward pressure becomes higher than the downward pressure (due to the foundation weight and applied load), the foundation will move upward as shown in Figure 2-11a. Behind most retaining structures, the frost pressure is oriented horizontally against the wall as shown in Figure 2-11b. The combination of frost and active earth pressures may cause the wall to slide horizontally along its foundation.

The behavior of frozen soil was of interest in the past century, particularly after the ground freezing techniques were developed. Vialov (Vialove 1965) was the first one who investigated the viscoelastic behavior of frozen soil comprehensively. The viscoelastic behavior is especially important in the estimation of creep in artificial ground freezing (Lackner et al., 2008; Klein, 1981). Estimation of frost pressures and relaxation is of interest in cold-regions

tunnel design. Klein (1981) developed a finite element time dependent model for investigating the behavior of temporary frozen earth support system in tunneling. Lai et al. (2000) used numerical inversion of Laplace transform for calculating forces and lining stress in tunnels. They assumed elastic-viscoelastic behavior for the frozen rock and used Poyting-Thomson model for illustrating the viscoelastic behavior in their model. Yuanming et al. (2005) assumed that the frozen soil is nonlinear elastic- plastic isotropic body and developed a finite element model for estimating the frost heaving pressure along a pile of a land bridge in china. Unfortunately, none of the mentioned researches conducted laboratory or field testing to evaluate their results.

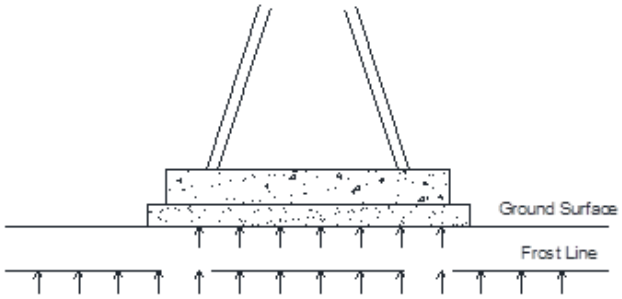

(a)

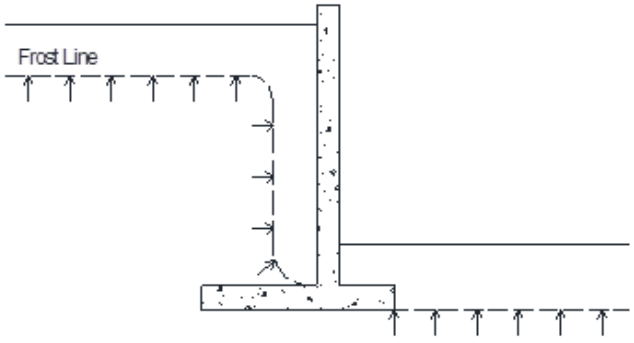

(b)

Figure 2-11 Frost action under foundation causing uplift pressure and behind retaining structure causing horizontal pressure

In field, there are different complications in estimating frost pressure. The pressure could be different when the amount of free water is different or when the level of homogeneity is different. Sometimes the ice penetrates along the cracks and fissure instead of through the pores

which results in lower frost pressures (Penner and Irwin, 1969). Different researchers reported measurements of frost pressure in different conditions and for different soil types. (Penner 1969; Penner and Gold 1971; Kinosita 1967). Kinosita measured frost pressure both in field and laboratory conditions. His results showed decrease in frost pressure when the frost depth penetration stops or slows down in the cycles of freeze and thaw. He assumed that the decrease is because of viscoelastic behavior of frozen soil; i.e. stress relaxation.

The results of field testing showed the following equation for decrease in frost force after a stop in frost penetration:

$$F = F_0(at + 1)^{-n} \qquad Equation\ 2-72$$

Where F_0= the force at the time of stoppage (Kg);

t= time from frost penetration stoppage (hr);

a and n= constants that can be obtained from experiments ; for temperature of -4^{o}C a and n are 35 hour^{-1} and 1/6, respectively.

By assuming a viscoelastic relationship between frost heave rate and force, he also suggested the following equation for estimation of frost heave force:

$$F(t) = \frac{Cb}{a(1-n)}\left\{1 - \frac{at(2n-1)+1}{(at+1)^n}\right\} \qquad Equation\ 2-73$$

Where b= constant frost heave rate;

C= constant; and

all other parameters are the same as before.

His laboratory results also showed that frost heave and frost pressure have very similar trend.

2.3 Thaw Depth and Seasonal Load Restrictions

This section consists of review of the literature regarding the thaw depth during spring season and the load restriction models.

2.3.1 Thaw Depth

With the assumptions of no heat transfer in the frozen zone and a linear temperature distribution in the thawed zone, to estimate the thaw depths over time, Stefan simplified Neumann's equation as follow (Jiji, 2009):

$$X = \sqrt{\frac{2k_u T_s}{\rho l}}\, t \qquad \text{Equation } 2-74$$

Where X= thaw depth (m);

t= time since the thawing starts (s);

k_u= thermal conductivity of the unfrozen soil (W/ (m.^{o}C);

T_s= applied constant surface temperature (^{o}C);

l= latent heat of fusion (J/Kg); and

ρ= density (Kg/m^3).

Nixon and McRoberts (Nixon and McRoberts, 1973) modified the Stefan solution for multi layered systems. They considered a two layered system, the first layer with the depth of H and thermal conductivity of k_1 and volumetric latent heat of L_1 overlying the second layer of soil with thermal conductivity of k_2 and volumetric latent heat of L_2. They calculated the time to thaw the upper layer completely using Equation 2-75. Re-arranging Equation 2-75 yields Equation 2-76. The product $t_0 T_s$ in the last equation is defined as the cumulative thawing degree day (CTDD) that is required to completely thaw the first layer. Further, they estimated the thaw depth for the second layer using Equation 2-77.

$$t_0 = \frac{H^2 L_1}{2k_1 T_s} \qquad \text{Equation } 2-75$$

$$t_0 T_s = CTDD = \frac{H^2 L_1}{2k_1} \qquad \text{Equation } 2-76$$

$$X = [(\frac{k_2}{k_1} H)^2 + 2\frac{k_2}{L_2} Ts(t - t_0)]^{1/2} - \left(\frac{k_2}{k_1} - 1\right) H \qquad \text{Equation } 2-77$$

Where the subscript 1 refers to the first layer;

t_0 = time to thaw the overlying layer (hr);

H = thickness of the first layer (ft);

L = volumetric latent heat of fusion (Btu/ft^3);

k = thermal conductivity (Btu/ft hr °F) ; and

T_s = the mean surface temperature during the thawing period (°C).

X= the thaw penetration depth (ft);

the subscripts 1 and 2 refer to first and second layer, respectively; and

All other factors are as before.

Thus, the estimation of thaw depths using Equations 2-75 through 2-77 requires knowledge of the thermal conductivity and latent heat of fusion of the soil. Since these inputs are

not always available or expensive to collect, average values are typically used in the calculations of frost depths.

2.3.2 Seasonal Load Restriction

A typical pavement structure consists of two or three layer system depending on the pavement class. The thicknesses of these layers vary substantially from one road class to another. For all Interstate and primary roads, the thicknesses of the layers are designed and constructed to provide adequate protection of the roadbed soil against freezing. Such protection is not provided for the majority of the secondary roads including most county roads, city streets and farm-to-market roads. During the winter season, available water in the pavement structure freezes creating ice lenses and causing increases in the stiffness of the various pavement layers. Over the winter months, the ice lenses grow in volume due to migration of water from the ground water table toward the freezing front. The growth of ice lenses causes the pavement to heave. During spring season, the frozen ice lenses melt from the top due to warmer temperature and from the bottom due to the internal heat of the earth. Melted water at the top of the ice lenses cannot drain by gravity because of the impermeable ice. Hence, the water from the melted ice saturate the pavement layers especially the upper portion of the roadbed soil. This causes substantial softening of the roadbed soil. It is at this critical time, the damage delivered by the traffic load increases substantially causing the well- known spring break-up of the pavement structures. To minimize this damage and to extend the life of the pavement structures, most highway authorities post seasonal load restriction (SLR) signs. The SLR causes hardship to the trucking industry and increases the number of trucks on the road. Thus, accurate knowledge of the time when the SLR signs should be posted and removed is crucial to the road owners and the road users. Such timely posting and removing the SLR signs cannot be had unless accurate prediction of frost and thaw depths as a function of time can be accomplished. In addition, accurate prediction of freeze-thaw cycles is critical to an effective load restriction approach (Ovik et al., 2000).

Several SLR models were developed to estimate the time for posting and removing the SLR signs. Some of these models and are being used by some State Highway Agencies. Three of these models are presented below.

- **Minnesota Seasonal Load Restriction Policy**

For the placement and removal of SLR signs, The Minnesota Department of Transportation (MnDOT) developed a method and policy based on the cumulative thawing degree days (CTDD)

and the cumulative freezing degree days (CFDD) (MnDOT, 2009). The MnDOT procedure for the calculation of the CFDD and CTDD is summarized in a flowchart format shown in Figure 2-11.

The decision to post and remove the SLR signs is based on the results of the calculation of the CFDD and CTDD and the corresponding reference temperatures listed in Table 2-1. The reference temperature accounts for the effect of the duration and intensity of the sun radiation on the pavement thawing. The MnDOT's SLR policy divides the state into six zones. The SLR is posted when the 3-day weather forecast shows that the CTDD for a given zone is more than 25 ^{o}F-degree day and the continued warmth is predicted for longer time period.

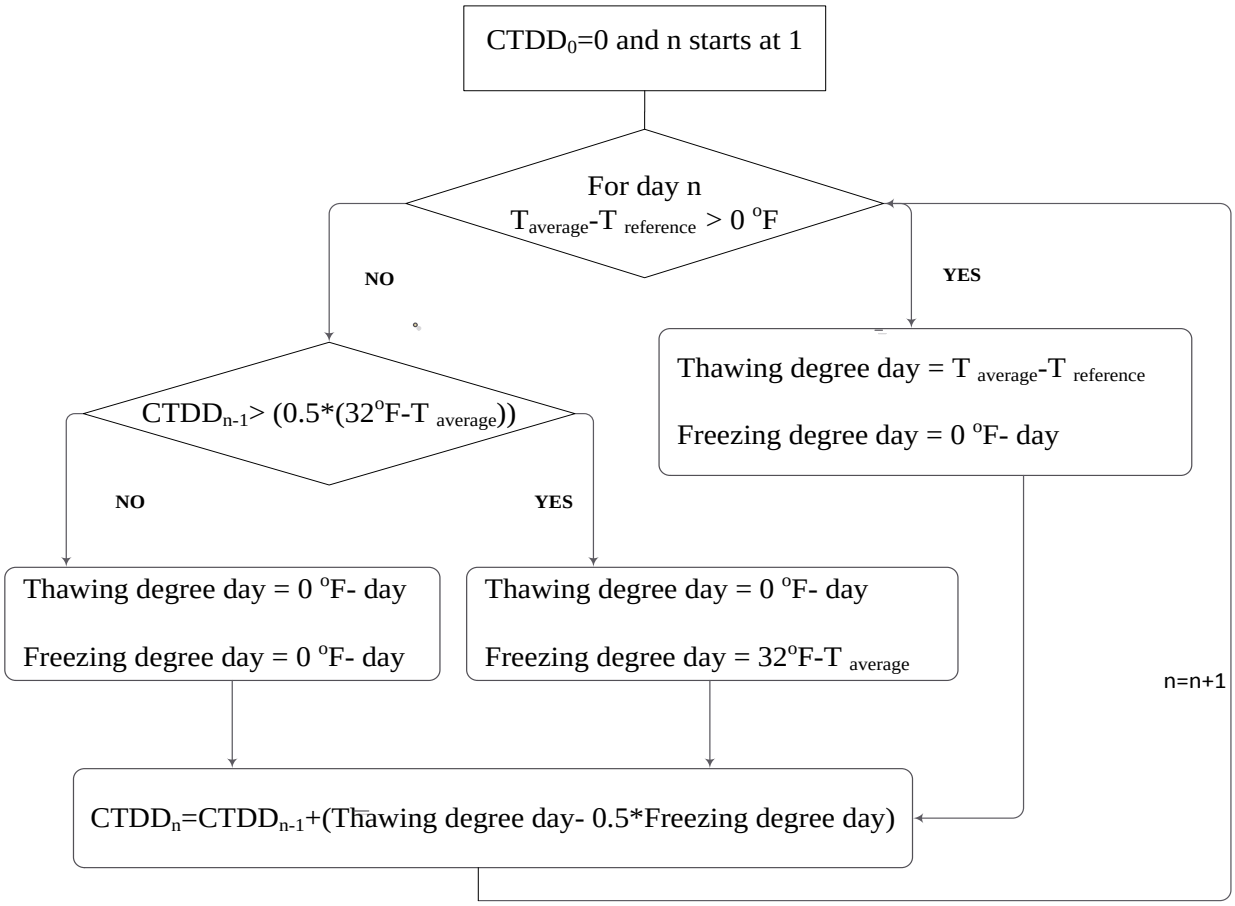

Figure 2-12 MnDOT CDTT calculation flowchart. In this flowchart $CTDD_n$ is the cumulative thawing degree day calculated over 'n' days , $CTDD_{n-1}$ is the cumulative thawing degree day calculated over 'n-1' days, $T_{average}$ is the daily average air temperature ($(T_{max}-T_{min})/2$) and the $T_{reference}$ is the reference temperatures listed in Table 2-1

Table 2-1 Reference temperature

Date	Reference Temperature (^{0}F)
January 1 – January 31	32
February 1 – February 7	29.3
February 8 – February 14	28.4
February 15 – February 21	27.5
February 22 – February 28	26.6
March 1 – March 7	25.7
March 8 – March 14	24.8
March 15 – March 21	23.9
March 22 – March 28	23
March 29 – April 4	22.1
April 5 – April 11	21.2
April 12 – April 18	20.3
April 19 – April 25	19.4
April 26 – May 2	18.5
May 3 – May 9	17.6
May 10 – May 16	16.7
May 17 – May 23	15.8
May 24 – May 30	14.9
June 1 – December 3	32

- **Wisconsin Restriction Policy**

Wisconsin Department of Transportation (WisDOT) has been using the SLR policy which was developed by Washington Department of Transportation. In this policy, the CTDD is calculated using Equation 2-78 (WisDOT, 2003)

$$CTDD_n = \sum_{i=1}^{n} Thawing\ degree\ day \qquad Equation\ 2-78$$

$$Thawing\ degree\ day = \left(\frac{T_{max}+T_{min}}{2} - T_{reference}\right) \qquad Equation\ 2-79$$

Where T_{max}= maximum daily air temperature;

T_{min} = minimum daily air temperature; and

$T_{reference}$ = 29°F.

Since various temperature measurements indicated that during the thawing period, the asphalt pavement surface temperature is 32°F when the air temperature is about 29°F, the reference temperature was set at 29°F.

Table 2-2 provides a list of Wisconsin's seasonal load restriction policy for thin and thick pavements. The posting of the SLR signs are based on the two levels listed in Table 2-2; should and must is placed when the 5-day weather forecast shows that the CTDD will reach the "should be posted or the must be posted" levels. The CTDD value for each level and pavement type is listed in Table 2-2.

Table 2-2 CTDD threshold for posting SLR

Pavement Structure	**CTDD**	
	"Should" Level	**"Must" Level**
THIN Asphalt 2" or less Base course 6" or less	10°F- degree day	40°F-degree days
THICK Asphalt more than 2" Base course more than 6"	25°F- degree days	50°F- degree days

Chapter 3

Data Mining

3.1 Data Base

The evaluation of the accuracy of existing frost depths and heave models or the development of new accurate and representative ones require field data that represent the environment and the various pavement structures (Tighe et.al, 2007). Fortunately, such data was available and obtained from the Michigan Department of Transportation (MDOT) and the Minnesota department of Transportation (MnDOT). The following data bases and their sources were used in this study:

1. Road Weather Information System (RWIS) for frost depth data measured in the state of Michigan. It should be noted that the RWIS subsurface sensors do not measure the frost depth directly, they measure the subsurface temperature. In the analyses, it was assumed that the ground water freezes at 32^{o}F.
2. National Oceanic and Atmospheric Administration (NOAA) weather data in the states of Michigan and Minnesota.
3. Minnesota Department of Transportation (MnDOT) database for frost depth measured in the state of Minnesota.
4. Michigan Department of Transportation (MDOT) database for frost heave measured in the state of Michigan.
5. Michigan State University Enviro-weather (MSU-EW) for weather data in the state of Michigan.

3.2 Frost Depth Data

3.2.1 The State of Michigan

RWIS uses different technologies that collect, transmit and publish weather and road condition information. The weather data is collected by the environmental sensor station (ESS). In these stations the sensors collect and transmit weather and pavement data (US DOT, 2002). In general RWIS may encompass:

1. Meteorological sensors for measuring atmospheric pressure, temperature, relative humidity, visibility, wind speed and direction, and precipitation (amount and type)

2. Pavement sensors for measuring pavement temperature and condition (wet, dry, snow), subsurface pavement temperature, the amount and type of deicing chemical used on the pavement surface
3. Pavement temperature and weather condition forecast based on the site (Boselly et al., 1993).

In this project, the RWIS database that was provided by MDOT was used for subsurface pavement temperature data (RWIS, 2012). RWIS consist of 25 stations located throughout the State of Michigan. However, only 18 stations were used (MDOT 2008, MDOT 2009a, and b) in this study due to partially missing data in seven stations. Figure 3-1 shows the stations location in the state of Michigan.

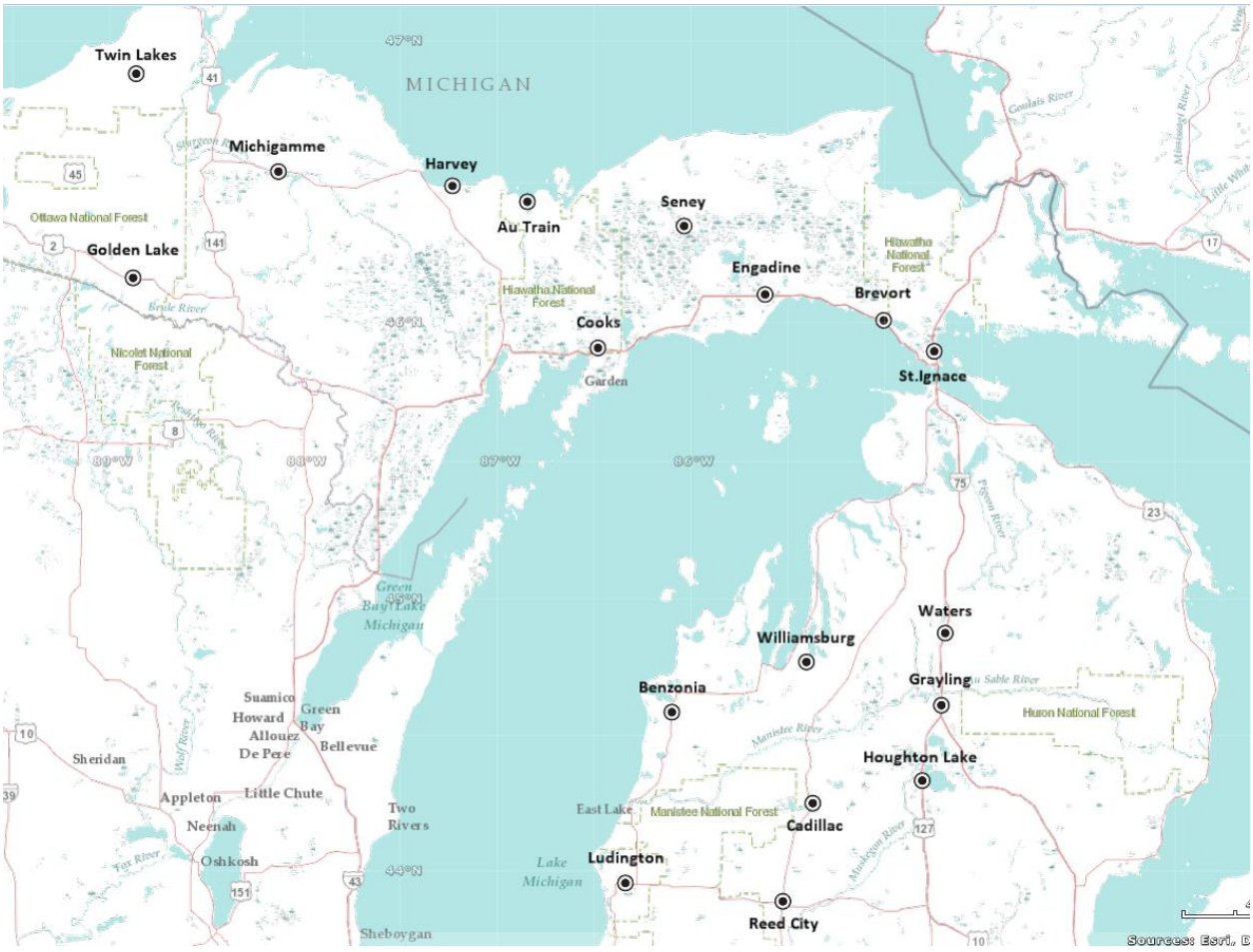

Figure 3-1 RWIS station locations, Michigan

Table 3-1 shows the RWIS stations ID, latitude, longitude and soil type. The detailed soil log for each station was provided by MDOT. In all stations one year data (2010-2011) were available and used except for Au Train, Harvey and Brevort Stations in the UP where two years of data (2009-2010) was available and used.

Table 3-1 RWIS stations in the State of Michigan

Region	Station	Latitude	Longitude	Subgrade Soil (up to 10 ft)
Upper Peninsula	Au Train	46.43	-86.84	Upper 3 Ft Of Sand With Gravel And Silt, Below Which Loose Moist Fine Sand
	Brevort	46.01	-85.01	Loose To Moderately Compact Moist Fine Sand
	Cooks	45.91	-86.48	Silty Clay With Sand
	Engadine	46.10	-85.62	Plastic Moist Sandy Clay
	Golden Lake	46.16	-88.88	Moderately Compact Moist Fine Sand With Gravel
	Harvey	46.49	-87.23	Loose To Moderately Compact Moist Fine To Medium Sand
	Michigamme	46.54	-88.13	Upper 5 Ft Clayey Sand,5 Ft And Below Wet Find To Medium Sand With Silt
	Seney	46.35	-86.04	Loose Moist To Wet Sand
	St. Ignace	45.90	-84.74	Silty Clay With Sand
	Twin Lakes	46.88	-88.86	Loose Moist Fine To Medium Silty Clayey Sand
Lower Peninsula	Benzonia	44.59	-86.10	Very Loose Fine To Medium Sand
	Cadillac	44.25	-85.37	Medium Compact Fine Sand
	Grayling	43.89	-85.53	Fine To Coarse Sand With Gravel
	Houghton Lake	44.77	-85.40	Loose To Medium Compact Fine Sand
	Ludington	45.36	-85.18	Very Loose Silty Sand With Trace Clay
	Reed City	44.61	-84.71	Loose To Medium Fine Sand With Trace Gravel
	Waters	44.33	-84.81	Medium Compact To Loose Fine Sand With Trace Gravel
	Williamsburg	45.76	-84.73	Medium Compact Fine Sand With 1.5 Ft Of Silty Clay

As mentioned before the RWIS collect meteorological as well as surface and subsurface pavement temperature data. The data were collected approximately every 10 minutes. The RWIS data were provided by MDOT and processed by the research team in order to be used in the study. Figure 3-2 depicts a soil profile showing the locations of temperature sensors at a typical RWIS station. The data were then used to develop a GIS contour map of maximum frost depth in a typical year in Michigan as shown in Figure 3-3.

Unfortunately the meteorological data were not available for the whole 2010-2011 winter. Therefore the NOAA and/or the MSU-EW weather data were used in the analyses (MSU-EW, 2012; NOAA, 2012). The selected NOAA and/or MSU-EW stations were within 10 miles of an RWIS station, otherwise the RWIS data were not used in the study. Table 3-2 shows the data availability in each database.

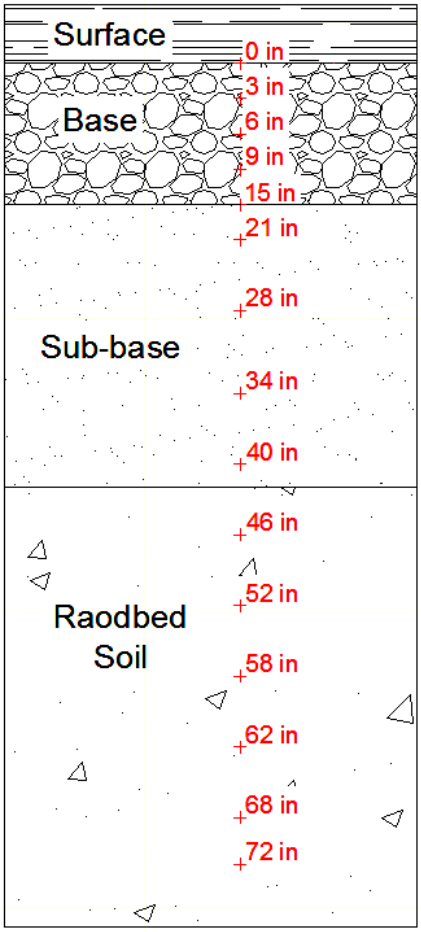

Figure 3-2 A soil profile at a typical RWIS station showing the depths of the temperature sensors

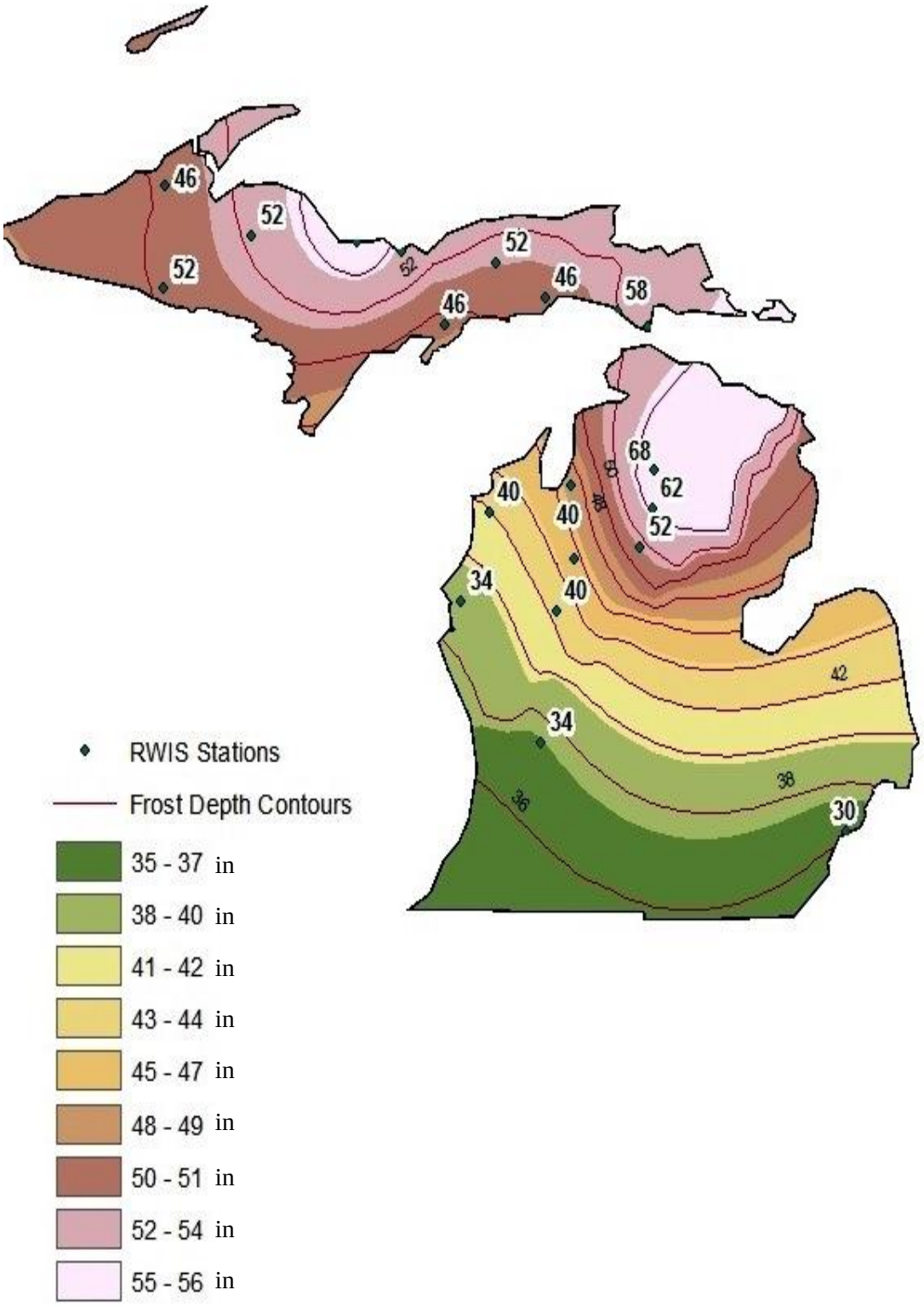

Figure 3-3 Maximum frost depth contours in a typical year in the State of Michigan

Table 3-2 Data availability in each database

Location	RWIS Station Name	Data base	Station Name	Precip.	Temp	Wind Speed	RH	Database	Station Name	Precip	Temp	Wind Speed	RH	Station Name	Temp	Precip.
lower peninsula	Benzonia	MSU-EW	Benzonia	✓	✓	✓	✓	NOAA	N/A	N/A	N/A	N/A	N/A	N/A	N/A	N/A
	Cadillac		McBain	✓	✓	✓	✓		N/A	N/A	N/A	N/A	N/A	N/A	N/A	N/A
	Grayling		N/A	N/A	N/A	N/A	N/A		Graying Army Airfied	✓	N/A	✓	✓	GHCND: USC00203391	✓	✓
	Houghton Lake		N/A	N/A	N/A	N/A	N/A		Roscommon Co.Airport	✓	✓	✓	✓	N/A	N/A	N/A
	Ludington		Ludington	✓	✓	✓	✓		N/A	✓	✓	✓	✓	N/A	✓	✓
	Reed City		N/A	N/A	N/A	N/A	N/A		Roben-Hood Airport	✓	N/A	✓	✓	Big Rapids Waterwork	✓	✓
	Williamsburg		Traverse City	✓	✓	✓	✓		N/A	N/A	N/A	N/A	N/A	N/A	N/A	N/A
	Waters		Gaylord	✓	✓	✓	✓		Gaylord-9 SW	✓	✓	✓	✓	N/A	N/A	N/A
upper peninsula	Michigamme	MSU-EW	N/A	N/A	N/A	N/A	N/A	NOAA	N/A	N/A	N/A	N/A	N/A	N/A	N/A	N/A
	Harvey		N/A	N/A	N/A	N/A	N/A		Sawyer Int. Airport	✓	N/A	✓	✓	Marquette	✓	✓
	Au Train		Chatham	✓	✓	✓	✓		N/A	N/A	N/A	N/A	N/A	N/A	N/A	N/A
	Brevort		McMillan	✓	✓	✓	✓		N/A	N/A	N/A	N/A	N/A	N/A	N/A	N/A
	Engadine		N/A	N/A	N/A	N/A	N/A		Luce County Airport	✓	N/A	✓	✓	Engadine MDOT	✓	✓
	Seney		McMillan	✓	✓	✓	✓		N/A	N/A	N/A	N/A	N/A	N/A	N/A	N/A
	Cooks		N/A	N/A	N/A	N/A	N/A		Schoolcraft Co. Airport	✓	N/A	✓	✓	Garden Corners	✓	✓
	Twin Lakes		N/A	N/A	N/A	N/A	N/A		N/A	N/A	N/A	N/A	N/A	N/A	N/A	N/A
	Golden Lake		N/A	N/A	N/A	N/A	N/A		Kings Land O' Lakes Airport	✓	N/A	✓	✓	STAMBAUGH 2 SSE	✓	✓
	St. Ignace		N/A	N/A	N/A	N/A	N/A		St.Ignace	✓	✓	✓	N/A	N/A	N/A	N/A

3.2.2 The State of Minnesota

In order to evaluate and generalize the frost depth model which was developed using the measured frost depth data in the state of Michigan, the Minnesota frost depth data were requested, received and used in this study. The MnDOT data consisted of 9 years of data (2003 to 2012) collected at 8 stations located throughout the State of Minnesota as shown in Figure 3-4. Similar to the Michigan case, the meteorological database from the nearest NOAA station was obtained and used in the study.

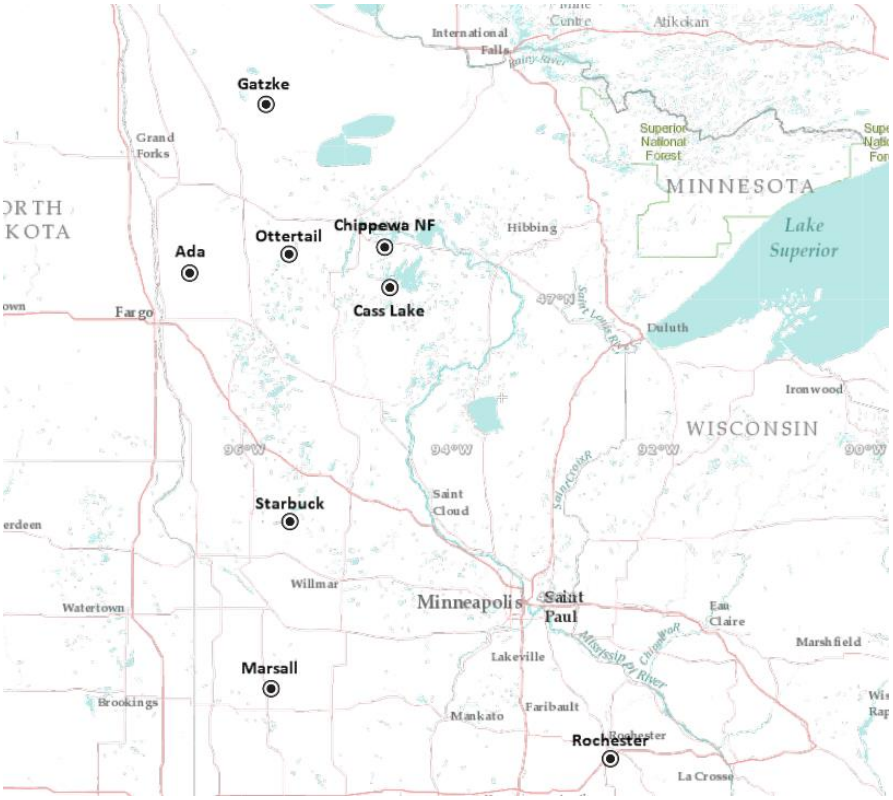

Figure 3-4 MNDOT stations location, Minnesota

3.3 Soil Properties Data

Disturbed soil samples from different RWIS stations in the State of Michigan were provided by MDOT. The thermal properties of the samples were then measured in the laboratory at Michigan State University. Since only disturbed soil samples were received, the insitu dry densities and water contents were unknown. Nevertheless, seven representative soil types were selected and their thermal properties were measured in the laboratory using KD2 pro thermal properties analyzer. The KD2 pro is a small and portable device with the capability of measuring different thermal properties of almost any material. The device has three sensors 6 cm single needle (KS-

1), 10 cm single needle (TR-1), and 3 cm dual-needle (SH-1). Each sensor could be used depending on the required thermal properties and types of the material.

The KS-1 sensor was used to measure thermal conductivity and thermal resistivity. The sensor is most accurate in liquid samples and insulating materials. In liquid samples free convection could be a source of error. Since the sensor applies small amount of heat to needles, free convection could be prevented making KS-1sensor a good choice for liquid samples. On the other hand, in granular samples like soil or powders, contact resistance could be a source of error. Size of the sensor and short heating time could maximize this error making the KS-1sensor a poor choice for these types of materials (Decagon Devices Inc., 2008).

The TR-1 sensor was also used to measure the thermal conductivity and thermal resistivity. TR-1 is a hollow needle and comes with drill bits. The size and relatively longer heating time could minimize the contact resistance error making this sensor the primary choice for soil and granular materials. The sensor complies fully with ASTM D5334-08 specification for measuring the thermal conductivity of soils (Decagon Devices, Inc., 2008).

The SH-1 sensor measures volumetric heat capacity, thermal diffusivity as well as thermal conductivity and thermal resistivity. This sensor could be used in most solid and granular material but not in liquid samples. Tables 3-3 summarize the applicability of each sensor for different materials (Decagon Devices, Inc., 2008).

Table 3-3 Sensor use guide (Decagon Devices Inc., 2008)

Sample Material	KS-1	TR-1	SH-1
Low viscosity liquids (Water)	Best	N/A	N/A
High viscosity liquids (glycerol, oil)	Best	OK	N/A
Insulation and insulating materials	Best	N/A	N/A
Moist soil	N/A	Best	OK
Dry soil, powders, and granular materials	N/A	Best	OK
Concrete and rock	N/A	Best	OK
Other solids	N/A	Best	OK

As stated before, seven types of soil were tested to obtain the required thermal properties. TR-1 and SH-1 sensors were used for measurements (Figure 3-5). In order to minimize the error five measurements were done on each sample as shown in Figures 3-6. The thermal properties of the samples were considered to be the average of these readings. Table 3-4 depicts the measured thermal properties of seven different types of soil in saturated condition. It is noteworthy that all soil samples were disturbed and were not compacted in the laboratory.

Figure 3-5 Thermal conductivity measurement using KD2 pro

As mentioned before, detailed soil log for each RWIS station were available in the State of Michigan. On the other hand, the soils at the State of Minnesota stations were categorized as clayey and sandy soils. Therefore in the model the average values of Table 3-4 for clayey and sandy soils were used for both states.

3.4 Frost Heave Data

Data from 5 sites in Oakland County, Michigan were provided by MDOT (Novak, 1968). The data was collected in the winter of 1962-63 in a six-mile section (EBI 63172, CR5H) along I 75, Figure 3-7 depicts the location of the sites. Table 3-5 shows soil type, the maximum measured frost heave and frost depth under pavement and shoulder and at different stations. The detailed measurements with time can be found in Appendix C.

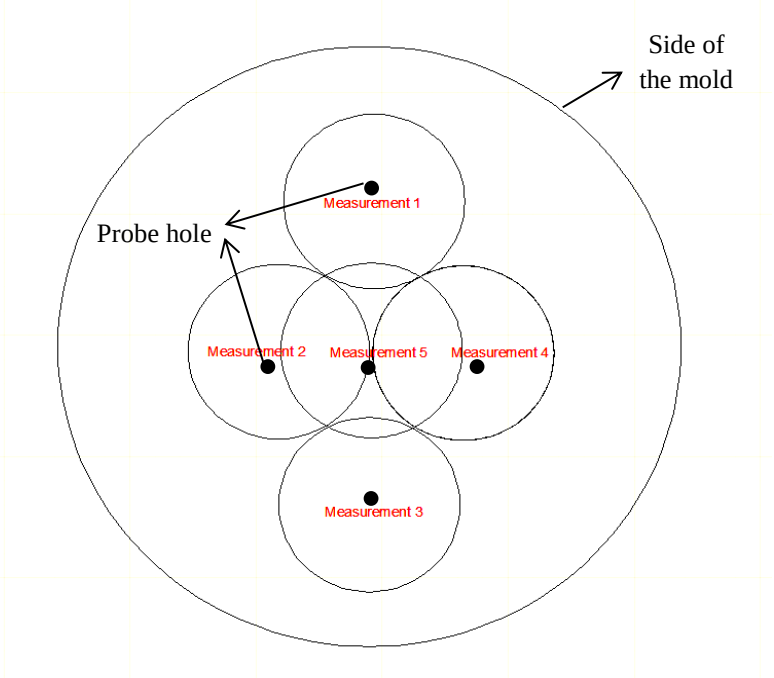

Figure 3-6 Five locations where the soil thermal properties were measured in each soil sample using KD2 pro

Table 3-4 Measured thermal properties of different types of soil using KD2 Pro

Station Name	Material	Moisture Condition	Thermal Conductivity (Btu/(ft.hr.^{o}F))	Heat Capacity (Btu/(ft^{3}.^{o}F))
Houghton Lake	Silty Fine Sand with Trace of Gravel	Saturated	1.49	39.84
	Fine Sand		1.48	42.37
Wolverine	Fine Sand with Trace of Gravel		1.44	40.13
	Fine Sand		1.40	40.13
	Soft Clayey Sandy , Some Silt & Some Gravel		1.01	44.46
Williamsburg	Silty Clay		0.88	46.25
Rudyard	Silty Clay		0.65	47.74

.

It should be noted that for station/528+88 the difference between the measured frost heave under the pavement and under the shoulder is approximately 0.35 inches which is much higher than the other sites. At this site, an undercut of approximately 12 inches was made while constructing the pavement for frost protection.

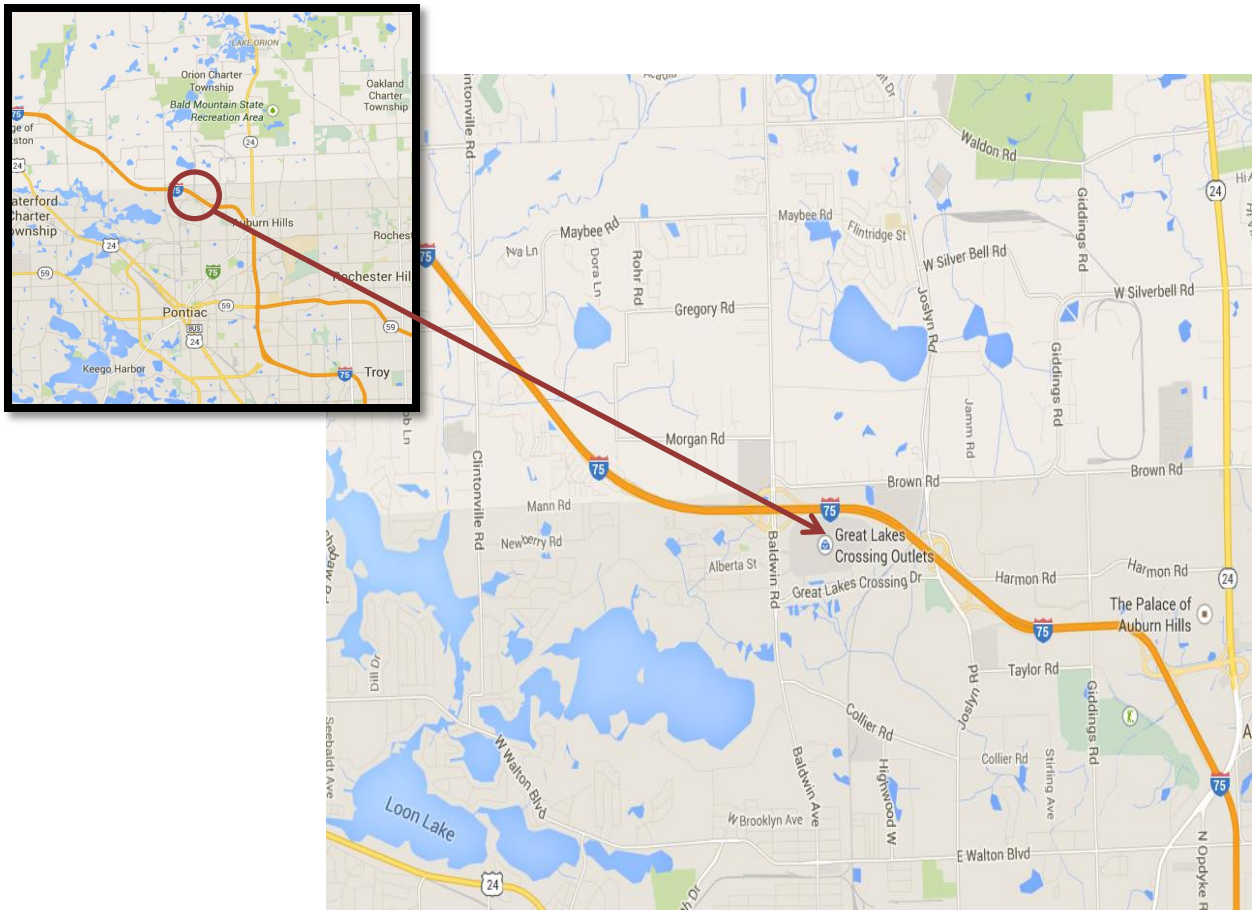

Figure 3-7 MDOT frost heave station locations, Oakland County, Michigan

Table 3-5 Measured total heave and frost depths in different soil types, I75, Oakland County, Michigan

Station Name	Soil Type	Frost depth (in)	Max heave in shoulder (in)	Max heave in pavement (in)	Duration (days)
Sta/724+00	Fine Sand and Silt with Pebbles	24	1	0.75	65
Sta/719+00	Fine Sand with Silt Pockets with Pebbles	28	0.85	0.75	40
Sta/652+00	Insitu Sub Soil Clayey, Silty, Gravely, Sand	34	0.9	0.85	60
Sta/528+88	Sandy Clayey Silt	30	0.75	0.4	70
Sta/474+00	Clayey Silt	25	1	0.9	55

Chapter 4

Analysis and Discussion of Frost Depth and Frost Heave

4.1 Introduction

Existing frost depth prediction models can be classified into numerical, analytical, semi-empirical, and empirical models. Some models require as inputs various thermal and hydraulic properties of soil and different meteorological data. Others require only the freezing index (FI) or the cumulative freezing degree day (CFDD). Any of these models can be used depending on the availability of the input data and the required accuracy. As mentioned in chapter 2, different numerical models were developed in the past three decades. In this chapter, UNSAT-H model was used to predict the frost depth. The results were then evaluated with the field data in Michigan. Furthermore, the accuracy of different analytical and semi-empirical frost depth prediction models including Stefan model (Jiji, 2009), Modified Berggren model (Aldrich et al., 1953) and Chisholm and Phang empirical model (Chisholm and Phang, 1983) were evaluated using the RWIS soil temperature data measured in the state of Michigan. Since none of the models yielded accurate results, revised empirical models that require only cumulative freezing degree day as input were developed. First, the data in the State of Michigan was used to develop an empirical model regardless of the soil types. Further, for model validation the 2003 to 2012 frost depth data from 8 stations in the State of Minnesota were used. Third, by considering the soil types two empirical models were developed for clayey and sandy soils. The two models were also evaluated using the Minnesota frost depth data. Finally, using the thermal conductivity data of each soil type, the two models were combined and one general model was developed which required CFDD and soil thermal conductivity. The accuracy of the general model was also checked using the frost depth data measured in the state of Minnesota.

4.2 UNSAT-H Model

As stated in chapter 2, UNSAT-H is a one dimensional finite difference heat and mass balance model. The model inputs are meteorological data including air temperature, precipitation, solar radiation, wind speed, cloud cover, dew point and soil hydraulic and thermal properties data. The soil can be modeled in different layers in UNSAT-H.

For evaluating the UNSAT-H model, one of the RWIS sites located in the Lower Peninsula of Michigan was chosen. The soil profile corresponding to the site is illustrated in Figure 4-1.

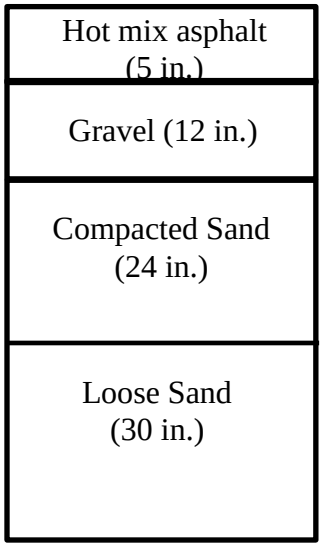

Figure 4-1 Schematic of the cross section of the modeled pavement site

Table 4-1 shows the hydraulic and thermal properties that were used for each layer. Using these properties and the weather data as the boundary conditions, soil temperature profile was estimated. Figure 4-2 shows the estimated and the measured freezing depths as a function of time. It can be seen from the figure that the model predicted the freezing front up to three weeks earlier than the measured front. This indicates that the model over predicts the freezing depth. In fact, the differences between the measured and the calculated frost depth could be as high as 10 inches. One main reason for the unfavorable results could be the unavailability of the proper input properties. That is the use of the estimated input properties contributed to the discrepancy between the estimated and the measured data. Unfortunately, the required input data are not available and are expensive to collect. Therefore, using this model at the state level may not be economically justified.

Table 4-1 Hydraulic and thermal properties for different layers in UNSAT-H model

Material	**θ_r**	**θs**	**α**	**Ks (cm/sec)**	**n**	**m (1-1/n)**	**Thermal Conductivity (W/m-K)**	**Volumetric Specific Heat (kJ/m^3-K)**
Asphalt	0.070	0.360	0.0050	5.60E-08	1.090	0.08257	3.9	2
Gravel	0.005	0.420	1.0000	1.00E+01	2.190	0.54338	1.25	1.36
Sand	0.020	0.375	0.0431	4.63E-01	3.100	0.67742	1.5	2.39

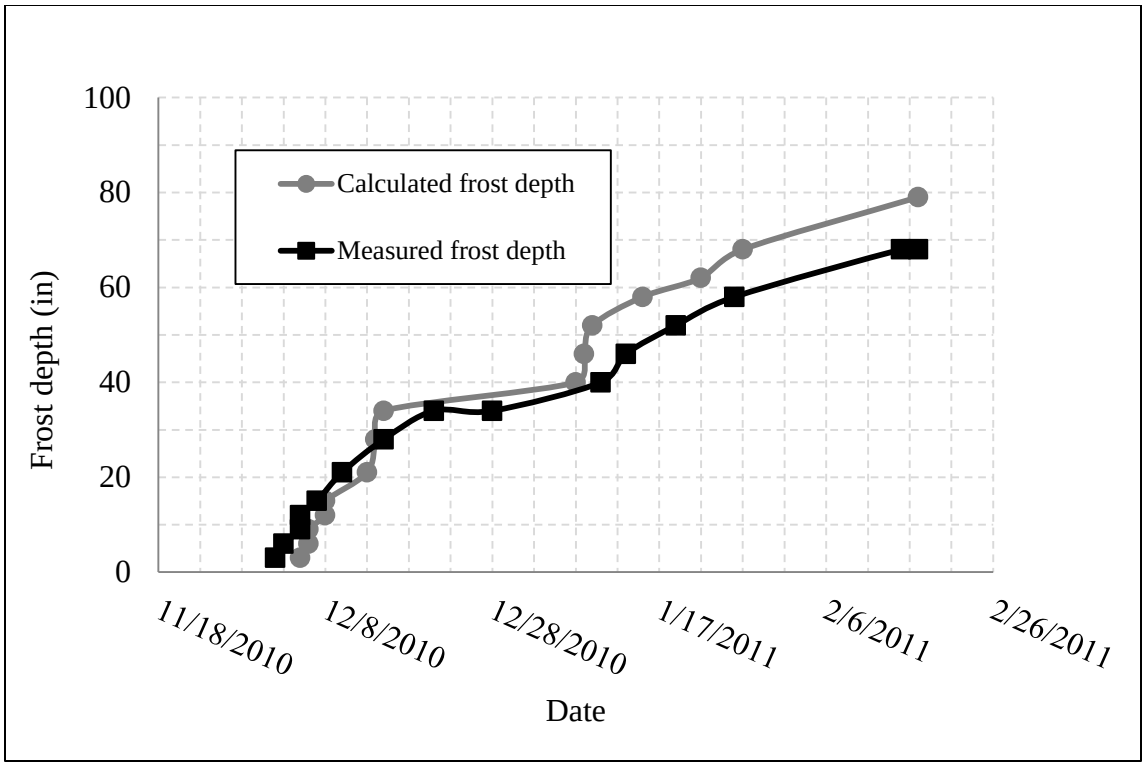

Figure 4-2 Calculated frost depth using UNSAT-H model and measured frost depth versus time in a RWIS station, Lower Peninsula, Michigan

4.3 Freezing Index and Freezing Degree Day Calculation

One of the common inputs to most analytical and semi-empirical models is the freezing index or the cumulative freezing degree day. Two different methods have been considered for calculating the cumulative freezing degree day; the Minnesota method (MnDOT, 2009) and Boyd method (Boyd, 1976).

4.3.1 Minnesota Cumulative Freezing Degree Day

The cumulative freezing degree day (CFDD) was calculated using Equation 4-1 (MnDOT, 2009):

$$CFDD_n = \sum_{i=1}^{n} Freezing\ Degree\ Day\ \leq\ 0 \qquad \text{Equation } 4-1$$

$$\text{Freezing Degree day} = \left(\frac{T_{max}+T_{min}}{2} - 32^{o}F\right) \qquad \text{Equation } 4-2$$

Where T_{max} = Maximum daily air temperature (°F); and

T_{min} = Minimum daily air temperature (°F).

It should be noted that in the Minnesota method, the cumulative freezing degree day is reset on July 1 of each year and the freezing index is the maximum CFDD at the end of the winter season. Table 4-2 lists an example calculation of the cumulative freezing degree day.

Table 4-2 Cumulative freezing degree day calculation, Waters station, Lower Peninsula

Date	Average Air Temperature (^{o}F)	Freezing Degree day (FDD) (^{o}F-day)	Cumulative freezing degree day (CFDD) (^{o}F-day)	Absolute Cumulative freezing degree day (CFDD) (^{o}F-day)
11/16/2010	42.44	10.44	0	0
11/17/2010	37.76	5.76	0	0
11/18/2010	30.29	-1.71	-1.71	1.71
11/19/2010	30.65	-1.35	-3.06	3.06
11/20/2010	29.75	-2.25	-5.31	5.31
11/21/2010	35.15	3.15	-2.16	2.16
11/22/2010	50.99	18.99	0	0
11/23/2010	39.47	7.47	0	0
11/24/2010	27.86	-4.14	-4.14	4.14
11/25/2010	27.77	-4.23	-8.37	8.37
11/26/2010	20.48	-11.52	-19.89	19.89
11/27/2010	28.49	-3.51	-23.4	23.4
11/28/2010	29.93	-2.07	-25.47	25.47
11/29/2010	34.07	2.07	-23.4	23.4
11/30/2010	38.75	6.75	-16.65	16.65

4.3.2 Boyd Cumulative Freezing Degree Day

If the CFDD is calculated and plotted as a function of time as shown in Figure 4-3, the graph will have a minimum value in the fall and a maximum value in spring. The Freezing Index (FI) for that winter is estimated as the difference between the maximum and minimum cumulative degree days as shown in the figure (Boyd, 1976).

Any spring or fall month that includes a seasonal maximum or a seasonal minimum degree days is called a "changeover" month. Boyd (1976) proposed that Equation 4-3 can be used for calculating the cumulative freezing degree day in the change-over month:

$$Y^2 + N * X * Y = N^2 k^2 \qquad \text{Equation } 4-3$$

where k = 2.5 constant;

N= number of days in the month;

$X = (T - 32^{\circ F})$;

T= the average temperature in the change-over month of N days; and

Y= Cumulative degree day of the change-over month.

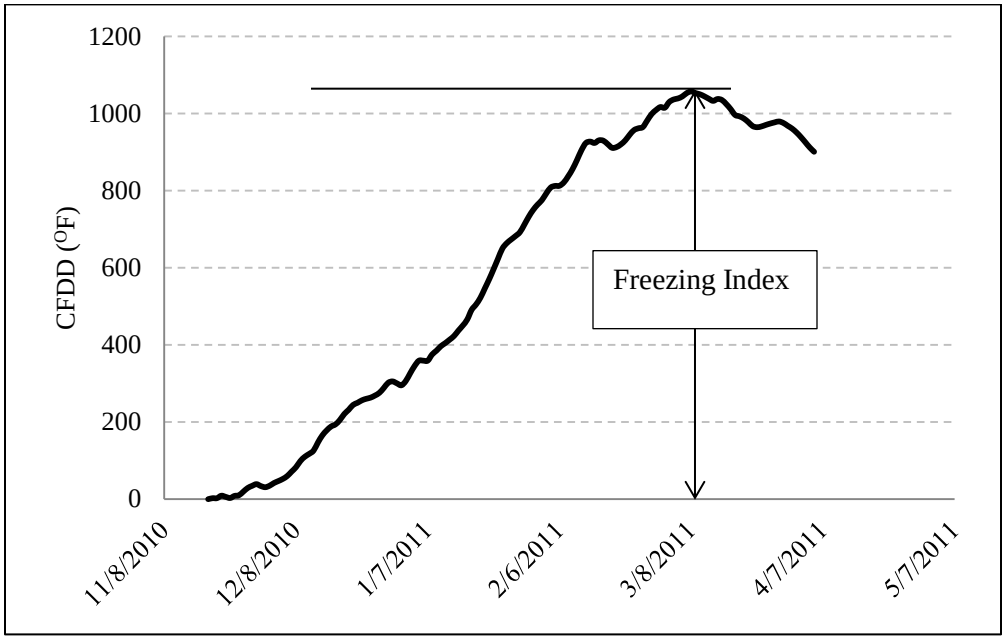

Figure 4-3 Calculation of freezing index using cumulative freezing degree day

The solution of this equation yields two values for Y; a positive and a negative value. For the changeover month, the cumulative freezing degree days (CFDD) for the month can be calculated using equation 4-4. Whereas, for all other months, the CFDD is calculated using Equation 4-5.

$$CFDD = |negative\ root\ of\ Y| \qquad \text{Equation } 4-4$$

$$CFDD = NX \qquad \text{Equation } 4-5$$

Where all parameters are the same as before.

CFDD values were calculated using both the Minnesota (Equation 4-1) and the Boyd methods and the data from different RWIS stations in Michigan. The results are plotted in Figure 4.4. It can be seen from the figure that the CFDD values calculated using Boyd equation could have more than 20% discrepancy relative to the CFDD values calculated using the Minnesota equation. This difference could be attributed to various reasons including:

1. The k value in Equation 4-3 is an empirical value based on the 10 years data collected at 22 stations across Canada. This value could change from one year to the next and from one region to another.

2. By using the monthly average temperature in the Boyd equation instead of the daily average temperature in calculating CFDD, the daily variations in the degree days are disregarded, which may lead to errors.

Because of the above reasons, in this study, the CFDD value were calculated using Minnesota equation (Equation 4-1)

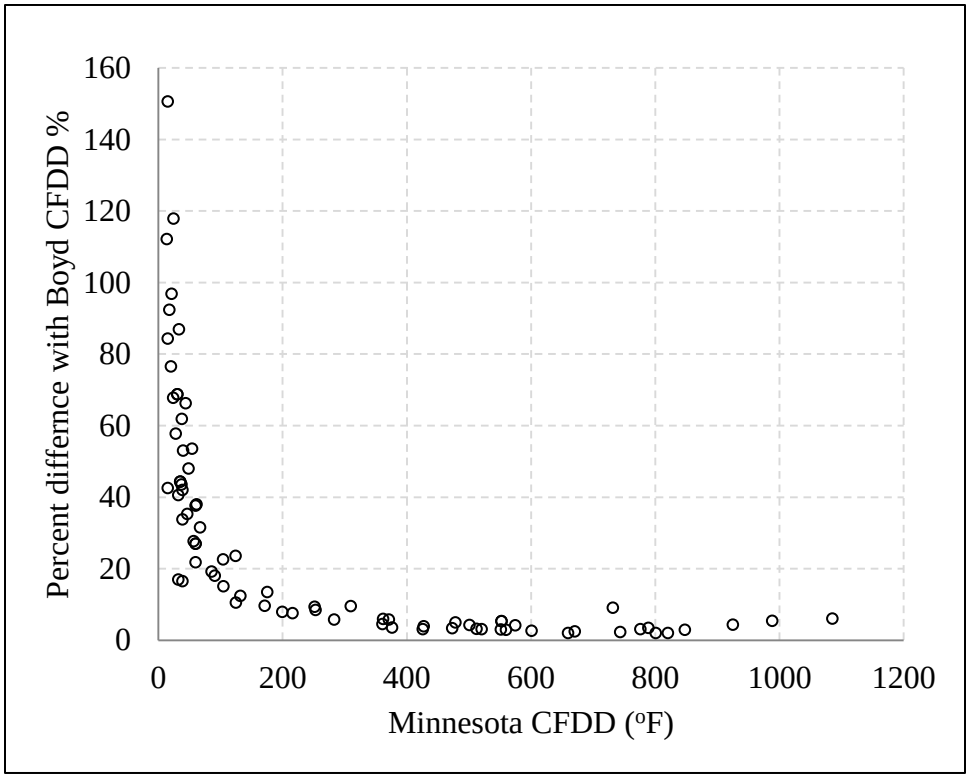

Figure 4-4 Comparison of calculated CFDD using Boyd (Boyd 1976) and Minnesota (MnDOT 2009) methods

4.4 Existing Frost Depth Prediction Models

There are several frost prediction models that were developed. Some of these models are empirical in nature, some others are semi-empirical, and still others are mechanistic. Some of these models are enumerated and discussed below.

4.4.1 Stefan Equation

As stated before, Stefan solved the heat transfer phase-change problem for the special case of no heat transfer in the unfrozen zone (Jiji, 2009) and estimated the frost depths. His solution is one of the first frost depth prediction models (see Equation 2-10 of Chapter 2) and modified versions of his solution are still being used by some State Highway Agencies (SHAs).

In order to evaluate the accuracy of Stefan Equation relative to the measured data in Michigan, measured frost depths at different RWIS stations in the state of Michigan were used. Unfortunately the in-situ water content and dry density data of the soils were not available. Therefore, the soil water content and dry density were estimated using the graphs developed by the U.S Army Corps of Engineers (USACE, 1998) and shown in Figure 4-5. The various curves in the figure relate thermal conductivity to dry density and moisture content in the frozen and unfrozen conditions of various soil types. For each soil type, the measured thermal properties were used and its dry density and water content were estimated from the graphs. Next, the volumetric latent heat of fusion (L) was calculated using Equation 2-11; as it was expected, the calculated values of L decreased as the water content decreased. The values of the freezing index for the years 2010 and 2011 were calculated using the NOAA data obtained from the appropriate weather stations. Finally, Equation 2-10 was used to calculate the frost depths as a function of time for the two years. The details of frost depth calculation for each RWIS station were presented in appendix A. Figure 4-6 and Table 4-3 depicts the maximum calculated versus the maximum measured frost depth data for saturated condition. In Figure 4-6 the straight line is the line of equality between the measured and the calculated frost depth data. It can be seen from the figure that, for all soil types, the calculated maximum frost depths in saturated condition are much higher (more than 25-inch) than the measured values. The discrepancy between the measured and calculated data could be related to:

1. The volumetric heat capacity of the soil and water, which were not considered in Stefan's Equation (Equation 2-10).
2. Errors in estimating the in-situ water content, dry density using the soil thermal conductivity and the Corps of Engineers graphs.

Given the significant differences between the measured frost depth data and the calculated ones using Equation 2-10, Stefan's equation was abandoned and the Modified Berggren equation was studied. The results are presented and discussed below.

4.4.2 Modified Berggren Equation

Aldrich et al., (1953) made the two assumptions listed below and modified the original Berggren's equation. Equation 2-12 was the resulting equation.

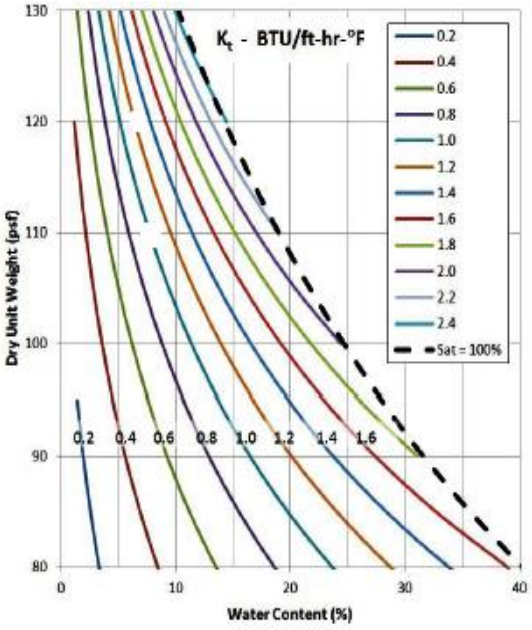

Figure 4-5(a) Frozen sand and Gravel

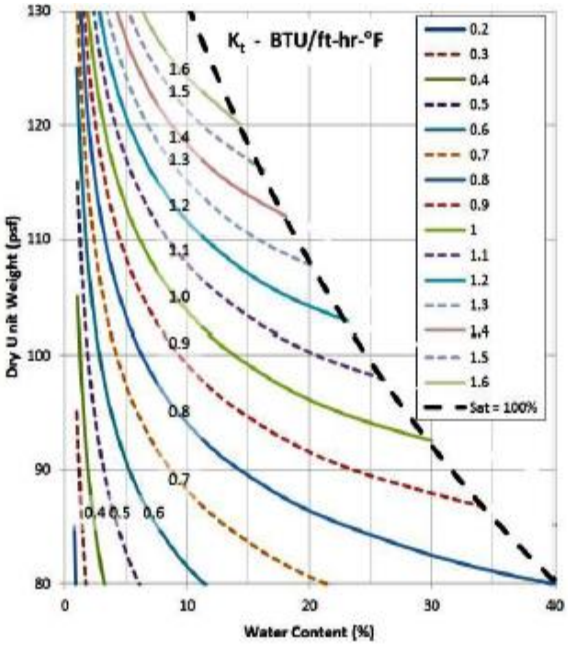

Figure 4-5(b) Unfrozen sand and Gravel

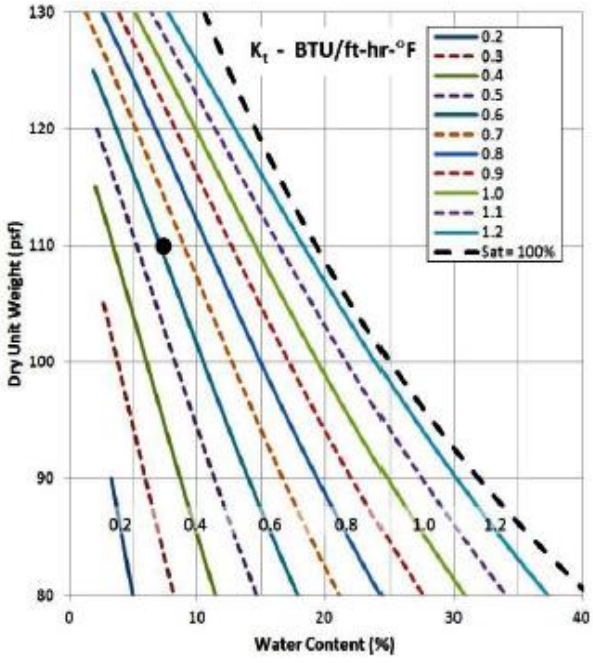

Figure 4-5(c) Frozen silt and clay

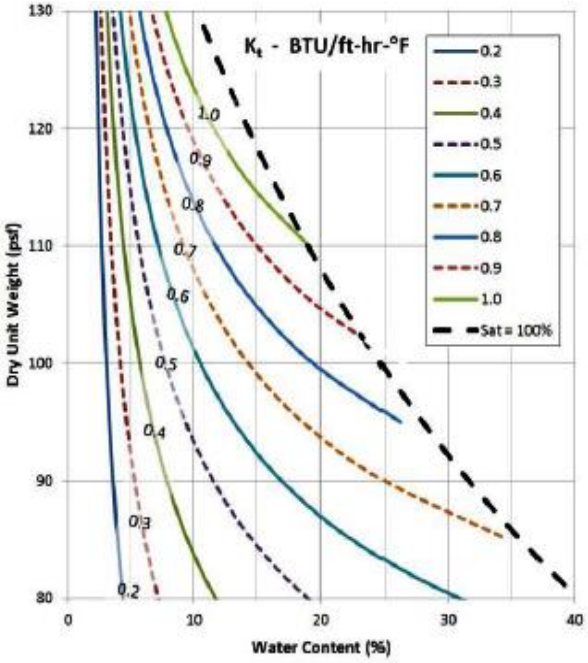

Figure 4-5(d) Unfrozen silt and clay

Figure 4-5 Soil Thermal conductivity of different types of soil based on water content and dry density obtained by US army cold region and engineering laboratory (CRREL) (Edgar, 2014)

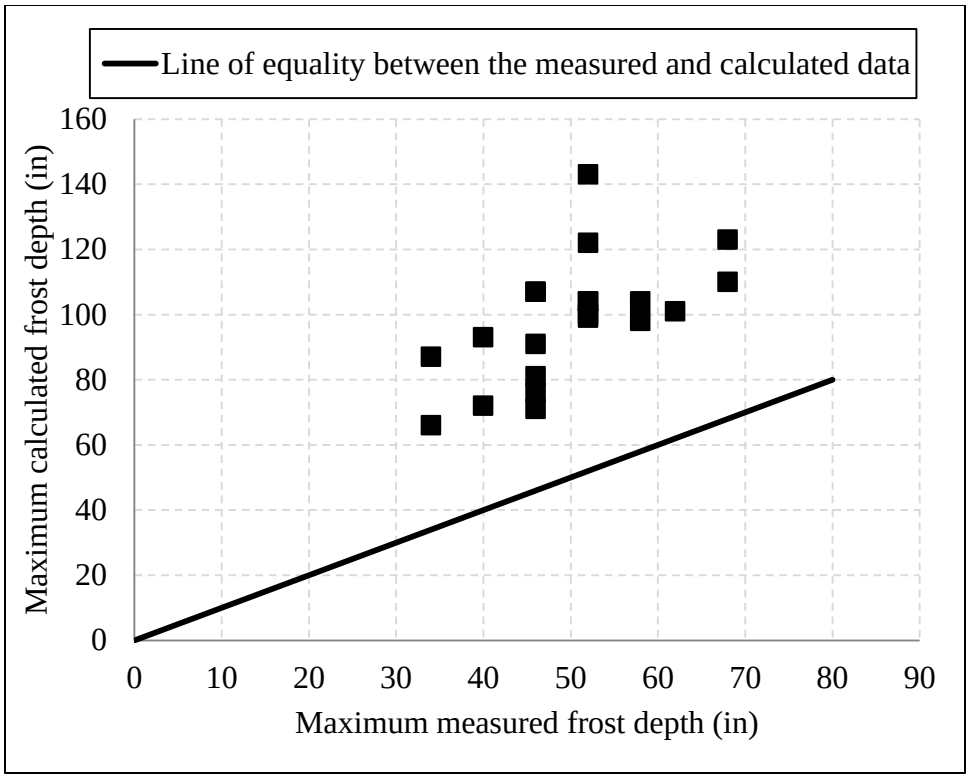

Figure 4-6 The maximum frost depths predicted by Stefan equation versus the measured maximum frost depths in Michigan

1. Heat transfer is one-dimensional problem and the soil is at its mean annual temperature before freezing begins (USACE, 1998).
2. At the beginning of the freezing season, the surface temperature decreases in a step-function manner from the mean annual temperature to some degrees below the freezing point and remains at this temperature (steady state) during the entire freezing season (Bianchini et al., 2012).

In this study, the maximum frost depths were calculated using the Modified Berggren equation for multilayered system (Equation 2-13). Table 4-4 shows an example of step by step frost depth calculation using Equation 2-13.

In the calculations, in order to obtain the correction factor (λ) from Figure 2.2, two dimensionless parameters (the thermal ratio (α) and the fusion parameter (μ)) must be calculated.

Table 4-3 Maximum frost depth predicted by Stefan equation for RWIS stations

Location	Station Name	Type of soil	Year	Maximum Measured Frost Depth (in)	Maximum Calculated Stefan Eq. (in)
Lower Peninsula	Benzonia	Loose Sand	2010-2011	34	87
	Cadillac	Dense Sand	2010-2011	46	107
	Grayling	Dense Sand	2010-2011	62	101
	Houghton Lake	Dense Sand	2010-2011	52	100
	Ludington	Loose Sand with clay	2010-2011	34	66
	Reed City	Compacted Sand	2010-2011	40	93
		Loose Sand			
	Waters	Compacted Sand	2010-2011	68	123
		Loose Sand			
	Williamsburg	Dense Sand	2010-2011	40	72
		Silty Clay			
Upper Peninsula	Au Train	Sand with Gravel and Silt	2009-2010	52	104
			2010-2011	52	143
		Loose Sand			
	Brevort	Loose Sand	2009-2010	46	91
			2010-2011	58	104
	Harvey	Sand with Gravel and Silt	2009-2010	58	98
			2010-2011	68	110
		Dense Sand			
	Golden Lake	Dense Sand with Gravel	2010-2011	52	122
	Seney	Loose Sand	2010-2011	52	99
	Cooks	Clayey Sand	2010-2011	46	107
	Michigamme	Clayey Sand	2010-2011	52	104
	St.Ignace	Silty Clayey Sand	2010-2011	46	71
	Twin Lakes	Silty Clayey Sand	2010-2011	46	81
	Engadine	Silty Clayey Sand	2010-2011	46	76

As stated in Chapter 2, fusion parameter (μ) depends on the volumetric heat capacity and latent heat of fusion of every layer and was calculated using Equation 4-6. The thermal ratio (α) is a fixed number for all layers and depends on the FI and annual average temperature; it was calculated using Equation 4-7.

$$\mu = \frac{C}{L} * v_s \qquad Equation\ 4-6$$

$$\alpha = \frac{v_0}{v_s} \qquad Equation\ 4-7$$

Where C=volumetric heat capacity (Btu/ft$^{3)}$;

L= latent heat of fusion (Btu/^{3}ft);

v_s= average temperature differential= $n(FI)/t$;

t= duration of winter period (used in calculation of v_s);

v_0= initial temperature differential = annual average temperature -32; and

All other parameters are as before.

After calculating α and μ, the correction factor λ was obtained from Figure 2-2 and the maximum frost depth was calculated using Equation 2-13 (See Table 4.4).

Using the Modified Berggren equation, the maximum frost depths were calculated for the RWIS stations in Michigan. The details of frost depth calculation for each station were presented in appendix A. The maximum calculated frost depths were compared to the maximum measured frost depth data in the State of Michigan in Figure 4-7 and Table 4-5. It can be seen from the figure that the Modified Berggren equation leads to more accurate results than the Stefan equation. However, the differences between the calculated and measured values in some cases are more than 20 inches. The discrepancy between the measured and calculated data could be related to:

1. Equation 2-13 does not account for the water movement in the soil.
2. Potential errors in estimating the thermal conductivity, water content and dry density.

Given the substantial differences between the measured frost depth data and the calculated ones using Equation 2-13, the Modified Berggren equation was also abandoned and the Chisholm and Phang equation was studied. The results are presented and discussed in the next section.

Table 4-4 Frost depth calculation using the Modified Berggren equation, Benzonia, Lower Peninsula, Michigan

Column No.	1	2	3	4	5	6	7	8	9	10	11	12	13	14	15
Material	**γ_d**	**w**	**d**	**C**	**k**	**L**	**Ĺ= ∑Ld/∑d**	**Ĉ= ∑Cd/∑d**	**μ= Ĉ / Ĺ *vs**	**λ**	**R**	**∑R**	**∑R+R/2**	**FI**	**∑FI**
HMA	138	0	0.42	24	0.86	397	0	24	0	0	0.48	0.00	0.24	0	0
Gravel	130	0.075	1	30	1.5	1350	953	28	0.17	0.56	0.67	0.48	0.82	147	147
Loose Sand	125	0.09	1.9	42	1.4	1555	1298	36	0.16	0.58	1.36	1.15	1.83	670	822

γ_d = unit weight (pcf); w = water content (%); d = layer depth (ft); C= volumetric heat capacity(Btu/ft^3); k= thermal conductivity (Btu/(ft.hr.^{o} F); L= latent heat of fusion (Btu/^{3}ft); μ= fusion parameter; λ= correction factor; R= thermal diffusivity (hr °F/ Btu);

FI=freezing Index (^{o}F-day)

Step by step calculation

1. k values were obtained from the laboratory measurements (Table 3-4). γ_d and w values were obtained from Figure 4-5 using k values. d values were obtained from the pavement profile of RWIS station, and C values are assumed based on the soil type (Columns 1-5).
2. L and μ were calculated using Equation 2-11 and 4-6, respectively (Columns 6 and 9).
3. α can be calculated by Equation 4-7 as follow:
   FI=801 (^{o}F-day) ; v_s=0.9(801)/t = 5.6; v_0= 48.6-32=16.6 → $\alpha=v_0/v_s$=2.93
4. Using α and μ values, λ can be obtained from Figure 2-2 for each layer (Columns 10)
5. R values were calculated as R= d/K for each layer (Columns 11)
6. Freezing index required for each layer to freeze were calculated using Equation 2-13 (Columns 14)
7. The summation of freezing indexes in column 14 should be approximately equal to the seasonal freezing index (FI=801)

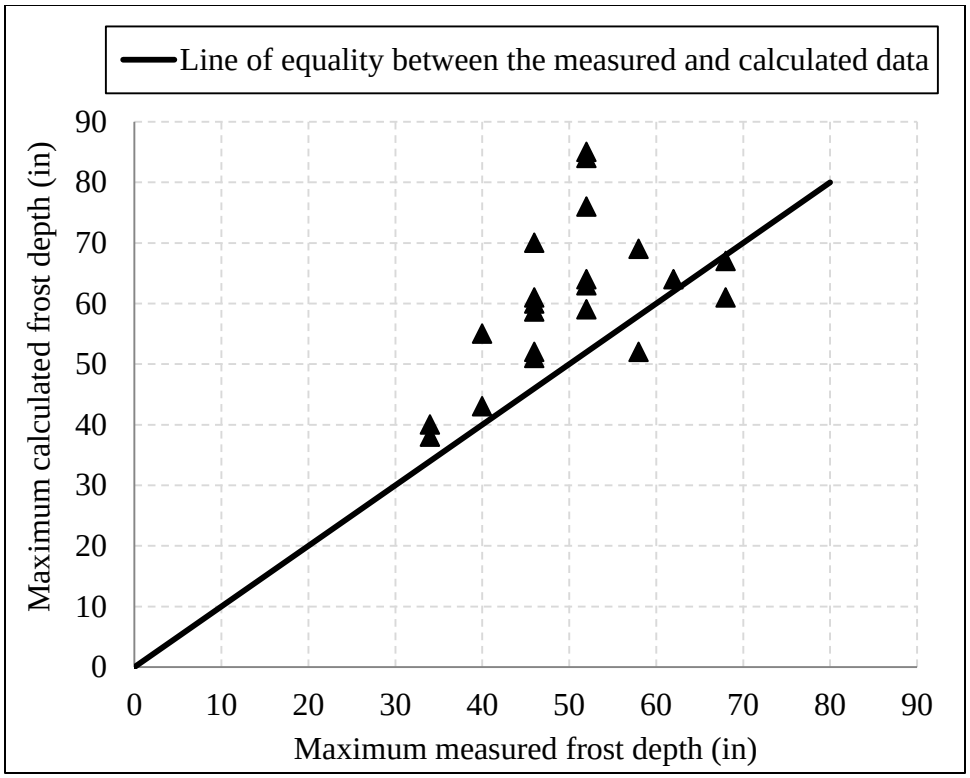

Figure 4-7 Measured maximum frost depths in Michigan versus the maximum calculated ones using the Modified Berggren equation

4.4.3 Chisholm and Phang Equation

The first empirical equation which relates CFDD and frost depth was developed by Chisholm and Phang in 1980 to predict frost depths under asphalt pavements in Ontario, Canada (Equation 2-14). It should be noted that since the local daily air temperature data were not available on a daily basis, the CFDD values were calculated using Boyd approach (Chisholm and Phang, 1980). Their results indicated that in their database, the frost depth predictions fall within 12 inches of the measured ones. Equation 2-14 was used to predict the maximum monthly measured frost depths at different RWIS stations in the state of Michigan. Figure 4-8 shows the results. It can be seen that in most cases, Equation 2-14 underestimates the maximum monthly frost depths. In fact, in some cases for small values of CFDD, the calculated frost depths could be negative. The differences between the predicted and the measured frost depths could be as high as 30 inches. Based on the fact that the empirical equation was developed using the measured frost depth data in Ontario, it can be concluded that the equation is regional and calibration is required for using it in other regions.

Table 4-5 Maximum frost depth predicted by Modified Berggren equation for RWIS stations

Location	Name of the Station	Type of Soil	Year	Maximum Measured Frost Depth (in)	Calculated Maximum Frost Depths Modified Berggren Equation (in)
Lower Peninsula	Benzonia	Loose Sand	2010-2011	34	37
	Cadillac	Dense Sand	2010-2011	46	55
	Grayling	Dense Sand	2010-2011	62	70
	Houghton Lake	Dense Sand	2010-2011	52	53
	Ludington	Loose Sand with clay	2010-2011	34	36
	Reed City	Compacted Sand	2010-2011	40	47
		Loose Sand			
	Waters	Compacted Sand	2010-2011	68	54
		Loose Sand			
	Williamsburg	Dense Sand	2010-2011	40	45
		Silty Clay			
Upper Peninsula	Au Train	Sand with Gravel and Silt	2009-2010	52	54
			2010-2011	52	71
		Loose Sand			
	Brevort	Loose Sand	2009-2010	46	57
			2010-2011	58	58
	Harvey	Sand with Gravel and Silt	2009-2010	58	49
			2010-2011	68	55
		Dense Sand			
	Golden Lake	Dense Sand with Gravel	2010-2011	52	75
	Seney	Loose Sand	2010-2011	52	52
	Cooks	Clayey Sand	2010-2011	46	55
	Michigamme	Clayey Sand	2010-2011	52	70
	St.Ignace	Silty Clayey Sand	2010-2011	46	55
	Twin Lakes	Silty Clayey Sand	2010-2011	46	60
	Engadine	Silty Clayey Sand	2010-2011	46	49

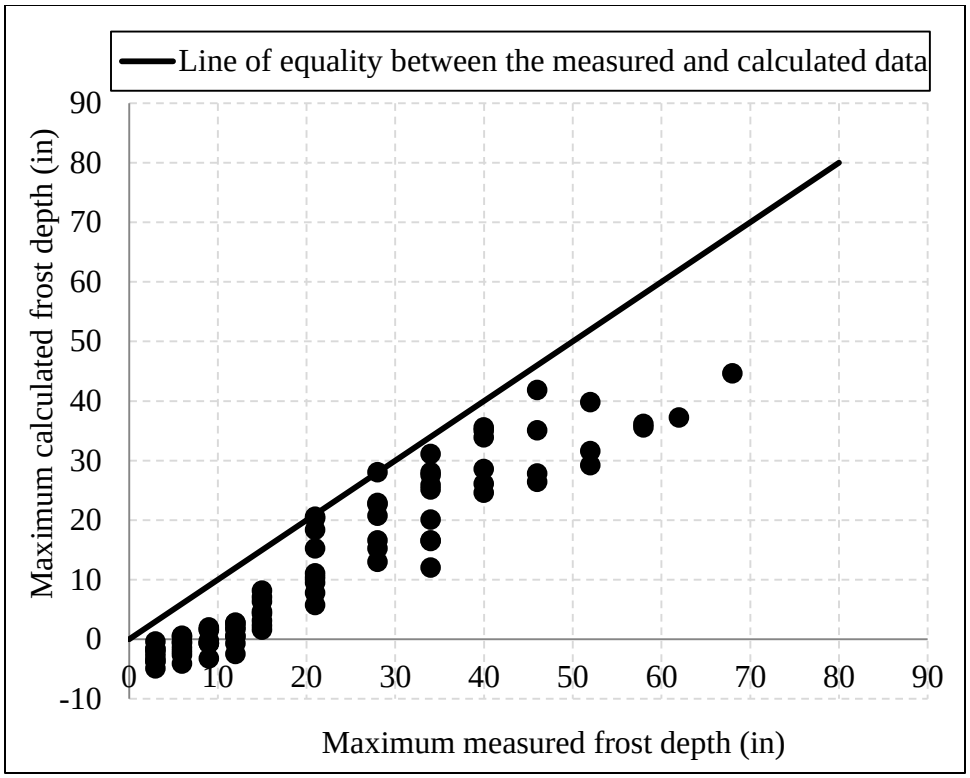

Figure 4-8 Measured maximum frost depths versus calculated ones using Chisholm and Phang equation

4.5 Empirical Models

Since none of the existing models yielded accurate frost depth results, new empirical models were developed in this study using the RWIS data in the State of Michigan. These new models are presented below.

Among the 25 RWIS stations located in the Upper and Lower Peninsulas of Michigan, 18 stations were used for developing empirical models. Seven stations were not considered due to incomplete data (some of the data are missing). For air temperature data the nearest NOAA station database was used due to higher consistency and accuracy with respect to the RWIS database. Sites not situated close to NOAA stations are not considered in this study. Due to data availability, only data from the winter of 2011 was used, expect for Au Train, Brevort and Harvey sites where data from the 2010 winter were also available.

First, the air temperature data was used to calculate the CFDD for each RWIS station location. The frost depth data and corresponding CFDD data for each RWIS station are presented in Appendix B. Second, the measured frost depth data in all RWIS stations and the calculated

CFDD values were used to develop one statistical prediction equation regardless of the soil type. This resulted in Equation 4-8.

$$P = 1.369(CFDD)^{0.5339} \qquad \text{Equation } 4-8$$

Equation 4-8 is more or less similar to 4-9, which was developed by the U.S. Corps of Engineers (Yoder, 1975)

$$P = 1.6575(CFDD)^{0.478} \qquad \text{Equation } 4-9$$

Where P = frost depth (inch); and

$CFDD$ = cumulative freezing degree day (^{o}F – day)

The results of both equations are depicted in Figure 4-9. The data in the figure indicate that Equation 4-9 under predicts the majority of the data. On the other hand, Equation 4-8 represents the measured frost depths more accurately. In fact, the calculated coefficient of determination (R^2) is 0.91. Figure 4-10 show the calculated frost depths using Equation 4-8 versus the measured ones. The solid straight line in the figure is the locus of equality between the measured and calculated data. Nevertheless, the majority of the calculated frost depth data are within a few inches from the measured values and the maximum difference is 10-inch. In other words, the 90% level of confidence interval is ± 10 inches.

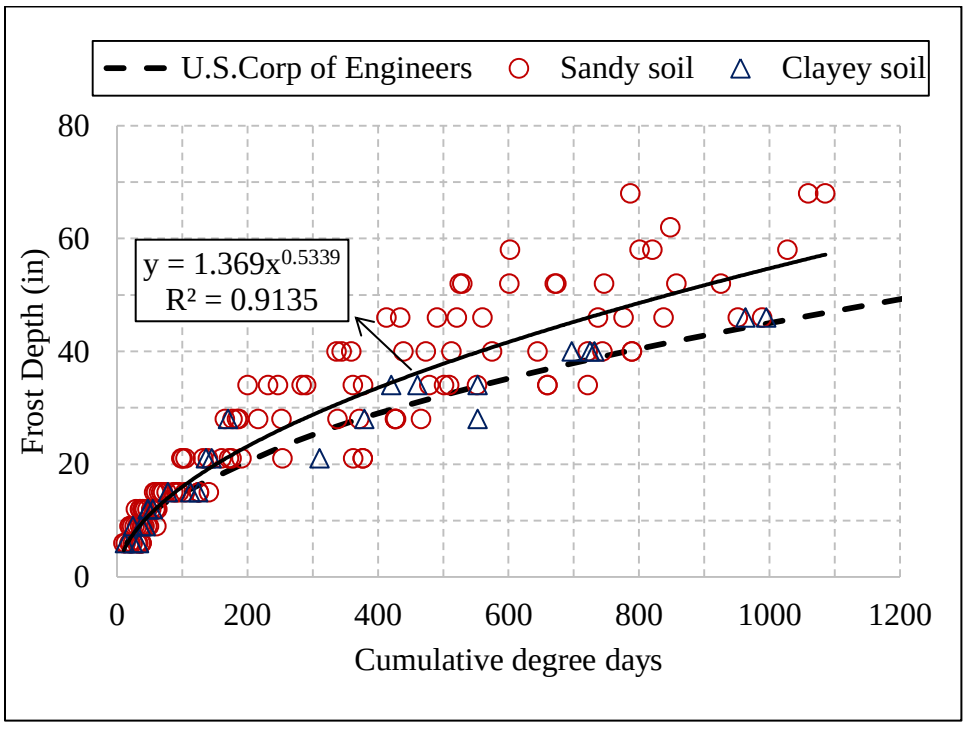

Figure 4-9 Frost depths versus cumulative freezing degree day for clayey and sandy soils in the State of Michigan

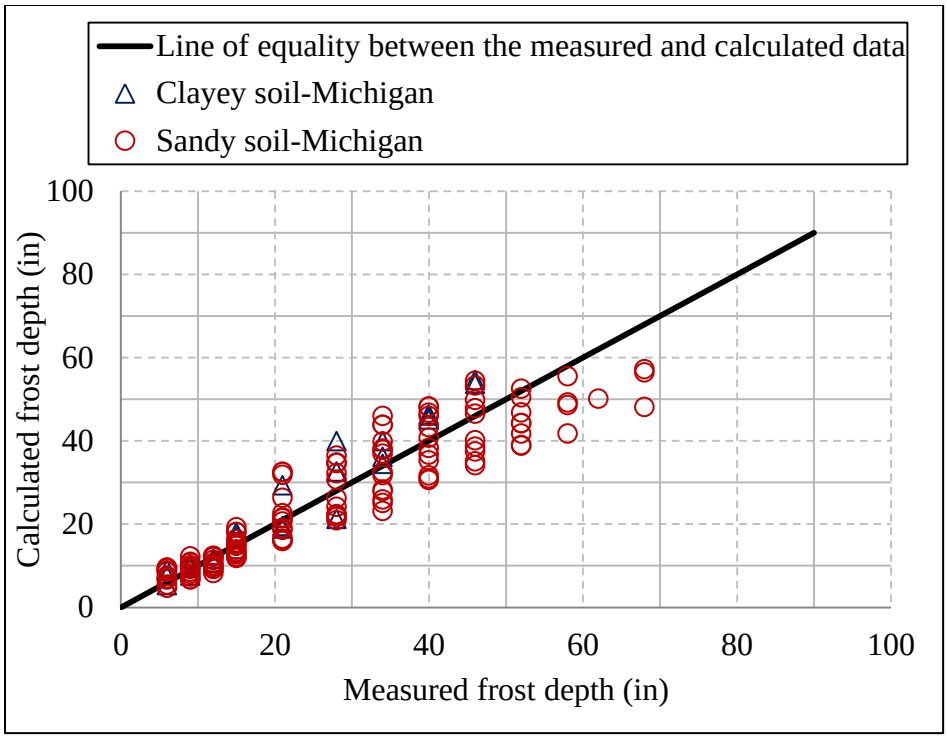

Figure 4-10 Measured frost depths in State of Michigan versus the calculated ones using Equation 4-8

As stated in Chapter 3, frost depth data measured from 2003 to 2012 in 8 stations in the State of Minnesota were requested and received from MnDOT. Equation 4-8 was then used to calculate the frost depth data at all 8 stations and for the ten year period. The measured frost depth data and the calculated ones are depicted in Figure 4-11. The straight line in the figure indicates the line of equality between the measured and the calculated values. Examination of the data shown in the figure indicates that Equation 4-8 does not predict the measured frost depth data in Minnesota accurately. In fact, Equation 4-8 over predicts the Minnesota frost depth data by as much as 40inches. Moreover, the calculated coefficient of determination (R^2) for the Minnesota data is 0.77 which is much lower than the calculated R^2 of 0.91 for the Michigan data.

Figures 4-12 and 4-13 show the calculated frost depths using Equation 4-9 versus the measured ones in the state of Michigan and Minnesota, respectively. The solid straight line in the figures is the locus of equality between the measured and calculated data. It can be seen that Equation 4-9 predict frost depths in clayey soils better than in sandy soils in both states. For the latter soils, the differences between the measured and calculated values could be as high as 25-inch. Please note that, like Equation 4-8, Equation 4-9 does not separate sandy from clayey soils.

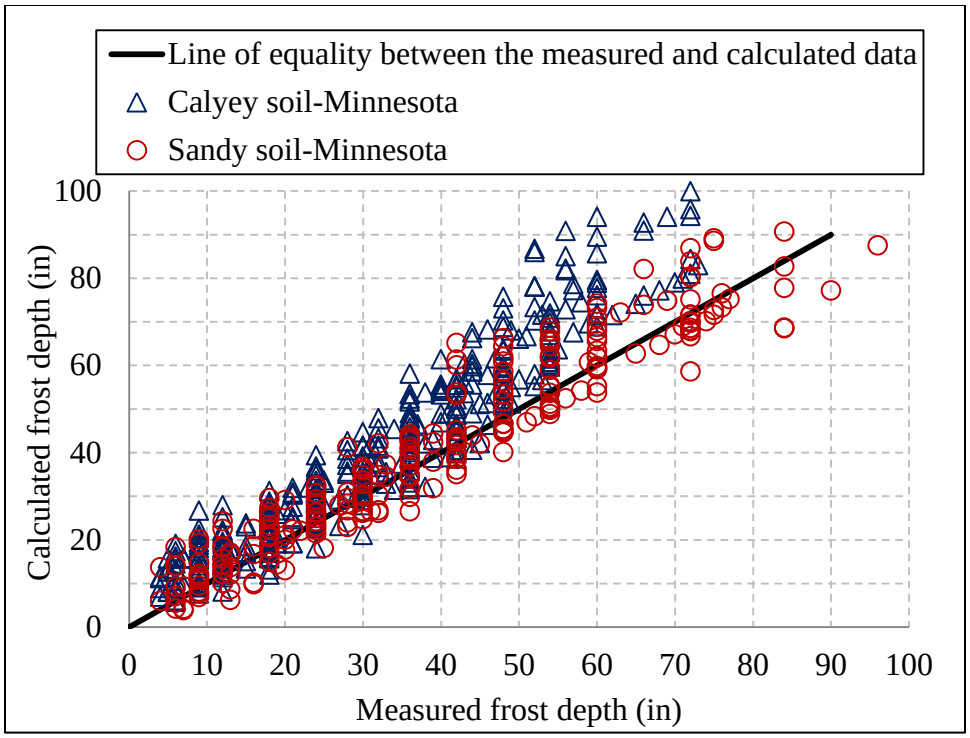

Figure 4-11 Measured frost depth in State of Minnesota versus the calculated ones using Equation 4-8

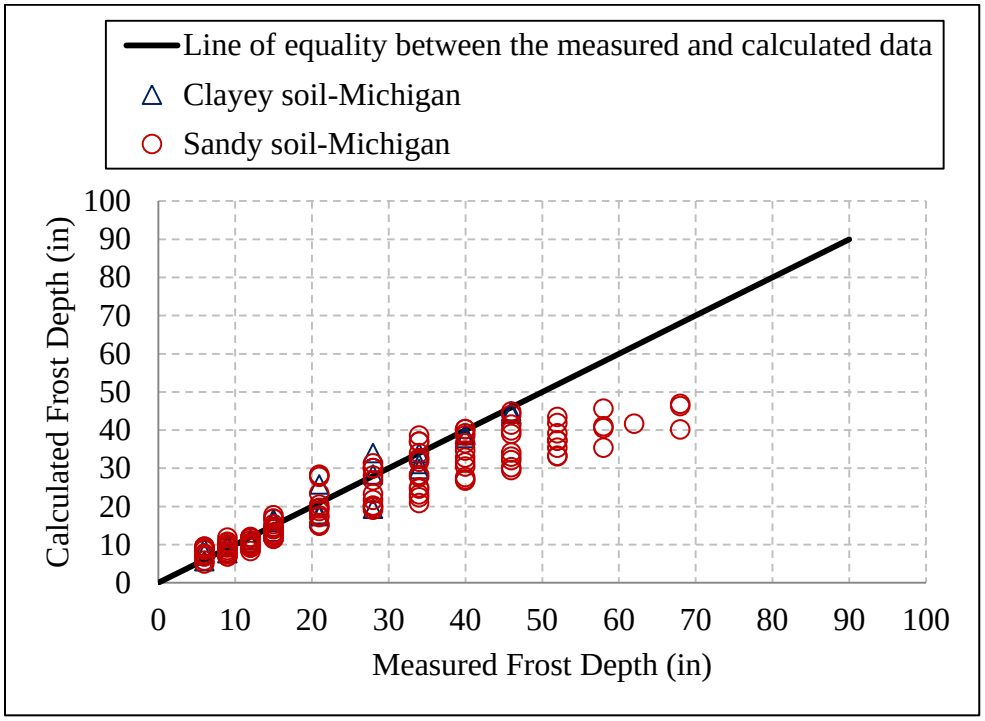

Figure 4-12 Measured frost depth in State of Michigan versus the calculated ones using Equation 4-9

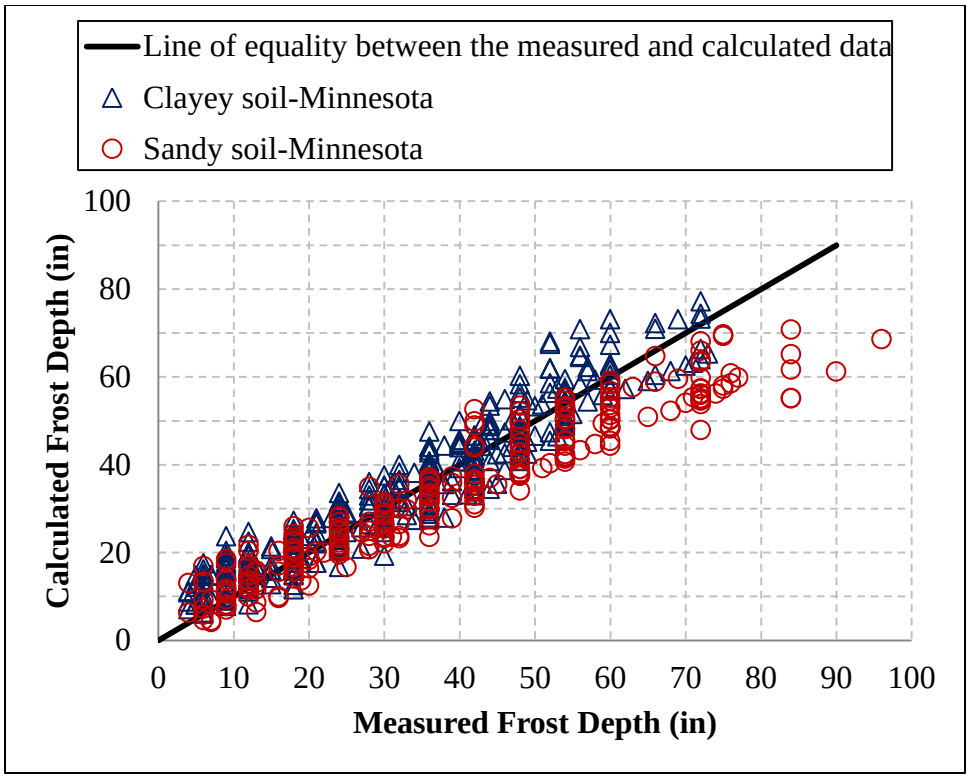

Figure 4-13 Measured frost depth in State of Minnesota versus the calculated ones using Equation 4-9

The results shown in Figure 4-11 were further scrutinized to improve the accuracy of Equation 4-8. Previous studies indicate that frost depths are a function of many variables including intensity and duration of the freezing period, water availability, soil permeability and capillarity, grain size and grain size distribution, and the soil thermal conductivity. Hence, it was hypothesized that these variables are a function of the soil type such as clayey and sandy soils. Therefore, the frost depth data measured at various RWIS stations in the state of Michigan was divided into two groups according to soil type at the stations; clayey and sandy soils. It should be noted that dividing data in two groups of clayey and sandy soil was based on the soil log provided by MDOT for each station.

After separating the data, a mathematical power function was used to model each group of frost depth data as a function of the calculated CFDD. This resulted in Equations 4-10 and 4-11 for clayey and sandy soils, respectively.

$$For\ clayey\ soils \qquad P = 1.5901(CFDD)^{0.4896} \qquad \text{Equation } 4-10$$

$$For\ sandy\ soils \qquad P = 1.3302(CFDD)^{0.5423} \qquad \text{Equation } 4-11$$

Figures 4-14and 4-15 depict the measured frost depth data in clayey soils in Michigan and the calculate frost depth data using Equation 4-10. Figure 4-14 also show the U.S. Corps of Engineers equation. It can be seen from the figure that Equation 4-10 and the U.S. Corps of Engineers equations fit the data very well. The coefficient of determination of Equation 4-10 is 0.94. Further, Figure 4-15 depicts the measured frost depth data in clayey soils in Michigan versus the frost depth data calculated using Equation 4-10. The solid line in the figure is the line of equality between the measured and the calculated data. The results in the figure indicate that Equation 4-10 predict the frost depth data in clayey soils in Michigan very well. In fact, the 90% confidence interval is ± 5 inches for the frost depth calculation.

Figures 4-16 and 4-17 depict the measured frost depth data in sandy soils in Michigan and the calculate frost depth data using Equation 4-11. Figure 4-16 also show the U.S. Corps of Engineers equation. It can be seen from the figure that Equation 4-11 represents the measured frost depth data much better than the U.S. Corps of Engineers equations. Indeed the coefficient of determination of Equation 4-11 is 0.91.

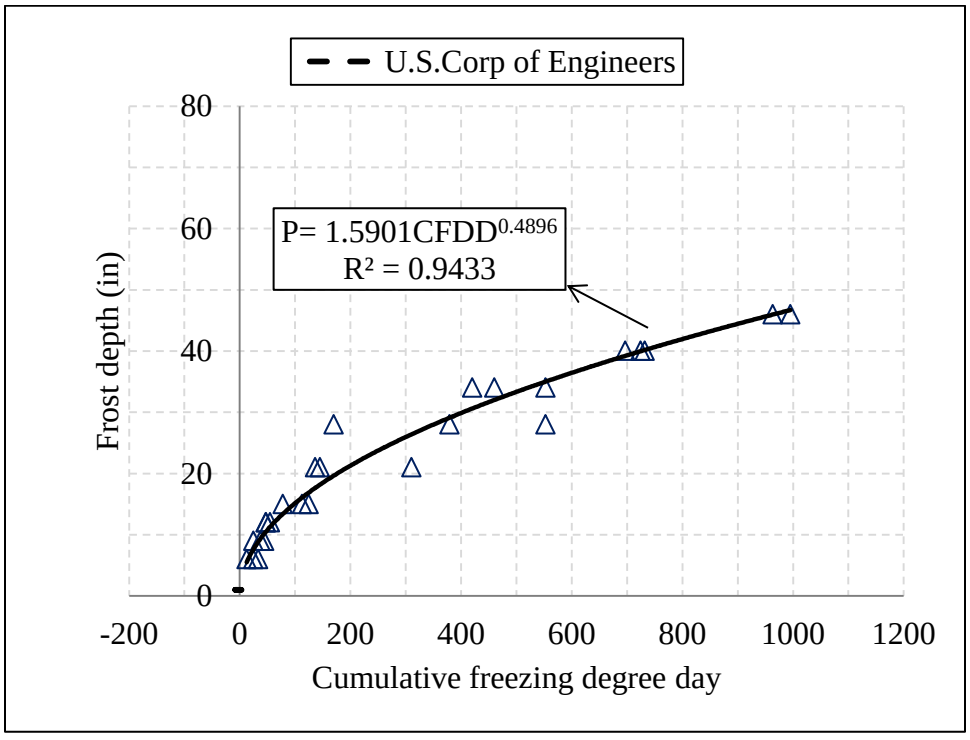

Figure 4-14 Measured frost depths in Michigan versus cumulative freezing degree day for clayey soil showing the best fit and the U.S. Corps of Engineers equations

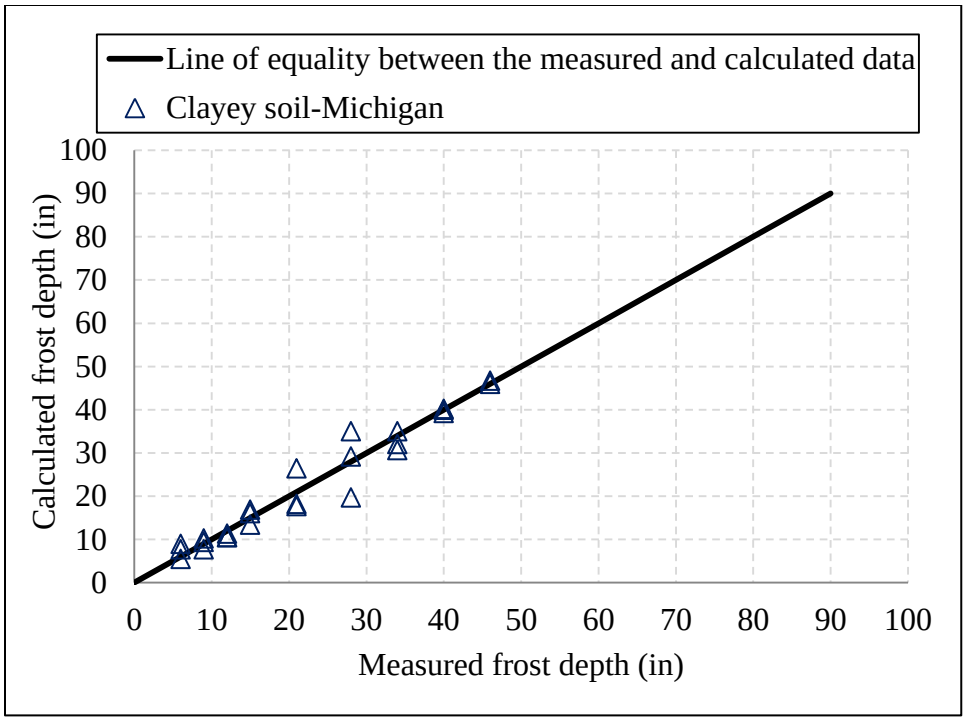

Figure 4-15 Measured frost depth data in clayey soils in Michigan versus the calculated ones using Equation 4-10

Further, Figure 4-17 depicts the measured frost depth data in clayey soils in Michigan versus the frost depth data calculated using Equation 4-11. The solid line in the figure is the line of equality between the measured and the calculated data. The results in the figure indicate that Equation 4-11 provides better prediction of the measured frost depth data relative to Equation 4-8. In fact, the 90% confidence interval is ± 8 inches for the frost depth calculation. It should be noted that for frost depth more than 50-inch in sandy soils in both states, Equation 4-12 underestimates the measured data by as much as 10-inch. Examination of the results depicted in Figures 4-14 through 4-17 indicate that Equation 4-10 predicts the frost depth data in clayey soils better than Equation 4-11 in sandy soils. The main reason is that the variability of the measured frost depth data in sandy soils is higher than that in clayey soil. Such variability is a function of the grain size and grain size distribution, which impact the distribution of water and the hydraulic conductivity of the soils. Unfortunately such data are not available at this time to improve Equation 4-11. Nevertheless, the equation does predict the frost depth data in sandy soils relatively accurately. One important point that should be noted is the number of measured data points in clayey soils is much less than in sandy soils. A total of 29 data points are available for clayey soils, whereas 129 data points are available in sandy soils.

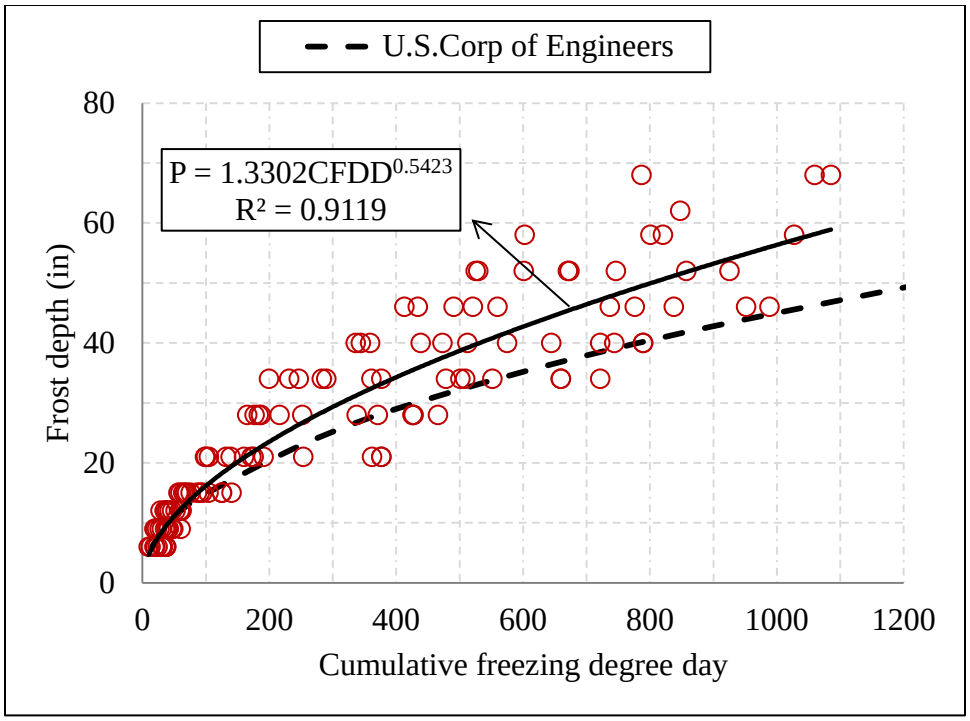

Figure 4-16 Frost depths versus cumulative freezing degree day for sandy soil showing the best fit and the U.S. Corps of Engineers equations in the State of Michigan

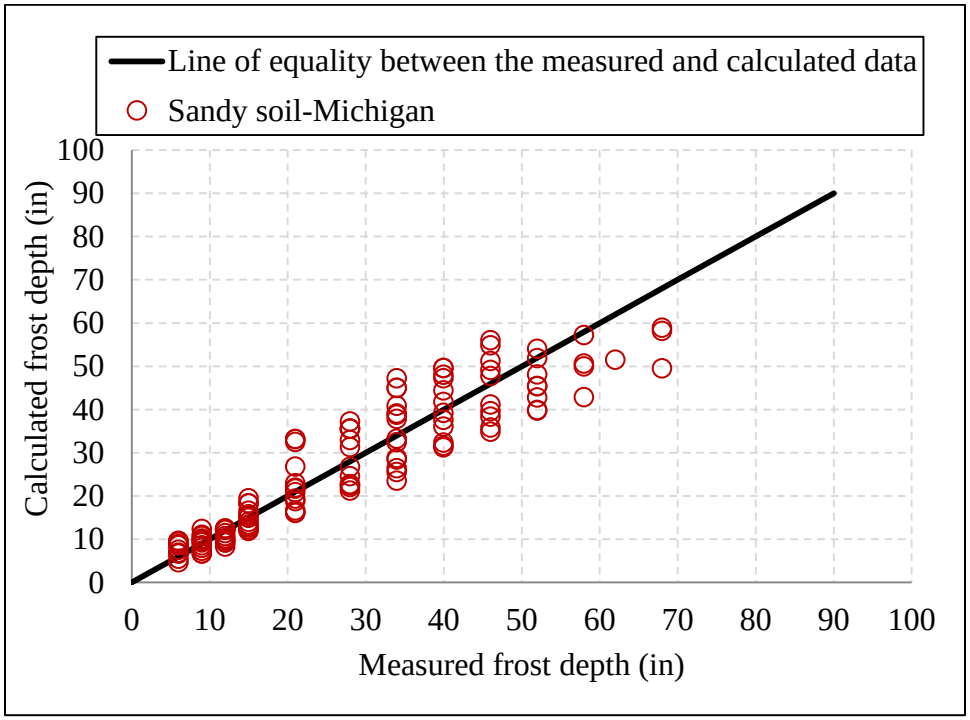

Figure 4-17 Measured frost depths in sandy soils in Michigan versus the ones calculated using Equation 4-11

Once again, to evaluate the accuracy of Equations 4-10 and 4-11, they were used to predict the measured frost depths in clayey and sandy soils in the State of Minnesota. Figures 4-18 and 4-19 depict the results. It should be noted that for clayey soil (Figure 4-18) the number of measured data points is 374 while for sandy soil (Figure 4-19) it is 247.

Examinations of Figures 4-18 and 4-19 indicates that the prediction of frost depth data in clayey and sandy soils in Minnesota using Equations 4-10 and 4-11 is significantly better and more accurate than the prediction using Equation 4-8 (see Figures 4-11, 4-18 and 4-19). In fact, for clayey and sandy soil the calculated coefficients of determination (R^2) are 0.88 and 0.9, respectively. The relatively high values of R^2 indicate that Equations 4-10 and 4-11 predict the frost depth data in clayey and sandy soils in the states of Michigan and Minnesota relatively accurately. The implication of this is that the two equations can be used in both states or perhaps at the regional level since both Michigan and Minnesota are located in the wet freeze region.

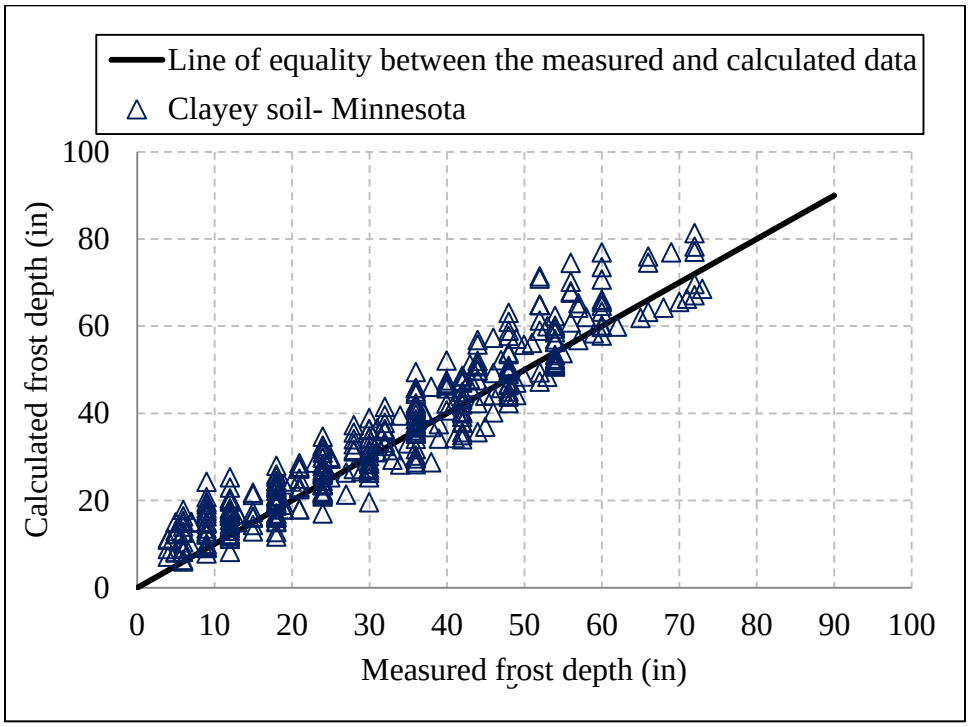

Figure 4-18 Measured frost depths in clayey soil in the state of Minnesota versus the frost depth values calculated using Equation 4-10

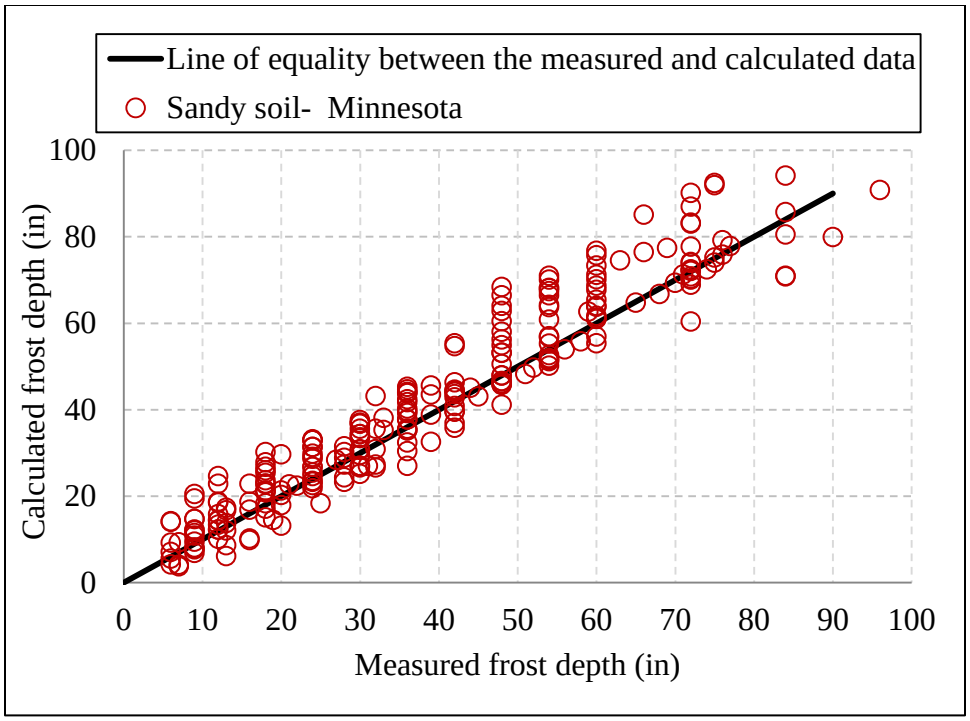

Figure 4-19 Measured frost depths in sandy soil in the state of Minnesota versus the frost depth values calculated using Equation 4-11

The thermal conductivity of any soil type (see Chapter 2) depends upon its water content, dry density, void distribution, and grain size and grain size distribution. These physical properties vary substantially from one soil type to another. Therefore, the disturbed clayey and sandy soil samples that were obtained by MDOT from various RWIS stations were saturated and the thermal conductivity of each soil type was measured in the laboratory at Michigan State University using the KD2 pro. The results are listed in table 3-4 of Chapter 3. To consolidate Equations 4-10 and 4-11 into one equation it was hypothesized that:

> "The various missing soil parameters (such as insitu density, water content, grain size, grain size distribution, soil permeability and capillarity) can be expressed by one related property; the saturated thermal conductivity of the soil".

Based on the hypothesis, the statistical parameters in Equations 4-10 and 4-11 were correlated to the average thermal conductivity of each soil type.

The statistical parameters of the two equations were then replaced by the resulting correlation equation, which yielded Equation 4-12 for both clayey and sandy soils. Figures 4-20

and 4-21 show the correlation between the statistical parameters and the average thermal conductivity of each soil type. Unfortunately, only two data points (two soil types) were available, hence the best correlation between the statistical parameters and the average thermal conductivity is a straight line as shown in the figures. It should be noted that such straight line correlations may not be accurate and may result in errors in the resulting frost prediction equations. To produce more accurate nonlinear equations (power, exponential or logarithmic function), data from three or more soil types must be available. Unfortunately, this was not the case and the straight line equations are the best scenario for the given data. Nevertheless, the equations for the two straight lines in Figures 4-20 and 4-21 were used to replace the statistical constants of equations 4-10 and 4-11. Equation 4-12 is the resulting equation for both types of soils clayey and sandy.

$$P = (-0.45\,k + 1.9614) * CFDD^{(.0913k+0.4143)} \qquad \text{Equation } 4-12$$

Where k= the average thermal conductivity of the soil (Btu/(ft.hr.^{o}F)); and

All other parameters are the same as before.

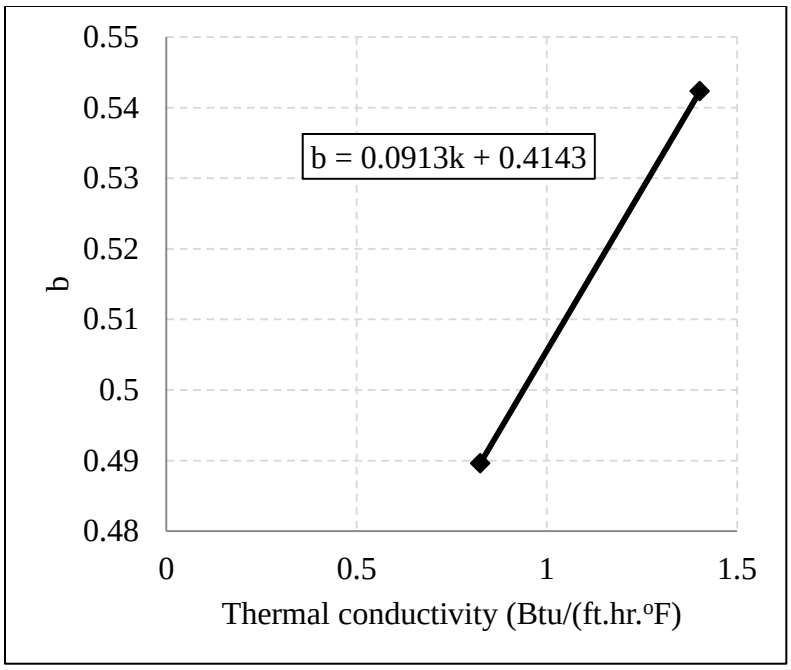

Figure 4-20 Correlation between the statistical power coefficient (b) of Equations 4-10 and 4-11 and the corresponding average thermal conductivity of the soil

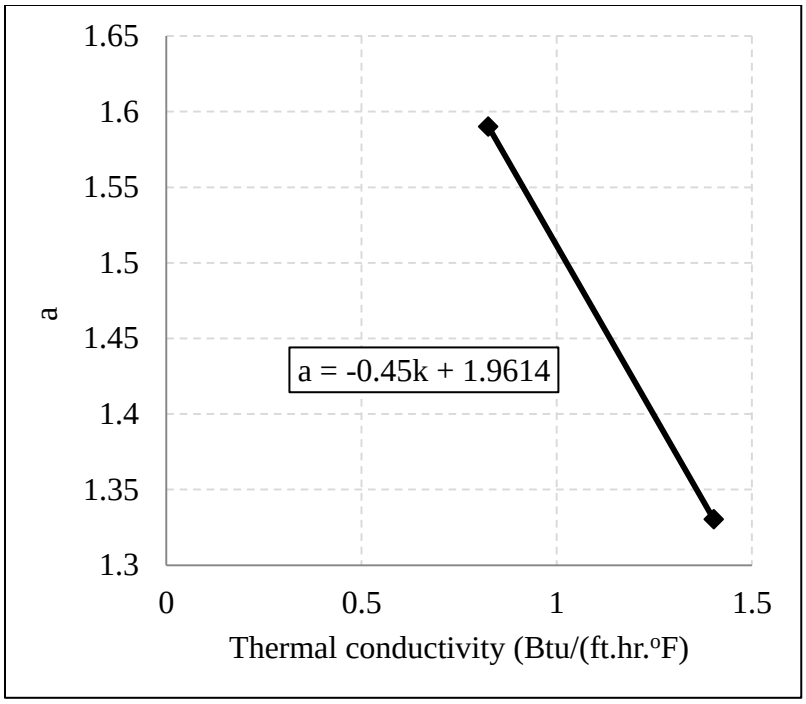

Figure 4-21 Correlation between the statistical coefficient (a) of Equations 4-10 and 4-11 and the corresponding average thermal conductivity of the soil

Equation 4-12 was then used to calculate the frost depths in clayey soils in the States of Michigan and Minnesota. The inputs to the equation consisted of the calculated CFDD for each state and the average measured thermal conductivity of the soil samples obtained from MDOT. Figures 4-22 and 4-23 depict the calculated and the measured frost depths in Michigan and in Minnesota, respectively. Comparing the results shown in the two figures and those shown in Figures 4-15 and 4-18 using Equation 4-10 indicate that the two equations produce similar results for clayey soils. Similarly, for sand soils in Michigan and Minnesota, Equations 4-12 and 4-11 produced almost the same results. These results can be seen in Figures 4-17 and 4-19 for Equation 4-11 and in Figures 4-22 and 4-23 for Equation 4-12.

Recall that the average thermal conductivity values obtained from seven different soil samples (two soil types) were used in the prediction of the frost depths in Michigan and Minnesota. This implies that:

1. If thermal conductivity data of more soil types are available, the prediction of frost depth could improve.
2. Equation 4-12 could perhaps be used at the regional level to estimate the frost depth data.

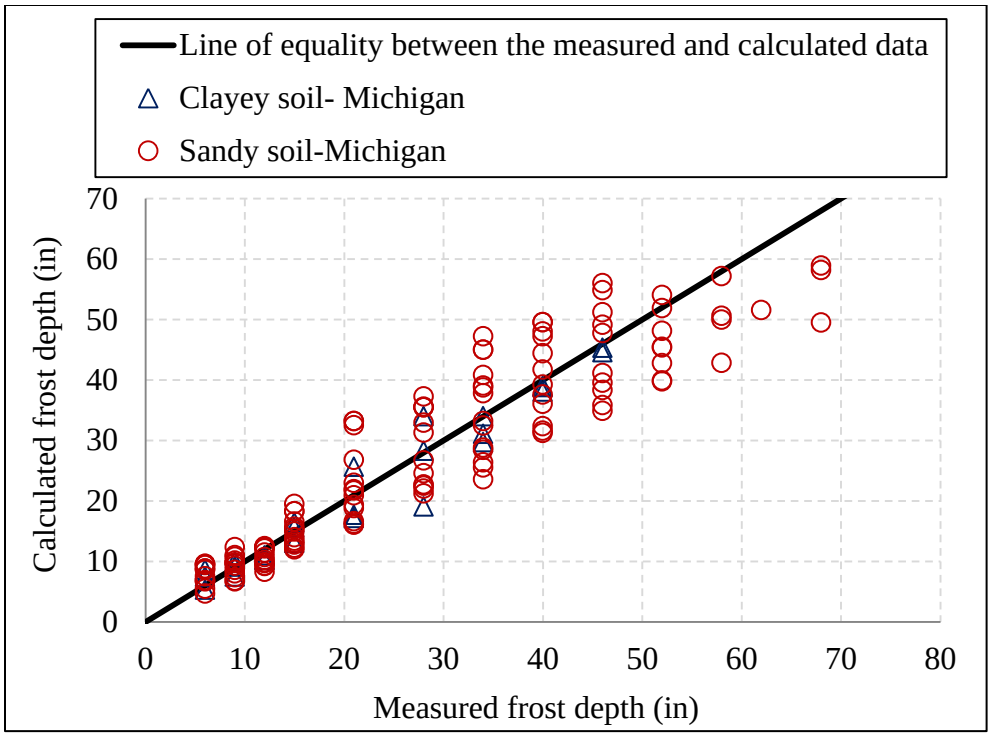

Figure 4-22 Calculated frost depths using Equation 4-12 versus the measured frost depth in clayey and sandy soil in the State of Michigan

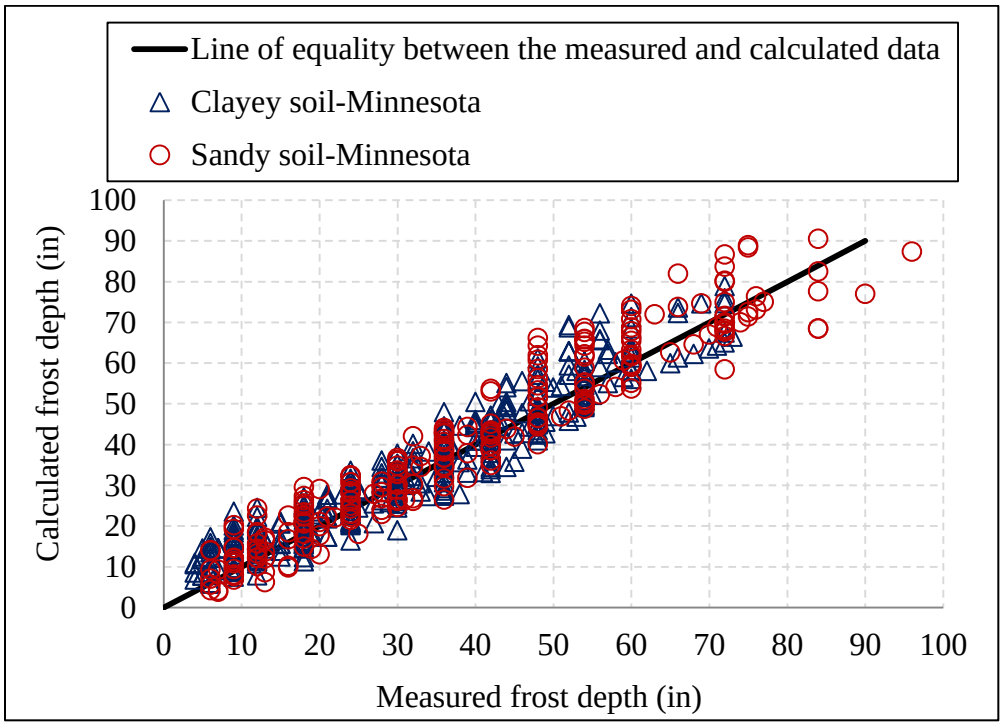

Figure 4-23 Calculated frost depths using Equation 4-12 versus the measured frost depth in clayey and sandy soil in the State of Minnesota

To further evaluate the validity of Equation 4-12, a statistical model was developed using the measured frost depth and the calculated CFDD for both soil types in Minnesota. The results are shown in Figures 4-24 and 4-25, respectively.

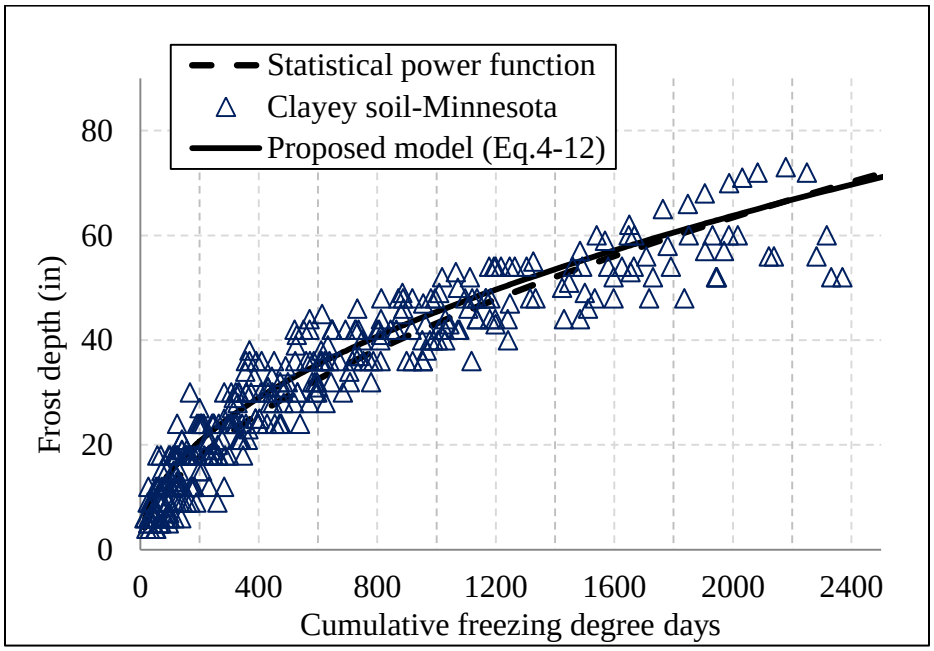

Figure 4-24 Frost depths versus cumulative freezing degree day for clayey soil showing the best fit statistical model and the proposed model (Equation 4-12) in Minnesota

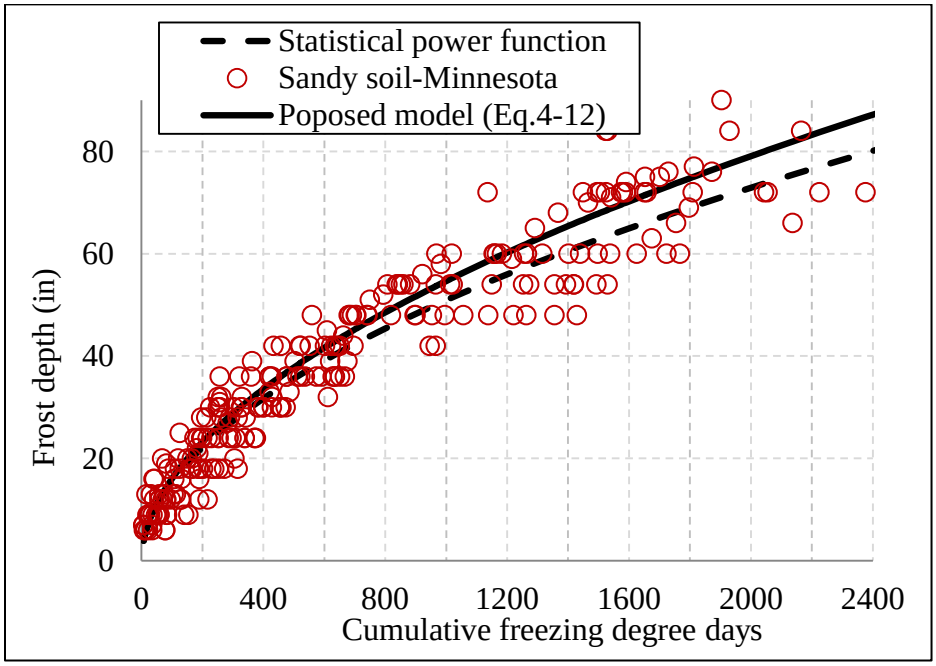

Figure 4-25 Frost depths versus cumulative freezing degree day for sandy soil showing the best fit and proposed model (Equation 4-12) in the State of Minnesota

The dashed and solid curves in Figures 4-24 and 4-25 represent the statistical model and Equation 4-12, respectively. Examination of Figure 4-24 indicates that Equation 4-12 and the statistical model produce almost the same results for clayey soils in Minnesota. On the other hand, the data in Figure 4-25 indicate that for sandy soil the differences between the results of the two models are less than 5 inches. This implies that Equation 4-12 can be used in Minnesota without calibration.

4.6 Thaw Depth

At the end of the freezing season, the soils start to thaw. The prediction of frost and thaw depths are crucial for estimating the amount of heave due to frost action and to estimate the proper time to post and remove seasonal load restriction signs. The calculation of frost depths is presented and discussed below.

4.6.1 Calculation of Cumulative Thawing Degree day (CTDD)

The cumulative thawing degree day (CTDD) was calculated using the approach proposed by MnDOT (See Section 2.3.2 of Chapter 2). Table 4-6 shows an example of CTDD calculation in one of RWIS stations, in Michigan.

4.6.2 Nixon and McRoberts Equation

After calculating the CTDD, Nixon and McRoberts equation (Equation 2-74) was used to estimate the depth of thaw at the various RWIS stations in the state of Michigan. Table 4-7 and Figure 4-26 depict the results. It can be seen from the figure that the results are not satisfactory. In fact, Equation 2-74 under predicts thaw depth by as much as 30 inches in some stations. The error could be related to the simplifying assumptions made in the equation, the lack of exact input data, or error in calculating the thaw index.

Although there are various methods and procedures for estimating the depth of thaw, the Nixon and McRoberts Equation is the only one that was evaluated in this study as specified in the proposal.

4.7 Frost Heave

Frost heave refers to the uplifting of the ground surface caused by freezing of water within the soil layers. In cold regions, frost heave could cause uplifting of the pavement structure, shoulders, and even unprotected foundations of bridges and trusses supporting highway signs

and utility lines (Liu et al., 2012). Frost heave can be influenced by various conditions including:

Table 4-6 Cumulative thawing degree day calculation, Waters, Lower Peninsula

Date	$T_{refrence}$ (F)	Average Air Temperature (^oF)	Thawing Degree Day (TDD) (^oF-day)	Freezing Degree Day (FDD) (^oF-day)	Cumulative Thawing Degree day (CTDD) (^oF-day)
2/3/2011	29.30	10.16	0	0	0
2/4/2011	29.30	18.46	0	0	0
2/5/2011	29.30	25.51	0	0	0
2/6/2011	29.30	31.36	2.06	0	2.06
2/7/2011	29.30	25.10	0	0	2.06
2/8/2011	28.40	10.15	0	0	2.06
2/9/2011	28.40	7.86	0	0	2.06
2/10/2011	28.40	8.70	0	0	2.06
2/11/2011	28.40	8.10	0	0	2.06
2/12/2011	28.40	14.13	0	0	2.06
2/13/2011	28.40	25.93	0	0	2.06
2/14/2011	28.40	33.67	5.27	0	7.33
2/15/2011	27.50	20.14	0	11.86	1.39
2/16/2011	27.50	25.97	0	0.00	1.39
2/17/2011	27.50	40.51	13.01	0.00	14.41
2/18/2011	27.50	41.76	14.26	0.00	28.66
2/19/2011	27.50	30.10	2.60	0.00	31.27
2/20/2011	27.50	19.68	0	12.32	25.11
2/21/2011	27.50	19.55	0	12.45	18.88
2/22/2011	26.60	12.87	0	19.13	9.317
2/23/2011	26.60	18.62	0	13.38	2.63
2/24/2011	26.60	24.64	0	0	2.63
2/25/2011	26.60	25.35	0	0	2.63
2/26/2011	25.70	24.15	0	0	2.63
2/27/2011	25.70	28.00	2.30	0	4.93
2/28/2011	25.70	17.13	0	0	4.93
3/1/2011	25.70	13.96	0	0	4.93

Table 4-7 Maximum thaw depth predicted by Nixon and McRoberts equation for RWIS stations

Location	Name of the Station	Type of Soil	Year	Maximum Measured Thaw Depth (in)	Maximum Calculated Nixon.Eq (in)
Lower Peninsula	Benzonia	Loose Sand	2010-2011	21	10
	Cadillac	Dense Sand	2010-2011	21	10
	Grayling	Dense Sand	2010-2011	46	20
	Houghton Lake	Dense Sand	2010-2011	46	25
	Ludington	Loose Sand with clay	2010-2011	34	16
	Reed City	Compacted Sand	2010-2011	28	10
		Loose Sand			
	Waters	Compacted Sand	2010-2011	21	14
		Loose Sand			
	Williamsburg	Dense Sand	2010-2011	21	14
		Silty Clay			
Upper Peninsula	Au Train	Sand with Gravel and Silt	2010-2011	46	19
		Loose Sand			
	Brevort	Loose Sand	2010-2011	46	21
	Harvey	Sand with Gravel and Silt	2010-2011	46	22
		Dense Sand			
	Golden Lake	Dense Sand with Gravel	2010-2011	62	24
	Seney	Loose Sand	2010-2011	40	23
	Cooks	Clayey Sand	2010-2011	46	20
	Michigamme	Clayey Sand	2010-2011	40	22
	St.Ignace	Silty Clayey Sand	2010-2011	34	21
	Twin Lakes	Silty Clayey Sand	2010-2011	40	19
	Engadine	Silty Clayey Sand	2010-2011	28	20

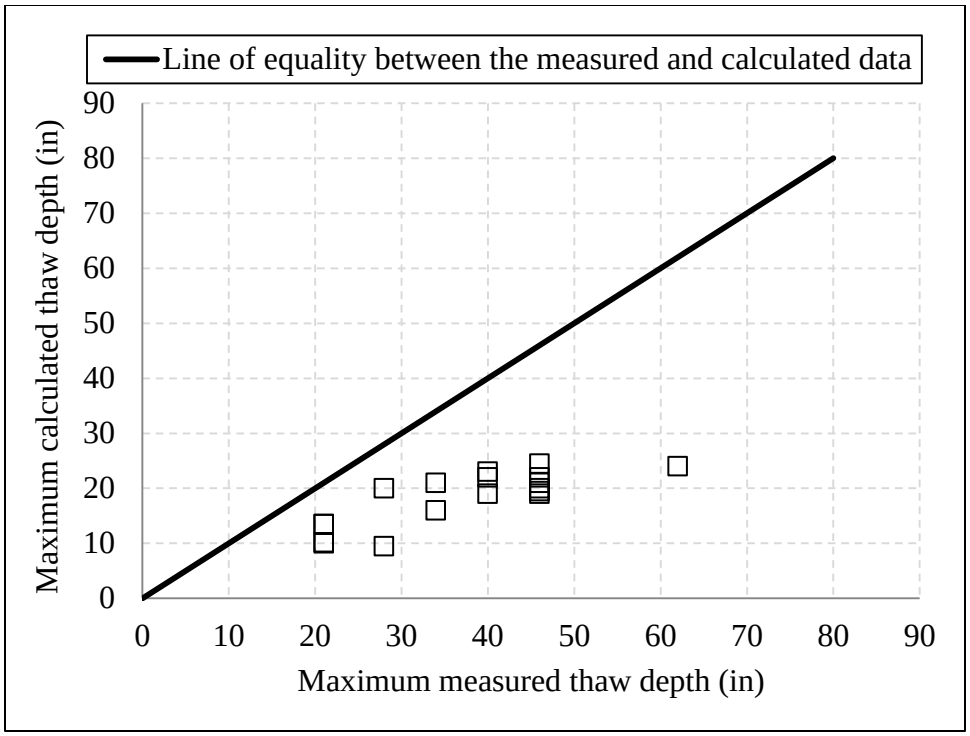

Figure 4-26 Maximum thaw depths predicted by Nixon and McRoberts equation versus the measured maximum thaw depths in Michigan

1. **Frost Susceptibility** – In general, the frost susceptibility of a soil is a function of its grain size and grain size distribution, which affect its capillarity and hydraulic conductivity (ACPA, 2008). There are various methods and criteria for the determination of soil frost susceptibility. In general frost susceptibility could be affected by soil type. In coarse material such as gravel and coarse sand hydraulic conductivity is high but capillary potential is low, whereas clay has low hydraulic conductivity and high capillary potential. Only fine sand and silt seem to have a balance between hydraulic conductivity and capillary potential. Figure 4-27 illustrates the dual effect of hydraulic conductivity and capillary potential on frost susceptibility. However, one of the most common criteria is based on the grain size distribution and the percent passing sieve number 200. The Canadian Department of Transportation developed another soil frost susceptibility criterion that also based on soil grain sized distribution as shown in Figure 4-28. Figure 4-29 and Table 4-8 show the susceptibility criteria developed by the U.S Corp of Engineers (COE).

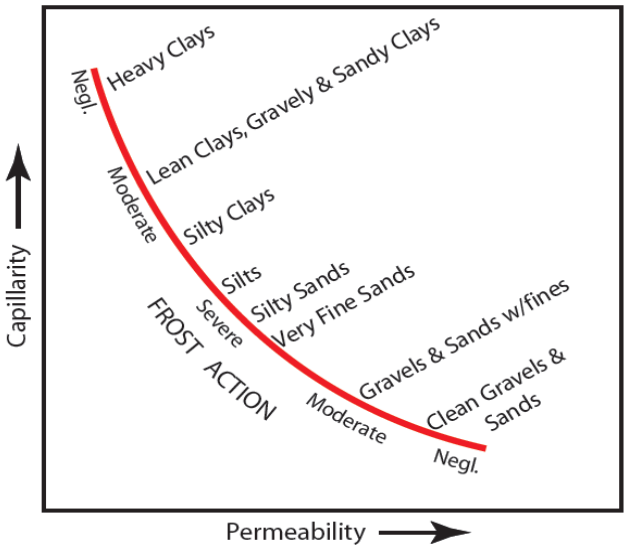

Figure 4-27 Effect of capillary potential and permeability on frost susceptibility (ACPA, 2008)

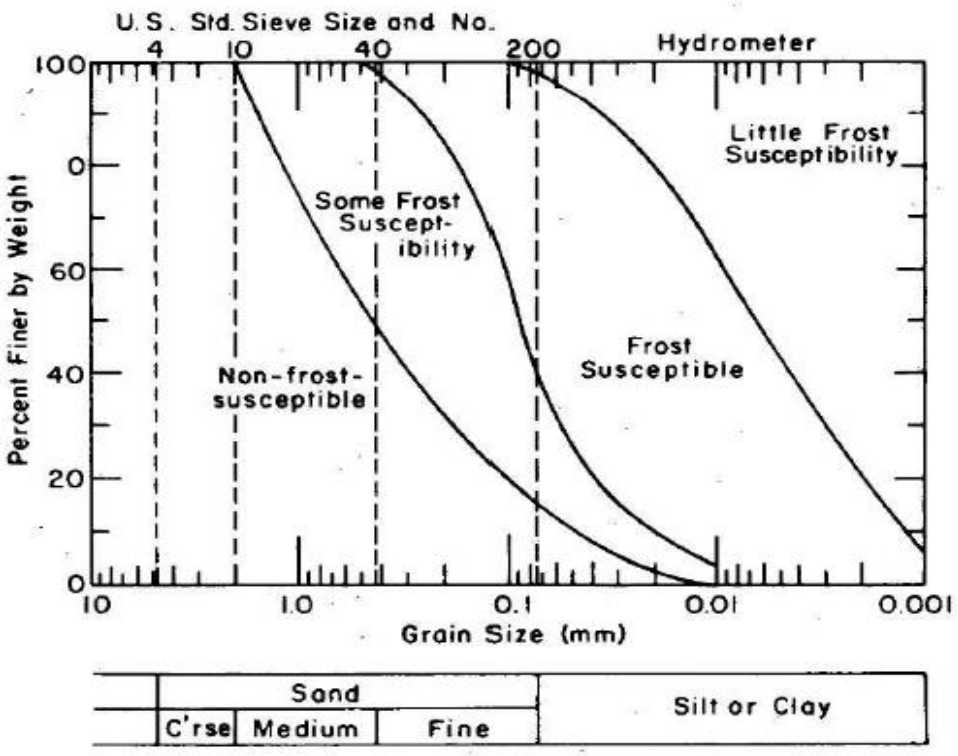

Figure 4-28 Frost susceptibility criteria, Canadian Department of Transportation (Edgar, 2014)

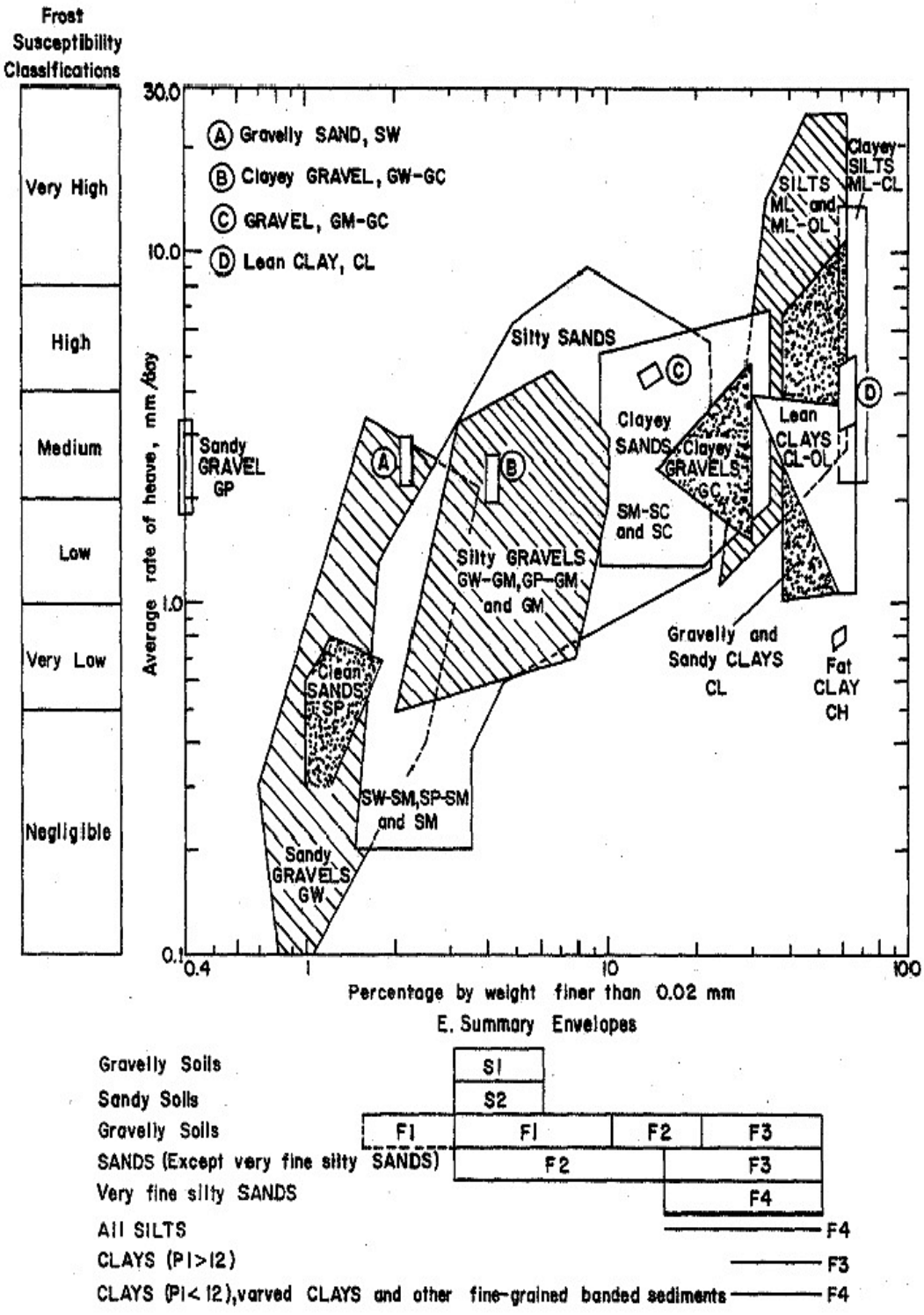

Figure 4-29 Heaving Rate in laboratory test on different disturbed soil types (COE, 1984)

Table 4-8 Frost susceptibility classification (COE, 1984)

Frost Group	Soil	Percentage Finer Than 0.02 mm by Weight	Typical Soil Types Under Unified Soil Classification System
Non-frost susceptible	(a) Gravel Crushed stone Crushed rock	0- 1.5	GW, GP
	(b) Sands	0- 3	SW,SP
Possibly frost susceptible, requires lab tests	(a) Gravel Crushed stone Crushed rock	1.5- 3	GW,GP
	(b) Sands	3- 10	SW,SP
S1	Gravely soils	3- 6	GW, GP, GW-GM, GP-GM
S2	Sandy soils	3- 6	SW, SP, SW-SM, SP-SM
F1	Gravely soils	6- 10	GM , GW-GM, GP-GM
F2	(a) Gravely soils	10- 20	GM , GW-GM, GP-GM
	(b) Sands	6- 15	SM , SW-SM, SP-SM
F3	(a) Gravely soils	Over 20	GM, GC
	(b) Sands, except very fine silty sands	Over 15	SM, SC
	(c) Clays, PI>12	---	CL, CH
F4	(a) Silts	---	ML, MH
	(b) Very fine, silty sand	Over 15	SM
	(c) Clays, PI< 12	---	CL, CL-ML
	(d) Varved clays and other fine-grained, banded sediments	---	CL, ML and SM, CL, CH and ML, CL, CH, ML and SM

2. **Below Freezing Temperature -** As stated in Chapter 2, freezing point depression occurs in pore water because of different reason such as intermolecular forces between water and soil (soil water surface tension) and salt solution. Therefore, pore water starts to freeze when the

air temperatures and consequently the ground surface temperature drops below the freezing temperature of 32^{o}F. The rate of water freezing is a function of the actual temperature below freezing and its duration. Colder and more sustainable below freezing temperatures accelerate the freezing rate and increases the depth of frost penetration and consequently increases the amount of ground heaving. Snow cover acts like insulator reducing frost depth substantially unless the air temperature and consequently the soil surface temperature drop significantly below the freezing temperature. However, for safety reasons, snow is typically removed from the pavement surface and accumulated near the shoulder as soon as possible. This causes higher frost depth and higher frost heave under the pavements relative to other areas covered by snow (Yoder, 1975). Further, salt and other deicing chemicals (typically used on roads during winter season) decrease the temperature at which water starts to freeze and causes decreases in frost depth and frost heave.

3. **Availability of Water Source –** If no free water is available, no water frost action will take place, hence, a source of water should be available under the pavement to start the free water freezing process. The water source could be as deep as 20 feet (Edgar, 2014). If the ground water level is shallow, frost heave can be observed even in course material (COE, 1984). Figure 4.30 shows the ASSHTO four different environmental regions in the United States. Only two regions, wet-freeze, and dry freeze are subjected to water freezing under the pavements. The wet freeze region is considered to be the most frost susceptible region (ACPA, 2008). As can be seen, the state of Michigan is located in the most frost susceptible region, the wet-freeze region. Hence, the estimation of frost depths and frost heave are two important factors that are typically considered in the design of pavement and bridge and other structural foundations.

4.7.1 Frost Heave Mitigation

The effects of frost heave on various structures vary from one structure to the next. Typically, structural foundations are constructed below the expected frost depths and hence, they are not affected by frost heave. Frost susceptible soils or free standing water behind bridge abutments and/or behind exposed retaining structures (such as retaining structures along depressed highways), are subjected to frost and frost heave causing active pressure against the structures. Basement retaining walls are rarely affected by frost due to heat loss from the basement interior that keeps the soil in the vicinity of the wall in relatively warm conditions. Pavement structures

are frost heave susceptible especially if the roadbed soils are not protected from frost action or if the granular base and subbase are subjected to saturation due to lack of proper drainage. Given the potential damage due to frost heave, different techniques have been proposed to mitigate frost heave damage especially in the pavement. The most common techniques are:

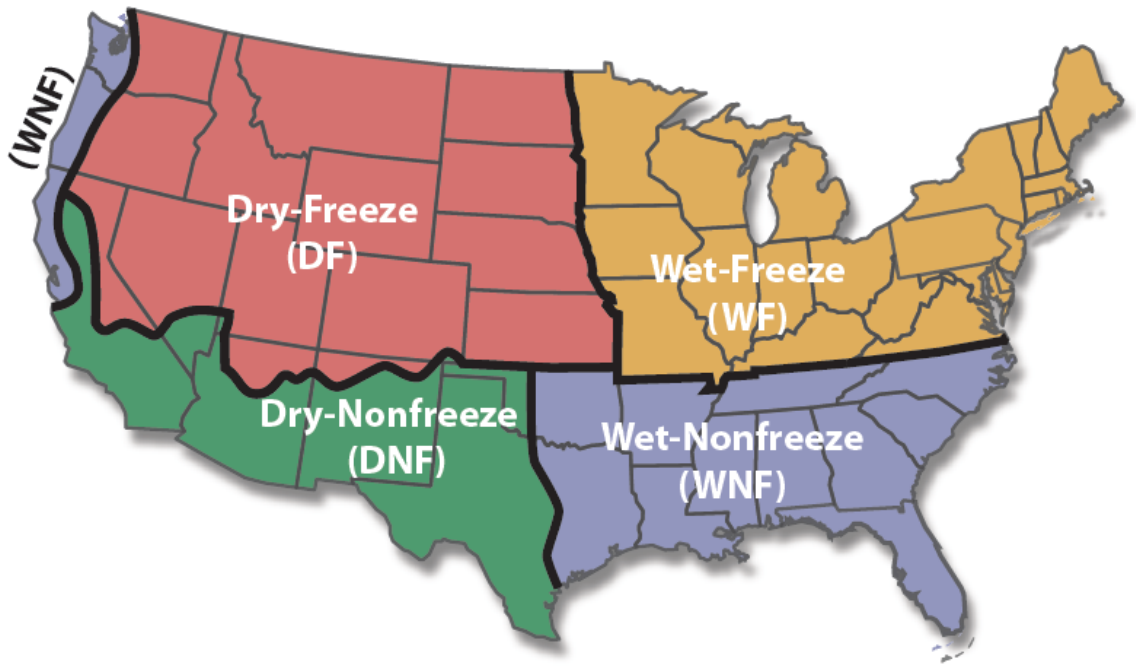

Figure 4-30 The AASHTO four environmental regions (ACPA, 2008)

1. **Cutting off the Water Source** - The source of water can be cut off in many different ways. One common technique is to install a barrier between the water source and the frost zone (Edgar, 2014). The barrier reduces the capillary action and consequently reduces frost heave. A blanket or a layer of gravel and crushed stone under the pavement or wrapping the roadbed soil by a geo-membrane layer could be effective in decreasing access to water (Wallace, 1987; Edgar, 2014). Another technique is to remove water using a proper drainage system. In pavements, drain tile, edge drain, and/or open side ditches can be built to remove the water. In retaining wall, weep holes can be installed at the foot of the wall which is exposed to frost (Wallace, 1987).
2. **Removing Frost Susceptible Soil** - As stated in the previous section, some soils are more frost susceptible than others. Such soils can be replaced by non-susceptible soils if the cost is

not prohibitive. In a typical scenario, the various frost heave mitigation options are assessed against their costs. The most cost effective option is typically chosen.

3. **Reducing Freezing Depth –** Although different approaches can be used to prevent frost penetration, two of these approaches are insulation and chemical additives to lower the water freezing temperature. Since insulation is the most common method, it is detailed further below.

Insulation Method – This method could be used in many different structures to decrease heat loss from the soil to the atmosphere. In pavements, an insulation layer is typically placed above the roadbed soils to protect the soils from freezing. Rigid polystyrene foams (RPF) are commonly used for frost protection under different building foundation and infrastructures. Two types of polystyrene have been used; expanded polystyrene (EPS) and extruded polystyrene (XPS).

The insulation materials are usually known by their thermal resistivity (R-value). R-value is an indication of material resistance to heat flow. It has inverse relationship with thermal conductivity of the material (Edgar, 2014). Table 4-9 shows the R-value of different RPF according to ASTM C578. It should be noted that the nominal R-value varies depending on moisture exposures condition. Moisture condition could vary from one site to another and it depends on the drainage system and on the direction along which the insulation is installed (vertical or horizontal). Therefore in the design process, the effective R-values are calculated or estimated and used.

Another important property of the PRF is the minimum thickness. Non-uniform distribution of moisture in RPF leads to edge effects and as the insulation thickness decreases it impacts the thermal performance of the RPF. It should be noted that the effect of the thickness varies depending on the insulation type and moisture conditions (Crandell, 2010). Table 4-10 shows the Design values for frost protected shallow foundation (FPSF) RPF based on ASCE 32-01.

Various researches investigated the effect of temperature and moisture conditions on the RPF properties. Ojanen and Kokko (1997) used data from different highway projects to evaluate the EPS performance. They found that the thermal conductivity measured at 23 ^{o}F is the most relevant to the highway conditions. Their data showed that with proper drainage, the long term moisture contents in EPS under highways are in the range of 0.5 to 2.5 %. Sandberg (1986) did

research on RPF performance under highways. He found that moisture content distribution is highly non-uniform in XPS which reduces the influence of moisture content on R-value in comparison to EPS (Crandell, 2010). Nevertheless, it is apparent that XPS performs consistently under different conditions. But EPS performance could vary based on the moisture content, density and manufacturing process (Crandell, 2010).

Table 4-9 Thermal resistance values (R-values) at different mean temperature

Classification	XI	I	VII	II	IX	XIV	XII	X	IV	VI	VII	V
Minimum density lb/ft^3	0.7	0.9	1.15	1.35	1.8	2.4	1.2	1.3	1.45	1.8	2.2	3.0
Mean Temperature	Thermal resistance of 1 inch thickness minimum ($F.ft^2.h/Btu$)											
25 ± 2 ^oF	3.45	4.20	4.40	4.60	4.80	4.80	5.20	5.60	5.60	5.60	5.60	5.60
40 ± 2 ^oF	3.30	4.00	4.20	4.40	4.60	5.00	5.40	5.40	5.40	5.40	5.40	5.40
110 ± 2 ^oF	2.90	3.25	3.45	3.65	3.85	3.85	4.30	4.65	4.65	4.65	4.65	4.65

Insulation Effect on The Frost Depth - As stated before, insulation is typically used to reduce heat flow and prevent heat loss in temperatures below 32 ^oF. Since the thermal conductivity of the insulation material is low, the heat loss decreases across the soil layer and the temperature remains above freezing point.

Equation 4-13, which is based on conservation of energy governs the Temperature variation in a soil layer (Jiji, 2009). Since no energy is generated in the freezing process, the equation can be rewritten as in Equation 4-14. Using Fourier's law, the heat flux can then be calculated using Equation 4-15;

Table 4-10 Design values for FPSF insulation materials based on ACSE 32-01

Insulation Type	**Minimum Density ($lb./Ft^{3)}$)**	**Effective Resistivity (R/In.)**		**Nominal Resistivity (R/In.)**	**Allowable Bearing Capacity (Psf)**	**Minimum Insulation Thickness (In.)**	
		Vertical	**Horizontal**			**Vertical**	**Horizontal**
ESP							
II	1.35	3.2	2.6	4.0	N/A	2	3
IX	1.80	3.4	2.8	4.2	1200	1.5	2
XPS							
X	1.35	4.5	4.0	5.0	N/A	1.5	2
IV	1.6	4.5	4.0	5.0	1200	1	1.5
VI	1.8	4.5	4.0	5.0	1920	1	1
VII	2.2	4.5	4.0	5.0	2880	1	1
V	3.0	4.5	4.0	5.0	4800	1	1

$$\dot{E}_{in} + \dot{E}_g - \dot{E}_{out} = \dot{E} \qquad \text{Equation } 4-13$$

$$\dot{E}_{in} - \dot{E}_{out} = \dot{E} \qquad \text{Equation } 4-14$$

$$\dot{E}_{in} - \dot{E}_{out} = -k\frac{\partial^2 T}{\partial z^2} \qquad \text{Equation } 4-15$$

Where $\dot{E}$ = rate of energy change within the region (Btu/hr);

$\dot{E}_{in}$ = rate of energy added (Btu/hr);

$\dot{E}_g$ = rate of energy generated (Btu/hr);

$\dot{E}_{out}$ = rate of energy removed (Btu/hr);

T= temperature in the soil layer (^{o}F);

k= Thermal conductivity of the soil layer (Btu/(ft.hr.^{o}F)); and

z= depth from the ground surface (ft).

The rate of energy change within the region can be calculated using Equation 4-16. Thus, Equation 4-14 can be rewritten as Equation 4-17 (Edgar, 2014).

$$\dot{\mathrm{E}} = C\frac{\partial \mathrm{T}}{\partial \mathrm{t}} \qquad \text{Equation } 4-16$$

$$C\frac{\partial T}{\partial t} = -k\frac{\partial^2 T}{\partial z^2} \qquad \text{Equation } 4-17$$

Where C= volumetric heat capacity (Btu/ (ft^3.^{o}F));

t= time (hr); and

All other parameters are the same

It should be noted that Equation 4-17 does not consider the phase change effect in the soil layer but since in RPF latent heat of fusion is negligible, this equation can be used for modeling an insulation layer. By assuming that surface temperature varies in a sinusoidal manner, solution to Equation 4-17 can be obtained using Equation 4-18 (Edgar, 2014).

$$T(z,t) = T_{ave} + A_0 * e^{\frac{-z}{d}} * \sin\left(\omega t - \frac{z}{d}\right) \qquad Equation\ 4-18$$

Where $T(z,t)$= temperature variation at depth for each time interval (^{o}F);

T_{ave}= the average temperature in soil layer (^{o}F);

A_0= amplitude of the sine wave which relates to surface temperature fluctuation;

d= depth that relates the reduction in temperature fluctuation A_0 to depth (^{o}F);

ω = time frequency; and

All other parameters are the same as before.

As stated above, the parameter "d" in Equation 4-18 is the characteristic depth that relates the reduction in surface temperature fluctuation to depth and can be calculated using Equation 4-19 (Edgar, 2014).

$$d = (\frac{2k}{C\omega})^{\frac{1}{2}} \qquad Equation\ 4-19$$

Where all parameters are the same as before.

According to Equation 4-19, adding a low thermal conductivity layer could significantly influence the temperature pattern in the soil. In fact, adding an RPF layer has the same effect as adding additional soil to the layer.

Therefore the thickness of the RPF can be modeled as :

$$t_{RPF} = d_{soil} * \sqrt{\frac{k_{RPF}}{k_{soil}}} \qquad Equation\ 4-20$$

Where t_{RPF} = insulation thickness (in);

d_{RPF} = depth of the soil layer (in);

k_{soil}= thermal conductivity of soil (BTU /(ft^2.hr.^{o}F))

k_{RPF}= the effective thermal conductivity of insulation layer (BTU /(ft^2.hr.^{o}F))

The thickness of the RPF can be calculated using Equation 4-12

$$t_{RPF} = \left((-0.45\ k_{soil} + 1.9614) * CFDD^{(.0913k_{soil}+0.4143)} - d_{RPF}\right) * \sqrt{\frac{k_{RPF}}{k_{soil}}} \qquad Equation\ 4-21$$

Where d_{RPF} = depth of insulation (in);

CFDD= cumulative freezing degree day in design year (^{o}F-day); and

All other parameters are the same as before.

- **Example**

  Calculate the thickness of the insulation for the given data.

  1. CFDD in design year = 800 ^{o}F-day;
  2. d_{RPF} = 36 in.
  3. k_{soil}= 1.4 (BTU /(ft^2.hr.^{o}F)).
  4. The effective insulation R-value=4.5 → k $_{RPF}$ =1/(4.5*12)= 0.0183 (BTU /(ft^2.hr.^{o}F)))

  The thickness of the insulation layer can be calculated using Equation 4-21.

$$t_{RPF} = ((-0.45 * 1.4 + 1.9614) * 800^{(.0913*1.4+0.4143)} - 36)\sqrt{\frac{0.0183}{1.4}} = 1.5\ in$$

4.7.2 Gilpin Frost Heave Model

Different theories and models for modeling frost heave are reviewed in Chapter 2 of this report. In this study, the Gilpin's model, which is based on frozen fringe theory, was used to predict the frost heave under field conditions. As stated before the original Gilpin model is a mechanistic-empirical model based on heat and mass balance equations and laboratory data. The Gilpin model is a laboratory based model and applying it to field conditions having different boundary values led to some errors in the results. Further, the required input data to the model are not available and are expensive to obtain. Therefore, in this study, the model was simplified to include the empirical frost depth prediction model developed by the research team. The resulting model was verified by comparing the predicted frost heave under pavements and shoulders to the measured values at 5 different sites in Oakland County, Michigan.

Basic Assumptions- A saturated, salt-free soil column was subjected to a constant overburden pressure (P_{OB}) as shown in Figure 4-31. The top of the column was subjected to a fixed sub-freezing temperature (T_{TOP}), whereas the bottom of the column (at the ground water table elevation) was at a fixed above freezing temperature (T_{BOT}). The soil column was assumed to consist of three zones; frozen zone at the top followed by a frozen fringe zone and then by an unfrozen zone. The top of the unfrozen zone begins at a point where water and ice can exist in the pore spaces of the soil at below freezing temperature (T_f). In this model frost penetration and frost heave were predicted using analytical iteration solution. In each iteration, it was assumed that

1. The temperature variation in each zone is linear.
2. The thermal conductivity in each zone is constant.
3. Each of the water content and permeability in the unfrozen zone is constant.
4. The water flow through the frozen fringe and unfrozen zones is at steady state.

Heat and Mass Balance Equations - As stated in Chapter 2, for simulating the heat transfer in his model, Gilpin used the phase-change heat transfer equations. After imposing the boundary conditions in each zone, Equation 2-42 and 2-43 were obtained for heat transfer between frozen and frozen fringe zones and frozen fringe and unfrozen zones, respectively.

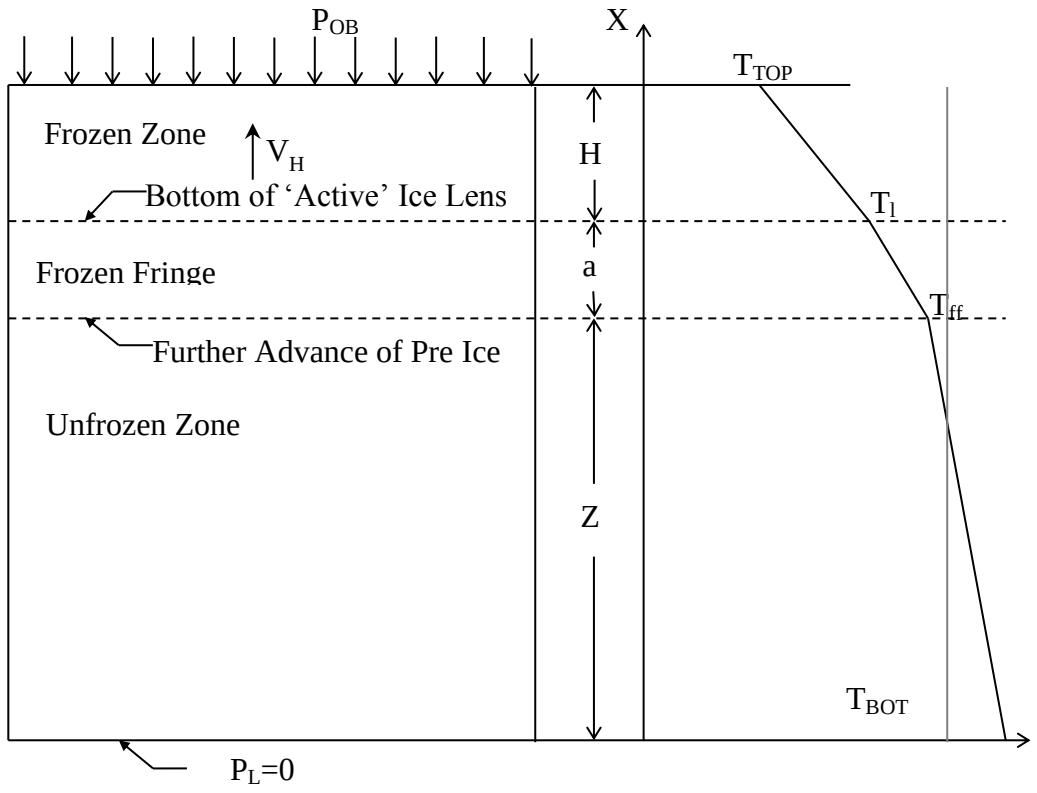

Figure 4-31 The schematic of frost heave model (Gilpin, 1980)

Using the mass balance equation and imposing boundary conditions, Gilpin proposed Equation 2-45 for calculating the water pressure at the bottom of the frozen fringe zone. Finally Equation 2-46 was obtained for frost heave calculation. It should be noted that Gilpin proposed semi-empirical models for estimating the hydraulic conductivity of frozen fringe and the temperature at the bottom of the frozen fringe zone, T_f (Gilpin 1980).

Ice Pressure Distribution in The Frozen Fringe Zone - Gilpin calculated the ice pressure distribution in the frozen fringe zone in order to model the initiation of new ice lenses. He assumed that the initiation of new ice lenses takes place where the ice pressure in the frozen fringe zone exceeds the critical pressure, which is also known as the separation pressure. This pressure is a function of the overburden pressure and water-ice curvature. Figure 4-32 illustrates

the ice pressure distribution. Based on Clapeyron equation, at zero flow rate in the frozen fringe zone, the ice pressure increases along the solid line ($L(-T)/(v_s T_a)$). Further, at non-zero flow rate the ice pressure increases along the P_s line so that it becomes equal to the overburden pressure at the top of frozen fringe zone. Ice pressure in the frozen fringe zone could be estimated using Equation 4-22.

$$V_H * \frac{v_w}{v_i} = K_{ff} \frac{v_i}{g} \frac{d}{dx} \left[P_i + \frac{LT}{v_i T_m} \right] \qquad Equation\ 4-22$$

Where v_w = specific volumes of water (m^3/Kg);

v_i = specific volumes of ice (m^3/Kg);

V_H= frost heave rate (m/s);

K_{ff} = the permeability in the frozen fringe (m/s);

g = acceleration of gravity (m/s^2);

P_i = pressure in ice (Pa);

L = latent heat of fusion of water (J/Kg);

T_m = bulk freezing temperature (^{o}K); and

T= temperature along the frozen fringe (^{o}C.).

For modeling the separation pressure, a pair of spherical soil particles was considered as shown in Figure 4-33. In the absence of ice, the overburden pressure is acting on the interface of the particles. This pressure could be transmitted from one particle to the other. However, at a critical ice pressure, the pressure at the contact point drops to zero allowing the ice to separate the particle from each other. This critical ice pressure was assumed to be the separation pressure. Where ice pressure in frozen fringe zone exceeds the separation pressure new ice lenses are formed. Estimation of the separation pressure was a matter of debate between researchers; Gilpin suggested the following equation for separation pressure:

$$P_{sep} = P_{OB} + \frac{2 * \sigma_{iw}}{D_{10}} \qquad Equation\ 4-23$$

Where P_{sep} = separation pressure (Pa);

D_{10}= particle size at 10 percent passing (m)

σ_{iw} = ice-water surface energy (N/m); and

P_{OB}= overburden pressure (Pa).

Other equations were developed and are available in the literature. However, in this study, the Gilpin equation was revised to simplify the required inputs and used to predict the frost heave potential.

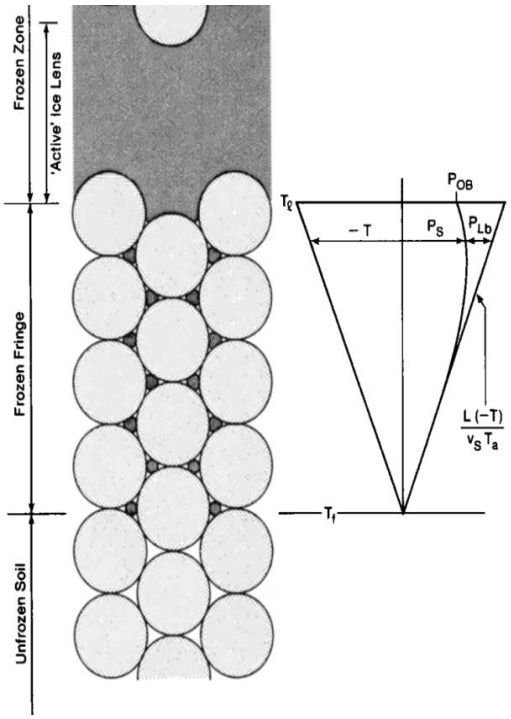

Figure 4-32 Ice pressure along frozen fringe zone (Gilpin, 1980)

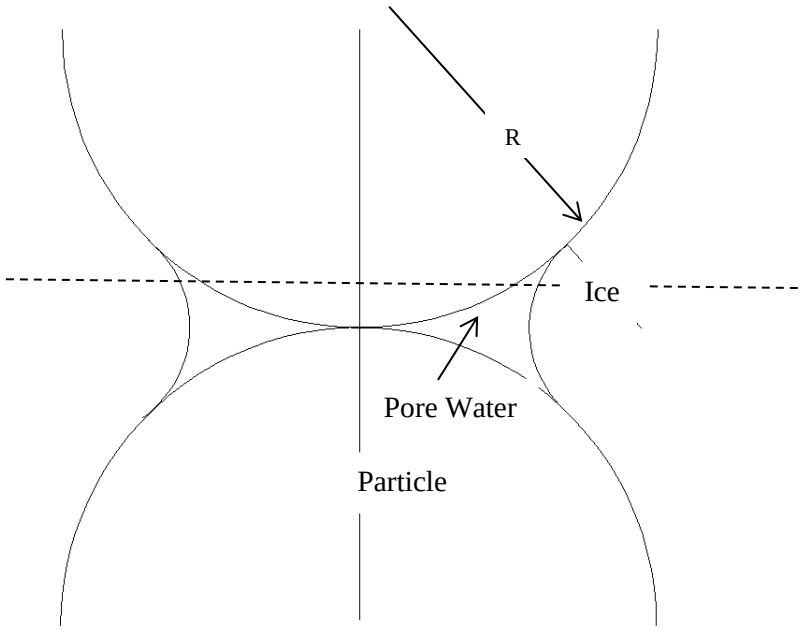

Figure 4-33 Particle separation pressure

4.7.3 Revised Frost Heave Model

In the Gilpin model at the beginning of the solution initial non-zero values were chosen for *a* and *H* in order to avoid the infinite temperature gradient (See Figure 4-31). At each iteration (Δt) , the systems of four equations were solved to calculate the four unknowns, i.e. V_H, P_{wf}, T_l and *dz/dt*. It should be noted that since Equation 2-46 is nonlinear the accuracy of the results are highly related to the nonlinear solution. After calculating V_H, ice pressure in the frozen fringe was calculated using Equation 4-22. If the ice pressure did not exceed the critical pressure then *H* was increased by $V_H * \Delta t$; *a* was increased by $dz/dt * \Delta t$ and the equations were solved for the next iteration. Otherwise a new ice lens was assumed to initiate where ice pressure exceeded the critical pressure, *H* was increased and *a* was decreased accordingly. Then V_H, P_{wf}, T_l and *dz/dt* were calculated again for the same time step (Gilpin, 1980).

In Gilpin model, the hydraulic conductivity of the frozen fringe zone (K_f) was estimated based on the laboratory data. Since laboratory conditions were not necessarily correlated well with the field conditions and field data were not available for calibration, an overall permeability (K_f) was assumed for the frozen fringe zone in order to avoid nonlinear solution. . Further, due to a large frozen zone thickness in the field, the frozen zone was assumed to be impermeable.

T_{ff} (temperature at the bottom of frozen fringe) was calculated using the following empirical equation (Gilpin 1980).

$$T_{ff} = -\frac{8\sigma_{iw}\nu_w T_m}{D_{10} * L} \qquad Equation\ 4-24$$

Where all parameters are the same as before.

In the revised model, instead of using Equation 2-43 for calculating the frost depth propagation, the empirical frost depth model that was developed based on the measured frost depths data Michigan was used (Equation 4-12). The analyses were conducted using analytical iterative solution. In each iteration, the frost depth propagation rate ($\frac{dz}{dt}$) was calculated using Equation 4-25 and 4-26 and the T_l was estimated using Equation 4-27.

$$\frac{dz}{dt} = 2.9 * 10^{-7}\left(-0.26\, k_{uf} + 1.9614\right)\beta \qquad Equation\ 4-25$$

$$\beta = \left((1.8 * \sum_{i=1}^{n} T_{Top}\,)^{(0.0528k_{uf}+0.4143)} - (1.8 * \sum_{i=1}^{n-1} T_{Top}\,)^{(0.0528k_{uf}+0.4143)}\right) Equation\ 4-26$$

$$T_l = T_{ff} - \frac{a}{k_{ff}} * (\rho_{si} L \frac{dz}{dt} + \frac{k_{uf}(T_{BOT} - T_{ff})}{Z}) \qquad \text{Equation } 4-27$$

Where T_{top}= subzero surface temperature (^oC- day); and

All parameters are the same as before

Furthermore, Equation 2-46 was revised into Equation 4-28 and by solving Equations 2-45 of Chapter 2 and Equation 4-28, the values of V_H *and* P_{wf} were calculated.

$$P_{wf} = -g\frac{z}{\nu_w}\left(1 + \frac{\nu_w}{\nu_i}\frac{\left(V_H + \rho_{st}\Delta\nu\frac{dz}{dt}\right)}{K_{uf}}\right) \qquad \text{Equation } 2-45$$

$$V_H = \frac{\nu_i^2}{g\nu_w}\frac{K_{ff}}{a}\left[\frac{L(-T_l)}{\nu_w T_m} - P_{OB} + P_{wf}\right] \qquad Equation\ 4-28$$

Where K_{ff} = over all permeability of frozen fringe (m/s); and

All other parameters are the same as before.

Finally, the ice pressure variation in the frozen fringe zone was calculated using Equation 4-22. New ice lens formation was assumed where the pressure value is higher than the separation pressure. Therefore the thicknesses of the frozen fringe and the frozen zone were changed accordingly and consequently, the calculations of $V_{H,}$ T_l, P_{wf} were repeated.

The total frost heave was then estimated using the following equation:

$$\Delta h_{total} = \Delta h_u + \Delta h_i = V_H * \Delta t + 0.09 * n * H \qquad 4-29$$

Where Δh_{total} = total frost heave (m);

Δh_u = frost heave due to water uptake (m);

Δh_i = heave due to freezing of in-situ pore water (m);

Δt = time interval (s);

n = soil porosity, and 0.09 is the ratio of volumetric expansion of water in phase change (Nixon 1982); and

All other parameters are the same as before.

4.7.4 Discussion of the Results of the Revised Frost Heave Model

At the beginning of the frost, the heave rate is high therefore the ice pressure in the frozen fringe zone could surpass the separation pressure and the frozen zone keeps lowering in the soil column. As frost progresses, the heave rate decreases and consequently the ice pressure

decreases and it does not exceed the separation pressure anymore. This causes growth in the frozen fringe zone. Since the hydraulic conductivity of the frozen fringe zone is less than that of the unfrozen zone the larger frozen fringe zone leads to lower heave. The extent of the frozen fringe zone depends on the types of the soil and overburden pressure.

1. **Soil Type** - The hydraulic conductivity of fine sand is higher than the clayey silt so the flow rate is greater in fine sand. However, as mentioned before, capillary pressure is mainly responsible for the frost heave phenomenon. Due to the aggregate size, suction is smaller in fine sand than in clayey silt, therefore larger frost heave rates are expected in clayey silt. Further, in fine sands relative to clayey silts a larger frozen fringe zone is observed. Figure 4-34 and 4-35 depicts the calculated frost heave and frozen fringe thickness in three different types of soil versus time, respectively.

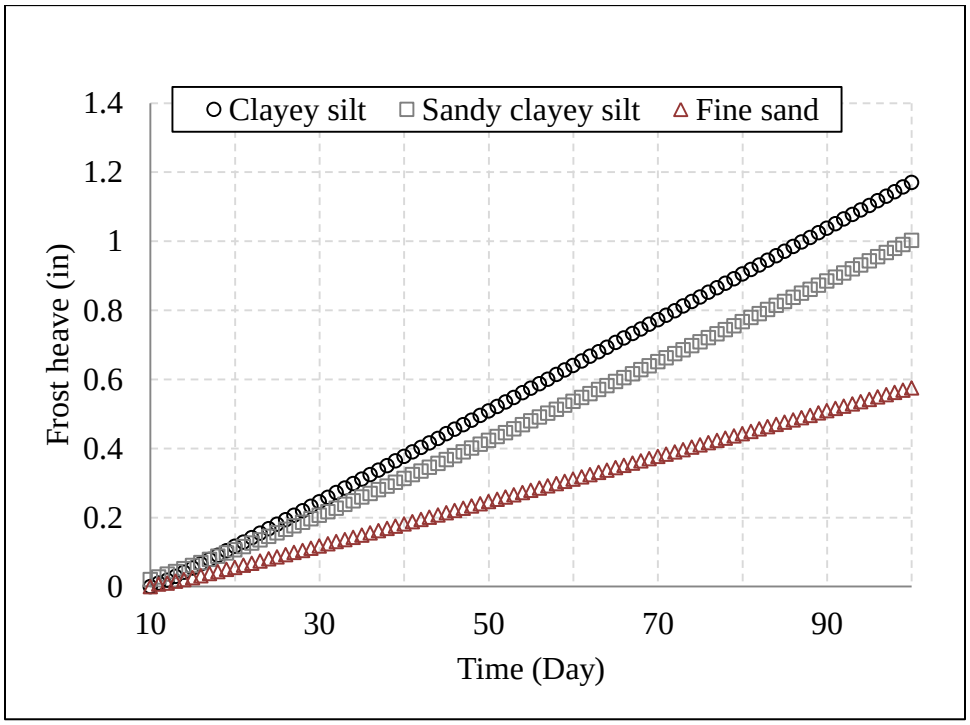

Figure 4-34 Calculated frost heave for three soil types when GWL= 30 ft, T_{TOP}= 29 ^{o}F for 100 days

2. **Overburden Pressure –** Various overburden pressures were used to assess the impact of overburden pressure on the frost heave and frozen fringe zone. Konrad and Morgenstern (1982) found out that the overall permeability of the frozen fringe zone decreases approximately by 25% as the overburden pressure increases up to 400kPa. Accordingly, in the revised model, the frozen fringe zone permeability was reduced as the overburden

pressure was increased. Figure 4-36 to 4-39 show the model results for total heave in different overburden pressures for different Z values when the T_{TOP} was fixed at 26 ^{o}F for 100 days in different soil types. As can be seen in the figures, when the ground water table is deep, for the same freezing time period, less amount of water can reach the frozen zone and therefore the frost heave decreases.

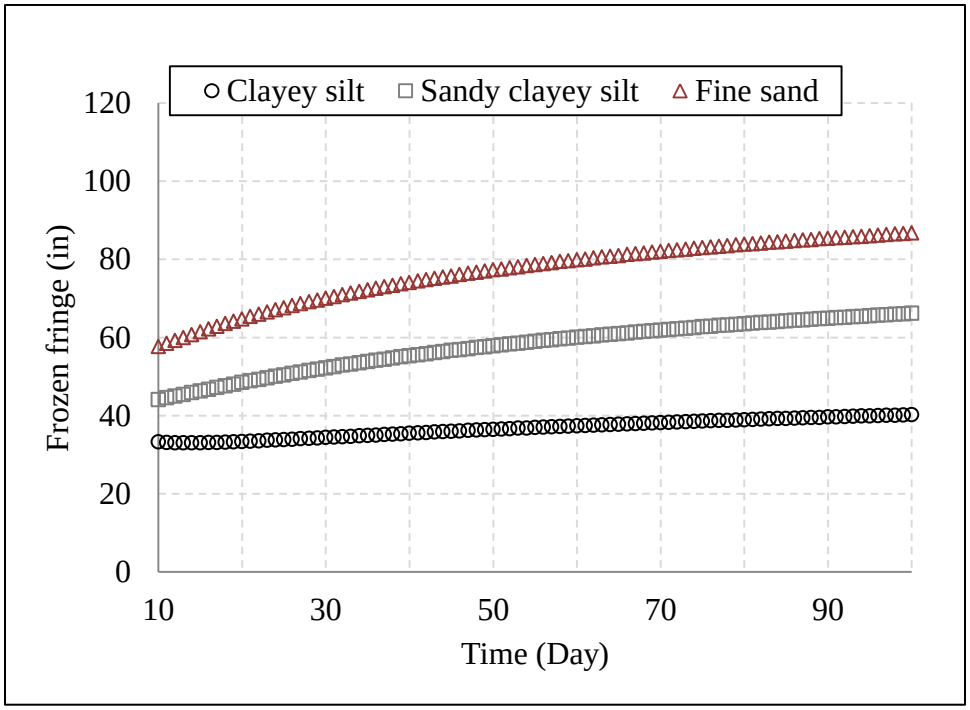

Figure 4-35 Calculated frozen fringe for three soil types when Z= 30 ft, T_{TOP}= 29 ^{o}F for 100 days

At higher overburden pressures, the separation pressure is larger therefore it is expected that the frozen fringe zone thickness increases as the overburden pressure increases. This leads to lower frost heave values in higher overburden pressures.

In order to assess the impact of surface temperature (i.e. T_{TOP}), the model was assessed with a fixed T_{TOP} and with a changing T_{TOP} but a fixed rate of cooling. In both scenarios the freezing index was the same. The results are depicted in Figure 4-40. It can be seen from the figure that the results are almost the same in both assessments, therefore using a fixed T_{TOP} based on the cumulative freezing index and length of frost period is a good assumption.

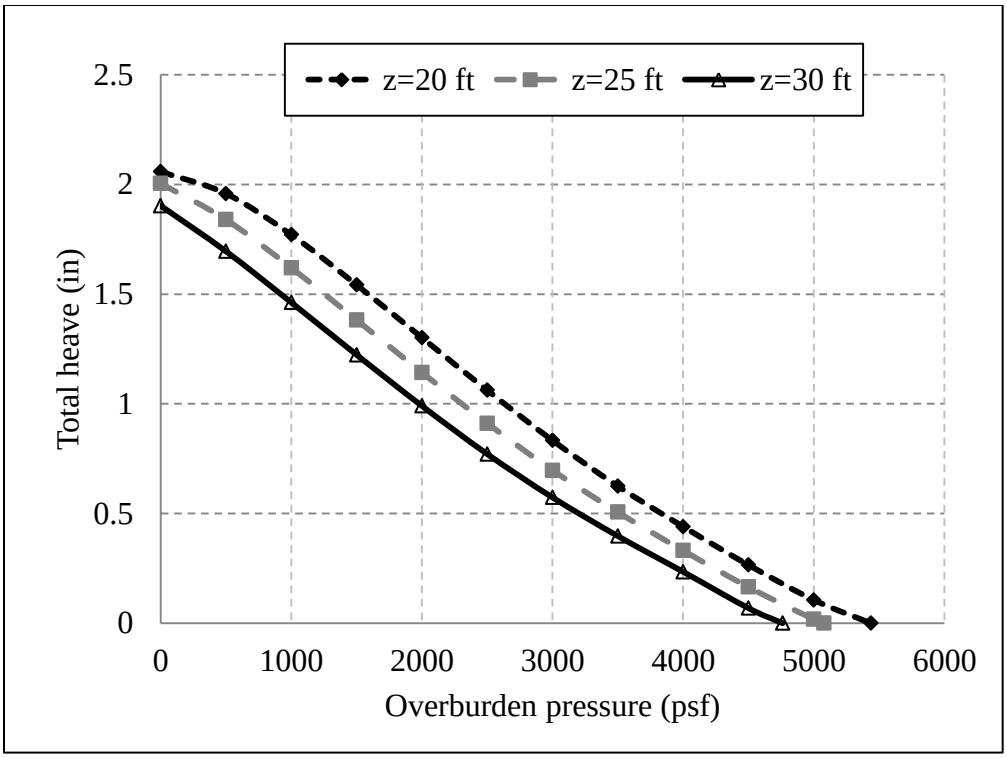

Figure 4-36 Calculated total heave versus overburden pressure for clayey silt in different ground water table depths when T_{TOP}= 26 ^{o}F in 100 days

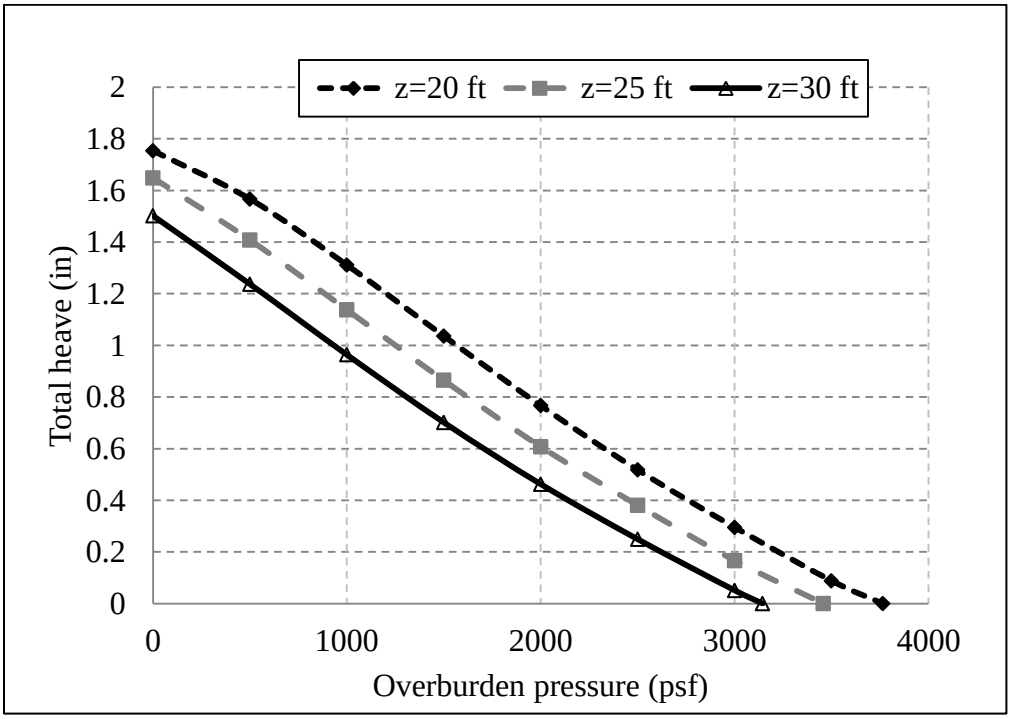

Figure 4-37 Calculated total heave versus overburden pressure for sandy clayey silt in different ground water table depths when T_{TOP}= 26 ^{o}F in 100 days

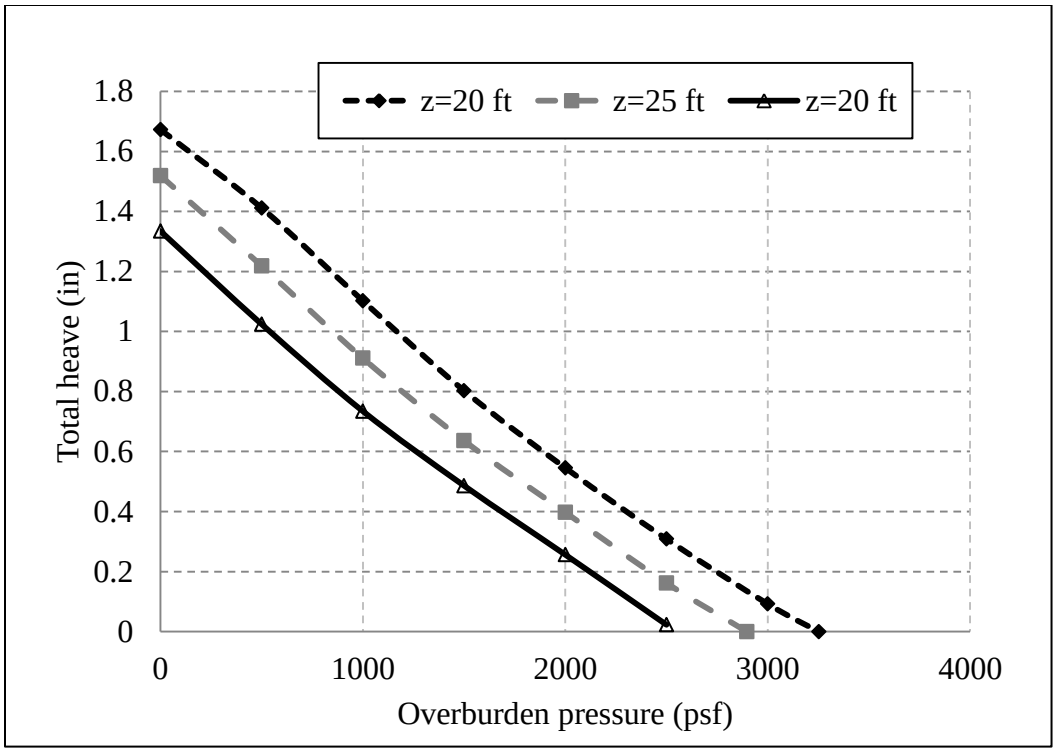

Figure 4-38 Calculated total heave versus overburden pressure for fine sand and silt with pebbles in different ground water table depths when T_{TOP}= 26 ^{o}F in 100 days

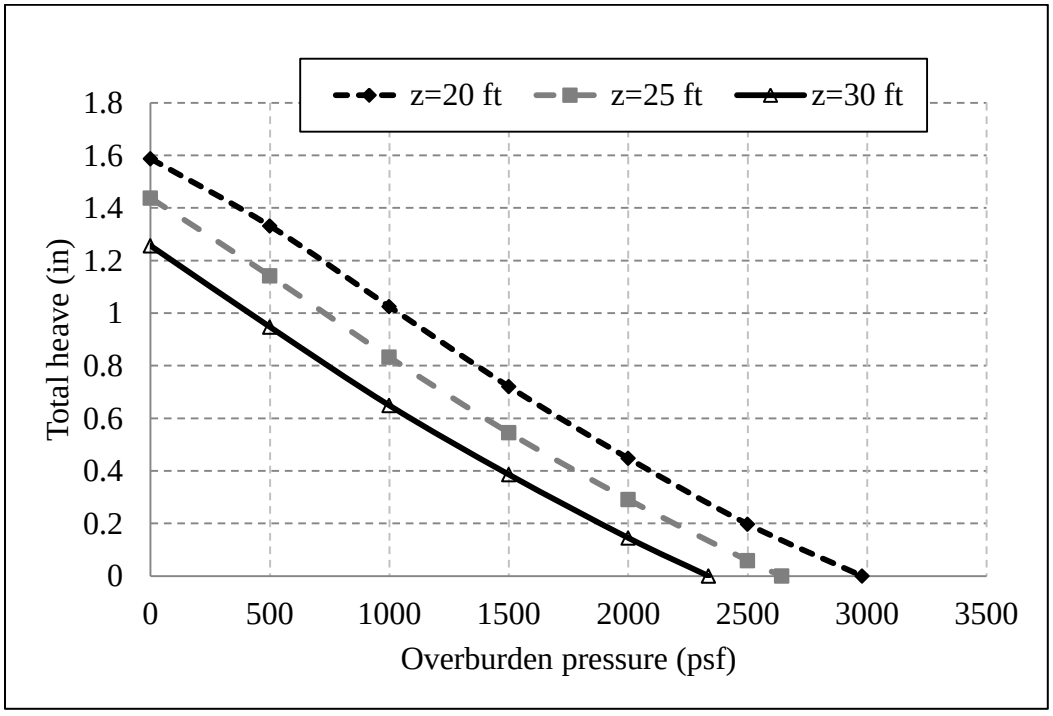

Figure 4-39 Calculated total heave versus overburden pressure for clayey, silty, gravely, sand in different ground water table depths when T_{TOP}= 26 ^{o}F in 100 days

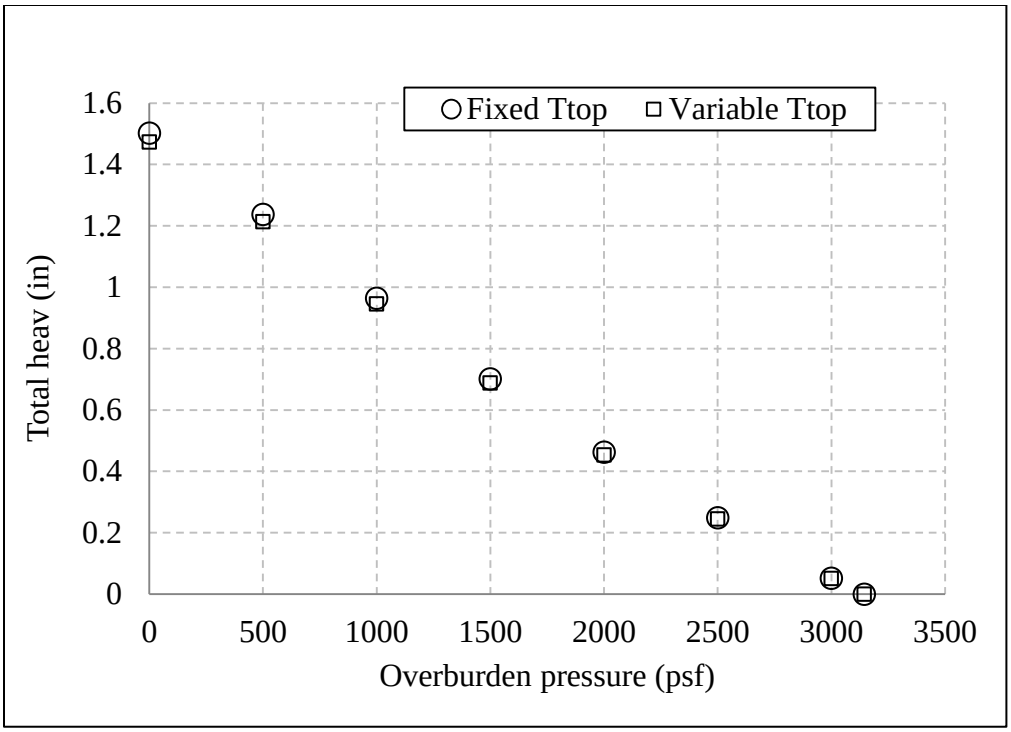

Figure 4-40 Total heave versus overburden pressure for clayey silt when T_{TOP} is fixed at 26 ^{o}F and when T_{TOP} is decreasing with a rate of -.057 per day in 100 days

Furthermore, the revised model was used to predict the frost heave under shoulder and pavement. Data from 5 sites located in Oakland County, Michigan were provided by the Michigan Department of Transportation (See Chapter 3-4). In order to validate the revised model, this data was used. According to each soil description and size distribution, hydraulic conductivity and D_{10} values were chosen. Thermal conductivity values were chosen according to the soil type from the measured thermal conductivity values (See Table 3-4).

Furthermore by using the measured frost depth at maximum heave and Equation 4-12 the CFDD values and the T_{TOP} for each site were calculated. The inputs for each soil type are shown in Table 4-11.

As stated before, the frost heave occurs when water migrates from water table to the frozen layer. Therefore, the controlling layer is the natural soil. It can be assumed that frost heave could be calculated by a single layer model consisting of the natural soil under the pavement layers. The weight of the asphalt, base and subbase layers can be considered as the overburden pressure.

The frost heave was estimated under the shoulder and pavement in Oakland County sites. The results are shown in Figures 4-41. The only difference between the two models is the

overburden pressure. The overburden pressure was modeled by a 20-inch thick soil layer having density of 125 (psf) for the shoulder and a 30.5-inch thick soil layer with the same density for the pavement. It should be noted that the ground water table was set at the average measured ground water table level in Oakland County.

Figures 4-41 indicates that in both cases the calculated frost heave values are within 0.1 inches of the measured ones. It can be concluded that different simplifications and modifications which were applied to the Gilpin model did not affect the accuracy of the model significantly, indeed, it produced better results.

Table 4-11 Different input values for each site, I75, Oakland County, Michigan

Station Name	Duration (days)	T_{top} (^{0}F)	Hydraulic Conductivity (ft/day)	GWT (ft)	D_{10} (mm)
Sta/724+00	65	28.5	1.43*10^-1	30	0.03
Sta/719+00	40	26.5	1.43*10^-1	30	0.03
Sta/652+00	60	25	2.83*10^-1	30	0.01
Sta/528+88	70	28.5	2.83*10^-2	30	0.004
Sta/474+00	55	28.5	1.43*10^-2	30	0.001

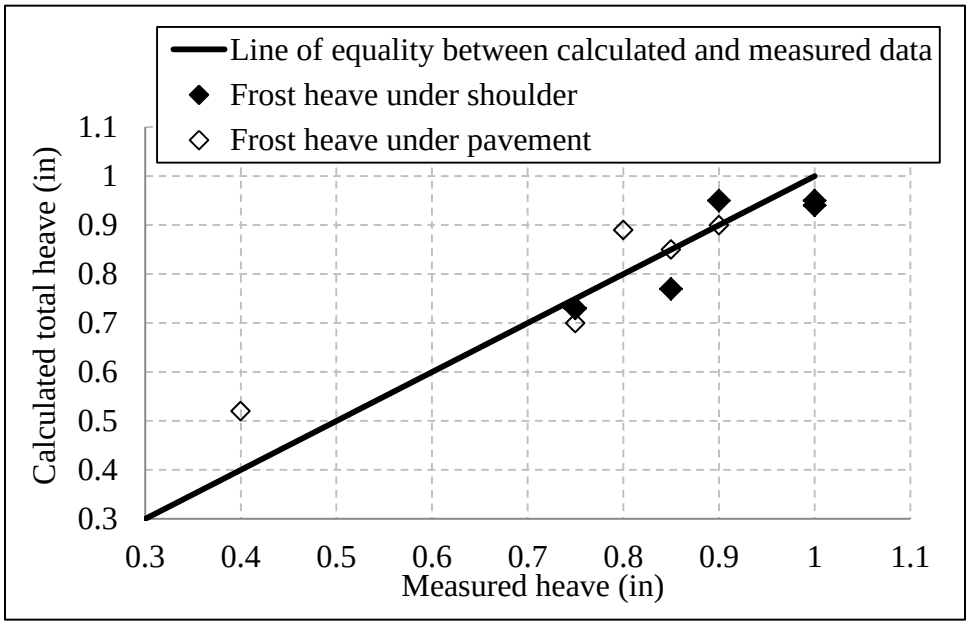

Figure 4-41 Measured versus calculated frost heave under the shoulder and pavement in 5 sites, Oakland County, Michigan

It is noteworthy that for station 528+88 (See Table 4-11); the measured frost heave under the pavement is approximately 0.35 inches less than that under the shoulder (See Table 3-5). This difference is higher than those at the other sites (about 0.1-inch). At station 528+88, an undercut of approximately 12 inches was made for frost protection of the roadbed soil. Therefore, the frost penetration in the clayey silt roadbed soil decreased by 12 inches and hence, as it was expected, the frost heave decreased. In the analyses, the undercut was modeled as a part of the overburden pressure against the surface of the clayey silt roadbed soil. The results are also shown in Figure 4-41.

4.7.5 Heave Pressure

Heave pressure can cause real stability issues in different structures such as retaining walls, utility poles and shallow foundations.

In the revised frost heave model presented in the previous section, frost heave can be calculated as a function of overburden pressure. If the overburden pressure is equal to or greater than the heave pressure, no heave will occur. That is equilibrium scenario is reached. Otherwise, frost heave will take place due to the net pressure against the structure in question. The heave pressure can be calculated as follows:

$$P_{FH} = P_E - P_{OB} \qquad 4-30$$

Where P_{FH} = pressure due to heave (psf);

P_E = the equilibrium overburden pressure (see Figure 4-36), (psf);

P_{OB} = the actual overburden pressure (psf); and

All other parameters are the same.

In order to develop a model for estimating the frost heave pressure, the following three steps were used:

1. For four soil types, the revised heave model (Equations 4-25 to 4-29) was used to calculate the amount of heave as a function of the overburden pressure and the depth to the ground water table (see Figures 4-36 through 4-39). Table 4-12 shows the different input values for each soil type. For each scenario, the corresponding equilibrium pressure was also calculated.

2. The data in Figures 4.36 through 4.39 were used to estimate (for each amount of heave and ground water depth), the corresponding overburden pressure.
3. The estimated overburden pressure and the equilibrium pressure were used as inputs to Equation 4-30 to estimate the heave pressure. Figure 4-42 shows the results for clayey silt. As can be seen the heave pressure is almost the same in different ground water table depth. Therefore, heave pressure can be estimated regardless of the ground water table depth as a function of frost heave. Figure 4-43 shows heave pressure verses frost heave in four soil types.

Table 4-12 Different input values for each soil type

Soil Type	**Hydraulic Conductivity (K_{uf}, (ft/day)**	**D_{10} (mm)**	**Thermal Conductivity (k_{uf},Btu/(ft.hr.^{o}F))**	**Dry unit Weight (γd, pcf)**	**Water Content (w%)**	**P_{OB} (psi)**
Clayey, silty, gravely, sand	2.83*10^-1	0.02	1.5	125	10	variable
Fine sand and silt	1.43*10^-1	0.01	1.4	120	15	
Sandy clayey silt	2.83*10^-2	0.002	1.01	115	20	
clayey silt	1.43*10^-2	0.001	0.88	100	25	

1- Soil type: can be obtained from the boring log on site (known)
2- Duration: the time period that CFDD (cumulative freezing degree day) is calculated over (known or assumed)
3- T_{top}: temperature at the ground surface= CFDD/Duration (known or assumed)
4- Hydraulic conductivity: can be measured on site or assumed based on the soil type
5- GWTD: ground water table depth (known)
6- D_{10}: the effective size of the soil; can be obtained from the soil distribution curve or assumed based on the soil type (known or assumed)
7- Thermal conductivity: measured at MSU soil laboratory (known)
8- T_{bottom}: temperature at the ground water table level; assumed based on GWTD (assumed)
9- Dry unit weight of soil: can be measured on site or obtained from the CRREL graphs based on the thermal conductivity values (known or assumed)
10- Water content: can be measured on site or obtained from the CRREL graphs based on the thermal conductivity values (known or assumed)
11- Void ratio: can be measured on laboratory or assumed based on the soil type and its density= 0.5 (known or assumed)
12- P_{OB}= overburden pressure

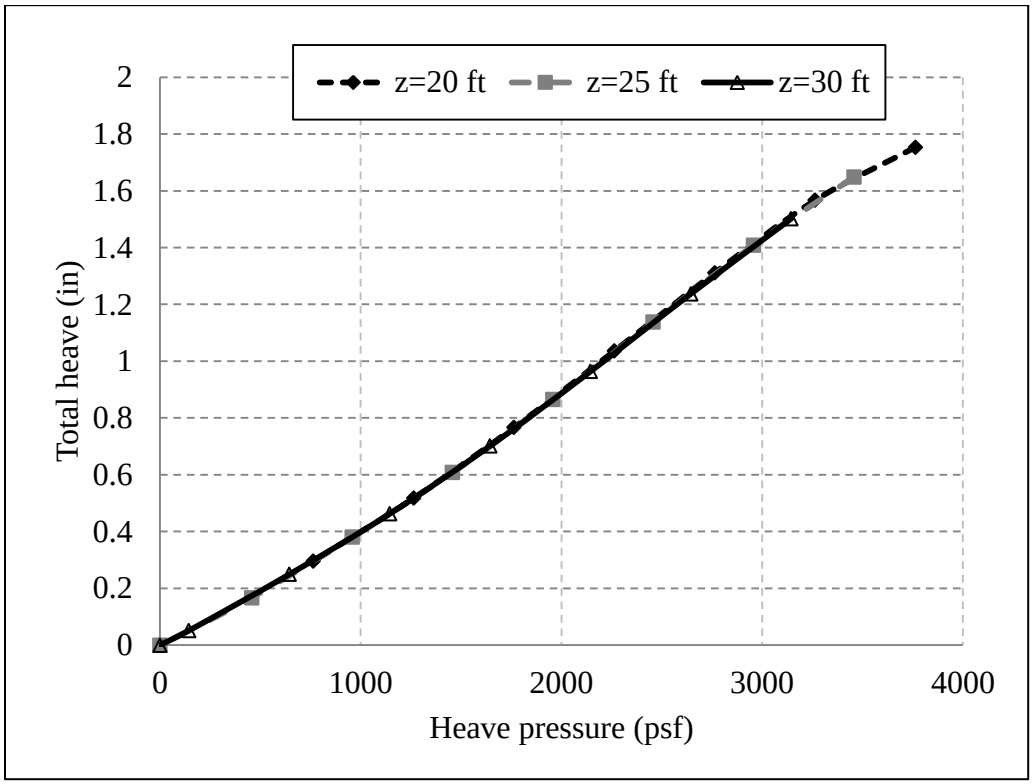

Figure 4-42 Heave pressure versus calculated total heave for clayey silt in different ground water table depths when T_{TOP}= 26 ^{o}F in 100 days

The results showed that in the same winter duration the heave pressure has a unique polynomial relationship with frost heave as follows:

$$P_{FH} = a * \Delta h_{total}^2 + b * \Delta h_{total} \qquad 4-30$$

Where a,b,c = constant values which are different in each soil type; and

all other parameters are the same.

It should be noted that in Equation 4-30 soil was considered to be saturated. Also, the effect of void ratio was not considered in the model. Table 4-13 shows statistical parameters of Equation 4-30 for each soil type.

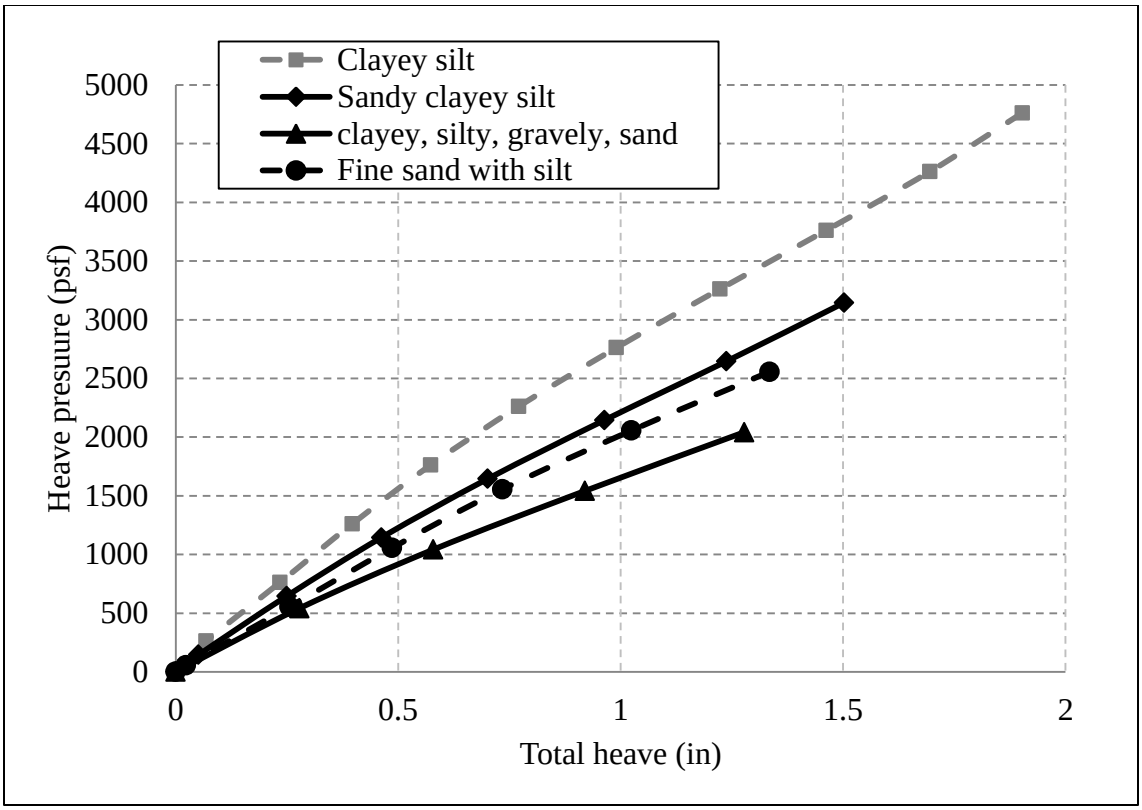

Figure 4-43 Heave pressure versus calculated total heave in four soil types when T_{TOP}= 26 ^{o}F in 100 days

Table 4-13 Statistical coefficients in Equation 4-30 for each soil type

Soil Type	Equation 4-30
clayey silt	$P_{FH} = -334.6\Delta h_{total}^{2} + 3069.7\Delta h_{total}$
Sandy clayey silt	$P_{FH} = -329.51\Delta h_{total}^{2} + 2570.1\Delta h_{total}$
Fine sand and silt	$P_{FH} = -302.89\Delta h_{total}^{2} + 2320.6\Delta h_{total}$
clayey, silty, gravely, sand	$P_{FH} = -291.35\Delta h_{total}^{2} + 1963\Delta h_{total}$

It should be noted that field data for evaluating the accuracy of the results were not available. Therefore the model should be validated as data become available.

Chapter 5
Conclusions

5.1 Summary

5.1.1 Frost Depth Modeling

Frost depth is an important factor that affects the design of all infrastructures including pavements, retaining structures, building and bridge foundations and/or utility lines. Frost depth was modeled using finite difference model, UNSAT-H. The model requires various input data that some of which are not available and expensive to obtain. Hence, the missing data were estimated and the accuracy of the calculated results was assessed using the measured frost depth in the State of Michigan. It was found that the calculated frost depths were significantly different than the measured ones. The differences could be attributed in part to the lack and consequent estimation of the required input data. Further, the accuracy and reliability of three analytical and semi-empirical models (Stefan, Modified Berggren and Chisholm and Phang) were evaluated. Unfortunately, none of the models produced favorable results. Therefore, different statistical models were developed to predict frost depths.

First, a statistical model was developed relating the frost depth data measured in the state of Michigan and the calculated cumulative freezing degree day (CFDD). The accuracy of the resulting statistical model was then assessed using the measured frost depth data in the state of Minnesota along with the calculated CFDD values for Minnesota. Once again, the results were not favorable, and it was concluded that the developed statistical model cannot be used in another State without calibration.

To improve the accuracy of the model, Michigan frost depth data were divided into two groups according to the soil types; clayey and sandy soils. For each soil type, a statistical model was developed relating the frost depth to the calculated CFDD. Furthermore, the two statistical models were then validated using the Minnesota data. The two models produce reasonable estimates of the frost depth data measured in the State of Minnesota.

The resulting two statistical models were then combined using the average laboratory measured thermal conductivity of saturated clayey and sandy soil samples obtained from MDOT. The accuracy of the combined statistical model was then assessed using the frost depth data measured in the states of Michigan and Minnesota. The calculated frost depth data using the

combined statistical model were reasonable and closely represent the frost depth data measured in both states.

5.1.2 Thaw Depth Model

Nixon and McRoberts thaw depth predictions model was assessed using the calculated cumulative thaw degree day (CTDD) and the thaw depth data measured in the State of Michigan. The model did not produce accurate and acceptable results.

5.1.3 Frost Heave Model

As soils freeze, water migrates through the soil voids below the freezing zone toward the freezing front, coats and triggers ice lenses to grow, and causes excessive heave. Frost have can be mitigated by removing and replacing the frost susceptible soil by drainable materials, stopping water flow by intercepting its path using drainage lines, cutting off the source of water, and/or reducing the frost depth by installing insulation. In this study, reducing frost depth was considered as a means of frost heave mitigation. A semi-empirical model was developed based heat balance in the soil layer and the frost depth model developed in the study (Equation 4-12). This model estimates the required insulation thickness to reduce the frost depth to the desired depth.

Further, The Gilpin's mechanistic- empirical model was used to predict frost heave. The model yielded unreasonable results and did not simulate the frost depth data measured by MDOT. Consequently, the model was modified by replacing the heat balance equation for calculating the frost depths by the empirical frost depth model developed in this study (Equation 4-12). The modified Gilpin's model yielded relatively accurate results that represent the frost heave data measured at 5 sites in Oakland County, Michigan. Lastly, the results of the frost heave model was used and heave pressure models were developed for four soil types as a function of frost heave.

5.2 Conclusions

From the results it can be concluded:

1. The UNSAT-H numerical model requires various meteorological and soil properties data that were not available and/or expensive to collect. In the analyses, the values of the required input data were estimated and the results were not accurate.
2. Analyzed existing mechanistic and mechanistic-empirical models did not accurately predict the measured frost depth data in the States of Michigan. The models were based on the

assumptions that volumetric heat capacity and water movement can be neglected and on a set of input data that were not available or expensive to measure. Hence, the required inputs (such as water content, dry density and thermal conductivity of each layer under the pavement) were estimated using the average measured soil thermal conductivity and the Corps of Engineers chart.

3. The analyses of one empirical model yielded inaccurate results relative to the measured ones. This model was developed based on the frost depth data in Ontario, Canada and it requires calibration for implementation in Michigan.
4. A statistical model relating the measured frost depth data in Michigan and the CFDD was developed independent of soil type. The model did not produce accurate results for Michigan and Minnesota.
5. One statistical model was developed for each of clayey and sandy soils using the measured frost depth data in Michigan. The two models predicted the measured frost depth data in Minnesota relatively accurately.
6. The statistical model developed based on the average thermal conductivity of saturated clayey and sandy soils produced accurate results for both soils in the states of Michigan and Minnesota.
7. Results of the analyses of a mechanistic model for thaw depth prediction showed that the model was not able to predict the thaw accurately.
8. The Gilpin frost heave model was used to predict the measured frost heave data. The results were not acceptable. In this study, the model was modified (see Chapter 4). The modified model yielded frost heave data that are representative to the measured data under the shoulder and under the pavement in Michigan.
9. Heave pressure model was developed based on the result of frost heave model. However, since pressure data were not available, the accuracy of the model could not be evaluated.

5.3 Recommendation

Based on the results of this study and the enumerated conclusions, the following recommendations were made:

1. Undisturbed soil samples be collected from various soil types in Michigan and their thermal conductivity be measured. The resulting data be used to improve the accuracy of the statistical frost depth model developed in this study.

2. The developed frost model be implemented to calculate frost depth data in those areas where no temperature sensors are installed with depth.
3. The mechanistic Nixon and McRobert model as well as other mechanistic-empirical models be further analyzed, modified, and calibrated to provide more accurate prediction of thaw depths in the state of Michigan.
4. To increase the benefits of this study, it is recommended that the developed frost depth model be used in the development of procedures and policy to predict the time when seasonal load restriction (SLR) signs must be posted and removed.

References

1. American Concrete Pavement Association, "Frost-Susceptible Soils", 2008.
2. Aldrich Jr, P. Harl, and H. M. Paynter. "Analytical Studies of Freezing and Thawing of Soils", Technical Report No. 42, Arctic Construction and Frost Effects Laboratory, New England Division U.S. Army Corps of Engineers, Boston, MA, U.S. Arctic Construction and Frost Effects Lab Boston Ma, 1953.
3. Andersland, O. B., and D. M Anderson. "Geotechnical Engineering for Cold Regions", McGraw-Hill Inc, 1978.
4. ASTM C578-14a. "Standard Specification for Rigid, Cellular Polystyrene Thermal Insulation", ASTM International, West Conshohocken, PA, 2014, www.astm.org.
5. Berg, R. L. "Calculating Maximum Frost Depths At Mn/Road: Winters 1993-94, 1994-95 And 1995-96", No. MN/RC-97/21, 1997.
6. Bianchini, A., and R.G. Carlos. "Pavement-Transportation Computer Assisted Structural Engineering (PCASE) Implementation of the Modified Berggren (ModBerg) Equation for Computing the Frost Penetration Depth within Pavement Structures", Publication No. ERDC/GSL-TR-12-15. Engineer Research and Development Center Vicksburg Ms Geotechnical and Structures Lab, 2012.
7. Black, P. B. "Applications of the Clapeyron Equation To Water and Ice in Porous Media", No. CRREL-95-6. Cold Regions Research and Engineering Lab Hanover, 1995.
8. Boselly III, S. E., G. S. Doore, J. E. Thornes, C. Ulberg, and D. Ernst, "Road Weather Information Systems Volume 1", Research report. Strategic Highway Research Program Publication-SHRP-H-350, National Research Council, Washington, DC, 1993
9. Boyd, D. W. "Normal Freezing and Thawing Degree-Days from Normal Monthly Temperatures." Canadian Geotechnical Journal, Volume 13.2, pp.176-180, 1976.
10. Bradley ,H., M. A. Ahammed, S. Hilderman, and S. Kass "Responding to Climate Change with Rational Approaches for Managing Seasonal Weight Programs in Manitoba." Cold Regions Engineering, pp. 391-401, 2012.
11. Chapin, J., B. H. Kjartanson, and J. Pernia. "Comparison of Two Methods for Applying Spring Load Restrictions on Low Volume Roads", Canadian Journal of Civil Engineering, Vol. 39, Issue 6, pp.599-609, 2012.

12. Chisholm, R. A., and W. A. Phang. “Measurement and Prediction of Frost Penetration in Highway”, Transportation Research Record: Journal of Transportation Research Board, No 918, Transportation Research Board of the National Academies, Washington D.C., pp. 1-10, 1983.
13. Crandell, J. H., "Below-Ground Performance of Rigid Polystyrene Foam Insulation: Review of Effective Thermal Resistivity Values Used in ASCE Standard 32-01—Design and Construction of Frost-Protected Shallow Foundations”, Journal of Cold Regions Engineering, Volume 24.2, pp. 35-53, 2009.
14. Dash, J. G., A. W. Rempel, and J. S. Wettlaufer. “The Physics of Premelted Ice and Its Geophysical Consequences”, Reviews of Modern Physics, Vol. 78.3, pp. 695-741, 2006.
15. Departments of The Army and The Air Force, “Artic and Subarctic Construction Calculation Methods for Determination of Depths of Freeze and Thaw in Soil”, Technical Manual, No. 5-852-6, Air Force Regulation, AFR88-19, Volume 6, January, 25, 1988
16. Devices, Decagon. “KD2 Pro Thermal Properties Analyzer Operator's Manual, Version 10.0”, 2008.
17. Everett, D. H. “The Thermodynamics of Frost Damage to Porous Solids”, Transactions of The Faraday Society”, Volume 57, pp. 1541-1551, 1961.
18. Edgar, T. V. “Instrumentation and Analysis of Frost Heave Mitigation on WY-70, Encampment, WY”.No. FHWA-WY-14/01F, 2014.
19. Fowler, A. C., And W. B. Krantz. “A Generalized Secondary Frost Heave Model”, Siam Journal on Applied Mathematics, Volume 54.6, pp. 1650-1675, 1994.
20. Fayer, M.l J. “UNSAT-H Version 3.0: Unsaturated Soil Water and Heat Flow Model. Theory, User Manual, and Examples”, Pacific Northwest National Laboratory 13249, 2000.
21. Gilpin, R. R., “A Model of the 'Liquid-Like' Layer between Ice and a Substrate With Applications to Wire Regelation and Particle Migration”, Journal of Colloid Interface Science, Volume 68, pp.235-251, 1979.
22. Gilpin, R. R., “Theatrical Studies of Particle Engulfment”, Journal of Colloid Interface Science, Volume 74, pp.44-63, 1980
23. Gilpin, R. R., “A Model for the Prediction of Ice Lensing and Frost Heave in Soils”, Water Resources Research, Volume 16.5, pp. 918-930, 1980.

24. Gilpin, R. R., “A Frost Heave Interface Condition for Use in Numerical Modelling”, Proc. 4th Canadian Permafrost Conference, Calgary, Canada, pp. 459-465, 1982.
25. Han, S. J., and D. J. Goodings, “Practical Model of Frost Heave in Clay.”,Journal of Geotechnical and Geoenvironmental Engineering, Volume 132.1, pp.92-101, 2006
26. Harlan, R. L, “Analysis of Coupled Heat-Fluid Transport in Partially Frozen Soil”, Water Resources Research, Volume 9.5, pp. 1314-1323, 1973.
27. Hayhoe, H. N., and D. Balchin. “Field frost heave measurement and prediction during periods of seasonal frost.” Canadian Geotechnical Journal 27.3 (1990): 393-397.
28. Hsieh, C. K., C. Qin, and E. E. Ryder, “Development of Computer Modeling for Prediction of Temperature Distribution inside Concrete Pavements”, Report No. FL/DOT/SMO/90-374, Florida Department of, 1989.
29. Huen, K., S. Tighe, B. Mills, and M. Perchanok “Development of Tools for Improved Spring Load Restriction Policies in Ontario”, The Annual Conference of The Transportation Association of Canada (TAC), Charlottetown, Prince Edward Island, 2006.
30. Janoo, V., and E. Cortez. “Pavement Evaluation in Cold Regions.” Cold Regions Engineering, pp.360-371, 2002.
31. Jiji, L. M. “Heat Conduction”, Berlin: Springer, 2009.
32. Klein, J., "Finite element method for time- dependent problems of frozen soils." International Journal for Numerical and Analytical Methods in Geomechanics volume 5.3, pp. 263-283, 1981.
33. Kestler, M. A., R. L. Berg, B. C. Steinert, G. L. Hanek, M. A. Truebe, and D. N. Humphrey, “Determining When to Place and Remove Spring Load Restrictions on Low-Volume Roads: Three Low-Cost Techniques”, Transportation Research Record: Journal of the Transportation Research Board , Volume 1, pp. 219-229, 2007.
34. Kinosita, S. “Heaving force of frozen soils.” Physics of Snow and Ice: proceedings, Volume 1.2, pp. 1345-1360, 1967.
35. Konrad, J.M., and N. R. Morgenstern, “A Mechanistic Theory of Ice Lens Formation in Fine-Grained Soils”, Canadian Geotechnical Journal, Volume. 17.4, pp.473-486, 1980
36. Konrad, J-M., and N. R. Morgenstern, “Effects of applied pressure on freezing soils”,. Canadian Geotechnical Journal. Volume.19.4, pp. 494-505, 1982.

37. Lackner, R., C. Pichler, and A. Kloiber. "Artificial ground freezing of fully saturated soil: viscoelastic behavior." Journal of engineering mechanics volume 134.1, pp. 1-11, 2008.
38. Lai, Y, W. Hui, W. Ziwang, L. Songyu, and D. Xuejun. "Analytical viscoelastic solution for frost force in cold-region tunnels." Cold regions science and technology 31, Volume 3, pp. 227-234, 2000
39. Leong, P., S. Tighe, and G. Doré, "Using LTPP data to develop spring load restrictions: A pilot study", Proceeding the 84th Annual Meeting CD-ROM, Transportation Research Board, Washington, D.C.,2005.
40. Levinson, D. M., O. Mihai, V. Voller, I Margineau, B. Smalkowski, M. Hashami, N. Li, M. Corbett, and E. Lukanen., "Cost/Benefit Study of Spring Load Restrictions", 2005.
41. Liu, Z., X. Yu, Y. Sun, and B. Zhang, "Formulation and Characterization of Freezing Saturated Soils". Journal of Cold Regions Engineering, Volume 27(2), pp. 94-107, 2012.
42. Loch, J. P. G., and R. D. Miller. "Tests of The Concept of Secondary Frost Heaving", Soil Science Society of America Journal, Volume 39.6, pp. 1036-1041, 1975.
43. Marquis, B., "Mechanistic Approach to Determine Spring Load Restrictions in Main", Technical report No. 08-1, Main Department of Transportation, Bangor, Main, 2008.
44. Minnesota Department of Transportation (MnDOT), "Guidelines for Seasonal Load Limit Starting and Ending Dates", Policy, Safety & Strategic Initiatives Division Technical Memorandum. No. 09-09-MAT-02, 2009.
45. Michigan Department of Transportation (MDOT) "Plans of Proposed" .No. NH 0852(019), pp.17-18, 2008.
46. Michigan Department of Transportation (MDOT) "Plans of Proposed" .No. ARRA 0984(084), pp.27, 2009a.
47. Michigan Department of Transportation (MDOT) "Request For Proposals, Book 2 Project Requirements" .North and Superior Regions ITS Deployment, pp.81-110, 2009b.
48. Michigan State University Enviro Weather (MSU-EW) http://www.enviroweather.msu.edu/homeMap.php, Accessed November, 2012
49. Miller, H., C. Cabral, M. Kestler, R. Berg, and R. Eaton, "Calibration of a Freeze-Thaw Prediction Model for Spring Load Restriction Timing in Northern New England". Cold Regions Engineering, pp. 369-379, 2012

50. Mnhoney, J., R. Rutherford and G.Hicks "Guidelines for Spring Highway Use Restrictions." Report No. WA-RD-80.2, Washington State Department of Transportation, Olympia, WA, 1986.
51. National Oceanic and Atmospheric Administration (NOAA).
52. Nixon, J. and E. McRoberts, "A study of Some Factors Affecting the Thawing of Frozen Soils," Canadian Geotechnical Journal, Volume 10, pp. 439-452, 1973.
53. Novak, E. C., "Study of Frost Action in Class AA Shoulders near Pontiac", Research report No.671, Project 63E-27, Testing and Research Division, Department of State Highway, Michigan, 1968.
54. Ovik, J.M., J.A. Siekmeier, and D.A Van Duesen, "Improved Spring Load Restriction Guidelines Using Mechanistic Analysis", Minnesota Department of Transportation, Report No. MN/RC-2000-18, 2000.
55. Penner, E., "Frost heaving forces in Leda clay." Canadian Geotechnical Journal, Volume 7.1 , pp. 8-16, 1969.
56. Penner, E., and L. W. Gold. "Transfer of heaving forces by adfreezing to columns and foundation walls in frost-susceptible soils." Canadian Geotechnical Journal, Volume 8.4, pp. 514-526, 1971.
57. Penner, E., and W. W. Irwin. "Adfreezing of Leda clay to anchored footing columns." Canadian Geotechnical Journal. Volume 6, pp. 327-337, 1969.
58. Peppin, S. S., and R. W. Style, "The Kinetics of Ice-Lens Growth in Porous Media", Journal of Fluid Mechanics, Vol. 692, pp. 482-498, 2012.
59. Peppin, S. S., and R. W. Style, "The Physics of Frost Heave and Ice-Lens Growth", Vadose Zone Journal , Vol.12, 2013.
60. Road Weather Information System (RWIS). Road Weather Information System portal, Michigan. http://www.rwisonline.com/scanweb/swlogin.asp. Accessed November ,2012
61. Smith, J. M. "Introduction to Chemical Engineering Thermodynamic", McGraw-Hill, Boston, 2001.
62. Stormont,J., and S. Zhou, "Improving Pavement Sub-surface Drainage Systems by Considering Unsaturated Water Flow", U.S. Department of Transportation Federal Highway Administration, Department of Civil engineering University of New Mexico, 2001

63. Taber, S., “The Mechanics of Frost Heaving”, The Journal of Geology, Volume. 2, pp. 303-317, 1930.
64. Takagi, S., “Segregation Freezing as the Cause of Suction Force For Ice Lens Formation”, Engineering Geology, Volume 13.1, pp. 93-100, 1979.
65. Tighe, S. L., B. Mills, C.T. Haas., and S. Baiz, “Using Road Weather Information Systems (RWIS) to Control Load Restrictions on Gravel and Surface-Treated Highways”, Ministry of Transportation Engineering Standards Branch Report, 2007.
66. Thompson, M. R., Dempsey, B. J., Hill, H., and J. Vogel, “Characterizing Temperature Effects for Pavement Analysis and Design”, Transportation Research Record: Journal of Transportation Research Board, No 1121, Transportation Research Board of the National Academies, Washington D.C., pp. 14-22, 1987.
67. Transportation Officials “AASHTO Guide for Design of Pavement Structures.” ASSHTO, Volume 1, 1993.
68. US department of transportation, “An Introduction to Standards for Road Weather Information Systems (RWIS)”, Federal Highway Administration, 2002.
69. U. S. Army Corps of Engineers “Pavement Criteria for Seasonal Frost Conditions”. Department of the Army Technical Manual, EM 1110-3-138, 1984.
70. Vialov, S. S., V. G. Gmoshinskii, S. E. Gorodetskii, V. G. Grigorieva, Iu K. Zaretskii, N. K. Pekarskaia, and E. P. Shusherina. “The strength and creep of frozen soils and calculations for ice-soil retaining structures”. No. Translation 76. 1965.
71. Wallace, M., “How to Prevent Frost Heave”, Concrete Construction, Volume 32.4, pp. 369-372, 1987.
72. Wisconsin Transportation, “Using Weight Limits to Protect Local Roads”, Bulletin . No. 8, 2003
73. Yavuzturk, C., K. Ksaibati, and A. D. Chiasson, “Assessment of Temperature Fluctuations in Asphalt Pavements Due to Thermal Environmental Conditions Using a Two-Dimensional, Transient Finite-Difference Approach”, Journal of Materials in Civil Engineering, Volume.17.4, pp.465-475, 2005.
74. Yoder, El. J., and M. W. Witczak, “Principles of Pavement Design” John Wiley & Sons, 1975.

75. Yuanming, L., Xuefu, Z., Jianzhang, X., Shujuan, Z., & Zhiqiang, L. “Nonlinear analysis for frost-heaving force of land bridges on Qing-Tibet Railway in cold regions”. Journal of Thermal Stresses, Volume 28(3), pp. 317-331, 2005.
76. Zapata, C. E., and W. N. Houston “Calibration and Validation of the Enhanced Integrated Climatic Model for Pavement Design.” Transportation Research Board, Volume 602, 2008.

Appendix A
Frost and Thaw Depth Analysis

Appendix A

Frost and Thaw Depth Analysis

This appendix houses the details of frost depth calculations for the winter of 2010-2011 using Stefani equation and Modified Berggren equation for all RWIS stations in Michigan. Also provides the details of thaw depth calculations using Nixon and McRoberts equation for all of the stations. It should be noted that LP stands for Lower Peninsula and UP stands for Upper Peninsula.

Table A-1 Frost depth calculation for Benzonia LP station using Stefan equation

Material	γ_d	w	d	k	L	FI	∑FI
HMA	138	0	5.00	10.3	0	0	0
Gravel	130	0.075	12	17.9	1350	19	21
Sand	125	0.09	69.5	16.7	1555	780	800
γ_d = unit weight (pcf); w = water content (%); d = layer depth (in); k= thermal conductivity (Btu/(ft.hr.^{o} F/in); L= latent heat of fusion (Btu/^{3}ft); FI=freezing Index (^{o}F-day)							

Table A-2 Frost depth calculation for Benzonia LP station using Modified Berggren equation

Material	γ_d	w	d	C	k	L	Ĺ= ∑Ld/∑d	Ĉ= ∑Cd/∑d	μ= Ĉ / Ĺ *vs	λ	R	∑R	∑R+R/2	FI	∑FI
HMA	138	0	0.42	24	0.86	397	0	24	0	0	0.48	0.00	0.24	0	0
Gravel	130	0.075	1	30	1.5	1350	953	28	0.17	0.56	0.67	0.48	0.82	147	147
Sand	125	0.09	1.9	42	1.4	1555	1298	36	0.16	0.58	1.36	1.15	1.83	670	822
d = layer depth (ft); C= volumetric heat capacity(Btu/ft^3); k= thermal conductivity (Btu/(ft.hr.^{o} F); μ= fusion parameter; λ= correction factor; R= thermal diffusivity (hr °F/ Btu); FI=freezing Index (^{o}F-day)															
v_0= Annual Temp $_{average}$-32							16.3	**vs= n(CFI)/t**		5.6	**FI**	801	**α=v0/vs**		4.2

Table A-3 Thaw depth calculation for Benzonia LP station using Nixon and McRoberts equation

Material	γ_d	w	d	k	L	TI	∑TI
HMA	138	0	5.00	10.3	0	0	0
Gravel	130	0.075	12	17.9	945	11.6	12.7
FI=freezing Index (^{o}F-day)							

Table A-4 Frost depth calculation for Cadillac LP station using Stefan equation

Material	γ_d	w	d	k	L	FI	∑FI
HMA	138.0	0	5.00	10.3	0	0	0
Gravel	130.0	0.075	12	17.9	1350	19	19
Sand	125.0	0.09	90	16.7	1555	1307	1326
γ_d = unit weight (pcf); w = water content (%); d = layer depth (in); k= thermal conductivity (Btu/(ft.hr.^{o} F/in); L= latent heat of fusion (Btu/^{3}ft); FI=freezing Index (^{o}F-day)							

Table A-5 Frost depth calculation for Cadillac LP using Modified Berggren equation

Material	γ_d	w	d	C	k	L	Ĺ= ∑Ld/∑d	Ĉ= ∑Cd/∑d	μ= Ĉ / Ĺ *vs	λ	R	∑R	∑R+R/2	FI	∑FI
HMA	138	0.02	0.42	40	0.86	0	397	40	0.94	0	0.48	0.48	0.73	0	0
Gravel	130	0.075	1	30	1.5	1350	1070	33	0.29	0.760	0.67	0.48	0.82	80	91
Sand	125	0.09	3.9	42	1.4	1555	1426	39	0.26	0.770	2.79	1.15	2.54	1084	1175
d = layer depth (ft); C= volumetric heat capacity(Btu/ft^3); k= thermal conductivity (Btu/(ft.hr.^{o} F); μ= fusion parameter; λ= correction factor; R= thermal diffusivity (hr °F/ Btu); FI=freezing Index (^{o}F-day)															
v_0= Annual Temp $_{average}$-32							8.1	**vs= n(CFI)/t**		9.4	**FI**	1146	**α=v0/vs**		0.86

Table A-6 Thaw depth calculation for Cadillac LP using Nixon and McRoberts equation

Material	γ_d	w	d	k	L	TI	∑TI
HMA	138	0	5.00	10.3	0	0	0
Gravel	130	0.075	10	17.9	945	10.3	11.4
TI=Thawing Index (^{o}F-day)							

Table A-7 Frost depth calculation for Grayling LP using Stefan equation

Material	γ_d	w	d	k	L	FI	∑FI
HMA	138.0	0.0	5.0	10.3	0.0	0	0
Gravel	130.0	0.075	12.0	17.9	1350.0	19	19
Sand	125.0	0.09	90.0	16.7	1555.2	1307	1326
γ_d = unit weight (pcf); w = water content (%); d = layer depth (in); k= thermal conductivity (Btu/(ft.hr.^{o} F/in); L= latent heat of fusion (Btu/^{3}ft); FI=freezing Index (^{o}F-day)							

Table A-8 Frost depth calculation for Grayling LP using Modified Berggren equation

Material	γ_d	w	d	C	k	L	Ĺ= ∑Ld/∑d	Ĉ= ∑Cd/∑d	μ= Ĉ / Ĺ *vs	λ	R	∑R	∑R+R/2	FI	∑FI
HMA	138	0.02	0.42	40	0.86	0	0	40	0.00	0	0.48	0.48	0.73	0	0
Gravel	125	0.075	1	30	1.5	1350	953	33	0.29	0.66	0.67	0.48	0.82	106	106
Sand	120	0.09	3.6	42	1.4	1555	1385	39	0.24	0.69	2.57	1.15	2.44	1194	1300
d = layer depth (ft); C= volumetric heat capacity(Btu/ft^3); k= thermal conductivity (Btu/(ft.hr.^{o} F); μ= fusion parameter; λ= correction factor; R= thermal diffusivity (hr °F/ Btu); FI=freezing Index (^{o}F-day)															
v_0= Annual Temp $_{average}$-32							11.34	**vs= n(CFI)/t**		8.4	**FI**	1312	**α=v0/vs**		1.35

Table A-9 Thaw depth calculation for Grayling LP using Nixon and McRoberts equation

Material	γ_d	w	d	k	L	TI	∑TI
HMA	138	0	5.00	10.3	0	0	0
Gravel	125	0.075	12	17.9	945	10.3	11.4
Sand	120	0.09	5.00	16.7	1089	36.6	53
TI=Thawing Index (^{o}F-day)							

Table A-10 Frost depth calculation for Houghton Lake LP using Stefan equation

Material	γ_d	w	d	k	L	FI	∑FI
HMA	138.0	0.0	5.0	10.3	0	0	0
Gravel	130.0	0.075	12.0	17.9	1350	19	21
Loose Sand	125.0	0.09	83.0	16.7	1555	1112	1132
γ_d = unit weight (pcf); w = water content (%); d = layer depth (in); k= thermal conductivity (Btu/(ft.hr.^{o} F/in); L= latent heat of fusion (Btu/^{3}ft); FI=freezing Index (^{o}F-day)							

Table A-11 Frost depth calculation for Houghton Lake LP using Modified Berggren equation

Material	γ_d	w	d	C	k	L	Ĺ= ∑Ld/∑d	Ĉ= ∑Cd/∑d	μ= Ĉ / Ĺ *vs	λ	R	∑R	∑R+R/2	FI	∑FI
HMA	138	0.02	0.42	40	0.86	0	0	40	0.95	0	0.48	0.48	0.73	0	0
Gravel	130	0.075	1	30	1.5	1350	1070	33	0.29	0.76	0.67	0.48	0.82	80	94
Sand	125	0.09	3.8	42	1.4	1555	1423	39	0.26	0.78	2.71	1.15	2.51	1015	1109
d = layer depth (ft); C= volumetric heat capacity(Btu/ft^3); k= thermal conductivity (Btu/(ft.hr.^{o} F); μ= fusion parameter; λ= correction factor; R= thermal diffusivity (hr °F/ Btu); FI=freezing Index (^{o}F-day)															
v_0= Annual Temp $_{average}$-32							7.9	**vs= n(CFI)/t**		9.4	**FI**	1133	**α=v0/vs**		0.84

Table A-12 Thaw depth calculation for Houghton Lake LP using Nixon and McRoberts equation

Material	γ_d	w	d	k	L	TI	∑TI
HMA	138	0	5.00	10.3	0	0	0
Gravel	130	0.075	12	17.9	945	32.3	34
Loose Sand	125	0.09	5.00	16.7	1089	63.4	96
TI=Thawing Index (^{o}F-day)							

Table A-13 Frost depth calculation for Ludington LP using Stefan equation

Material	γ_d	w	d	k	L	FI	∑FI
HMA	138.0	0.0	5.0	10.3	0	0	0
Gravel	130.0	0.075	12.0	17.9	1350	19	21
Sand with Clay	115.0	0.15	49.0	16.7	2484	619	640
γ_d = unit weight (pcf); w = water content (%); d = layer depth (in); k= thermal conductivity (Btu/(ft.hr.^{o} F/in); L= latent heat of fusion (Btu/^{3}ft); FI=freezing Index (^{o}F-day)							

Table A-14 Frost depth calculation for Ludington LP using Modified Berggren equation

Material	γ_d	w	d	C	k	L	Ĺ= ∑Ld/∑d	Ĉ= ∑Cd/∑d	μ= Ĉ / Ĺ *vs	λ	R	∑R	∑R+R/2	FI	∑FI
HMA	138	0.02	0.42	40	0.86	0	0	40	0.57	0	0.48	0.48	0.73	0	0
Gravel	130	0.075	1	30	1.5	1350	1070	33	0.17	0.71	0.67	0.48	0.82	93	111
Sand with Clay	115	0.15	1.75	42	1.4	2484	1851	38	0.12	0.75	1.25	1.15	1.78	572	664
d = layer depth (ft); C= volumetric heat capacity(Btu/ft^3); k= thermal conductivity (Btu/(ft.hr.^{o} F); μ= fusion parameter; λ= correction factor; R= thermal diffusivity (hr °F/ Btu); FI=freezing Index (^{o}F-day)															
v_0= Annual Temp $_{average}$-32				9.06	**vs= n(CFI)/t**			5.6	**FI**		649	**α=v0/vs**		1.61	

Table A-15 Thaw depth calculation for Ludington LP using Nixon and McRoberts equation

Material	γ_d	w	d	k	L	TI	∑TI
HMA	138	0	5.00	10.3	0	0	0
Gravel	130	0.075	11	17.9	945	28.6	30
TI=Thawing Index (^{o}F-day)							

Table A-16 Frost depth calculation for Reed City LP using Stefan equation

Material	γ_d	w	d	k	L	FI	∑FI
HMA	138.0	0.0	5.0	10.3	0	0	0
Gravel	130.0	0.075	12.0	17.9	1404	20	20
Sand	125.0	0.09	75.0	16.7	1620	946	965
γ_d = unit weight (pcf); w = water content (%); d = layer depth (in); k= thermal conductivity (Btu/(ft.hr.^{o} F/in); L= latent heat of fusion (Btu/^{3}ft); FI=freezing Index (^{o}F-day)							

Table A-17 Frost depth calculation for Reed City LP using Modified Berggren equation

Material	γ_d	w	d	C	k	L	Ĺ= ∑Ld/∑d	Ĉ= ∑Cd/∑d	μ= Ĉ / Ĺ *vs	λ	R	∑R	∑R+R/2	FI	∑FI
HMA	138	0.02	0.42	40	0.86	0	0	40	0.57	0	0.48	0.48	0.73	0	0
Gravel	130	0.075	1	30	1.5	1404	1108	33	0.24	0.75	0.67	0.48	0.82	85	100
Sand	125	0.09	3.2	42	1.4	1620	1463	39	0.22	0.75	2.29	1.15	2.29	881	981
d = layer depth (ft); C= volumetric heat capacity(Btu/ft^3); k= thermal conductivity (Btu/(ft.hr.^{o} F); μ= fusion parameter; λ= correction factor; R= thermal diffusivity (hr °F/ Btu); FI=freezing Index (^{o}F-day)															
v_0= Annual Temp $_{average}$-32				8.5			**vs= n(CFI)/t**			8.2	**FI**	960	**α=v0/vs**		1.03

Table A-18 Thaw depth calculation for Reed City LP using Nixon and McRoberts equation

Material	γ_d	w	d	k	L	TI	∑TI
HMA	138	0	5.00	10.3	0	0	0
Gravel	125	0.075	11	17.9	945	28.6	30
TI=Thawing Index (^{o}F-day)							

Table A-19 Frost depth calculation for Waters LP using Stefan equation

Material	γ_d	w	d	k	L	FI	∑FI
HMA	138.0	0.0	5.0	10.3	0	0	0
Gravel	130.0	0.075	12.0	17.9	1350	19	19
Sand	125.0	0.075	24.0	17.9	1350	75	94
Loose Sand with Gravel	120.0	0.09	82.0	16.7	1555	1085	1179

γ_d = unit weight (pcf); w = water content (%); d = layer depth (in); k= thermal conductivity (Btu/(ft.hr.^{o} F/in); L= latent heat of fusion (Btu/^{3}ft); FI=freezing Index (^{o}F-day)

Table A-20 Frost depth calculation for Waters LP using Modified Berggren equation

Material	γ_d	w	d	C	k	L	Ĺ= ∑Ld/∑d	Ĉ= ∑Cd/∑d	μ= Ĉ / Ĺ *vs	λ	R	∑R	∑R+R/2	FI	∑FI
HMA	138.0	0.0	0.42	40	0.86	0	0	40	0	0	0.48	0.48	0.73	0	0
Gravel	130.0	0.075	1	30	1.5	1350	1070	33	0.29	0.77	0.67	0.48	0.82	78	92
Sand	125.0	0.075	2	30	1.5	1350	1234	31	0.24	0.79	1.33	1.15	1.82	328	420
Loose sand with Gravel	120.0	0.09	2.2	42	1.4	1555	1360	35	0.25	0.79	1.57	2.48	3.27	747	1167

d = layer depth (ft); C= volumetric heat capacity(Btu/ft^3); k= thermal conductivity (Btu/(ft.hr.^{o} F); μ= fusion parameter; λ= correction factor; R= thermal diffusivity (hr °F/ Btu); FI=freezing Index (^{o}F-day)

v_0= Annual Temp $_{average}$-32	7.4	vs= n(CFI)/t	9.6	FI	1180	α=v0/vs	0.77

Table A-21 Thaw depth calculation for Waters LP using Nixon and McRoberts equation

Material	γ_d	w	d	k	L	TI	∑TI
HMA	138	0	5.00	10.3	0	0	0
Gravel	130	0.075	11	17.9	983	25.1	25
Sand	125	0.075	4	17.9	945	10.3	35

TI=Thawing Index (^{o}F-day)

Table A-22 Frost depth calculation for Williamsburg LP using Stefan equation,

Material	γ_d	w	d	k	L	FI	∑FI
HMA	138	0.02	5.00	10.3	0	0.0	0
Gravel	130	0.075	12	17.9	1350	18.8	19
Sand	125	0.09	10.8	16.7	1555	18.8	38
Silty Clay	115	0.165	44	13.1	2732	698.8	736

γ_d = unit weight (pcf); w = water content (%); d = layer depth (in);

k= thermal conductivity (Btu/(ft.hr.^{o} F/in); L= latent heat of fusion (Btu/^{3}ft); FI=freezing Index (^{o}F-day)

Table A-23 Frost depth calculation for Williamsburg LP using Modified Berggren equation

Material	γ_d	w	d	C	k	L	Ĺ= ∑Ld/∑d	Ĉ= ∑Cd/∑d	μ= Ĉ / Ĺ *vs	λ	R	∑R	∑R+R/2	FI	∑FI
HMA	138	0.02	0.42	40	0.86	0	0	40	0.00	0	0.48	0.48	0.73	0	0
Gravel	130	0.075	1.42	30	1.5	1350	953	33	0.22	0.72	0.67	0.48	0.82	89	89
Sand	125	0.09	2.32	39	1.4	1555	1187	36	0.19	0.73	0.64	1.15	1.47	161	250
Silty Clay	115	0.165	3.62	42	1.1	2732	1742	41	0.15	0.75	1.18	1.15	1.74	458	708

d = layer depth (ft); C= volumetric heat capacity(Btu/ft^3); k= thermal conductivity (Btu/(ft.hr.^{o} F); μ= fusion parameter;

λ= correction factor; R= thermal diffusivity (hr °F/ Btu); FI=freezing Index (^{o}F-day)

v_0= Annual Temp $_{average}$-32	9.1	vs= n(CFI)/t	6.2	FI	735	α=v0/vs	1.45

Table A-24 Thaw depth calculation for Williamsburg LP using Nixon and McRoberts equation

Material	γ_d	w	d	k	L	TI	∑TI
HMA	138	0	5.00	10.3	0	0	0
Gravel	130	0.075	12	17.9	945	13.2	13
Sand	125	0.09	1	16.7	1089	2.6	16

TI=Thawing Index (^{o}F-day)

Table A-25 Frost depth calculation for Au Train UP using Stefan equation

Material	γ_d	w	d	k	L	FI	∑FI
HMA	138	0.02	5.00	10.3	0	0.0	0
Gravel	130	0.075	12	17.9	1404	19.6	20
Sand	125	0.09	19.2	16.7	1620	62.0	82
Loose Sand	120	0.09	107	16.7	1555	1848.0	1930

γ_d = unit weight (pcf); w = water content (%); d = layer depth (in);

k= thermal conductivity (Btu/(ft.hr.^{o} F/in); L= latent heat of fusion (Btu/^{3}ft); FI=freezing Index (^{o}F-day)

Table A-26 Frost depth calculation for Au Train UP using Modified Berggren equation

Material	γ_d	w	d	C	k	L	Ĺ= ∑Ld/∑d	Ĉ= ∑Cd/∑d	μ= Ĉ / Ĺ *vs	λ	R	∑R	∑R+R/2	FI	∑FI
HMA	138	0.02	0.42	40	0.86	0	0	40	0.00	0	0.48	0.48	0.73	0	0
Gravel	130	0.075	1	30	1.5	1404	991	33	0.53	0.78	0.67	0.48	0.82	79	79
Sand	125	0.09	1.6	42	1.4	1620	1325	38	0.45	0.79	1.14	1.15	1.72	298	377
Loose Sand	120	0.09	4	42	1.4	1555	1456	40	0.44	0.79	2.86	2.29	3.72	1546	1923

d = layer depth (ft); C= volumetric heat capacity(Btu/ft^3); k= thermal conductivity (Btu/(ft.hr.^{o} F); μ= fusion parameter;

λ= correction factor; R= thermal diffusivity (hr °F/ Btu); FI=freezing Index (^{o}F-day)

v_0= Annual Temp $_{average}$-32	6.9	vs= n(CFI)/t	15.8	FI	1930	α=v0/vs	0.44

Table A-27 Thaw depth calculation for Au Train UP using Nixon and McRoberts equation

Material	γ_d	w	d	k	L	TI	∑TI
HMA	138	0	5.00	10.3	0	0	0
Gravel	125	0.075	12	17.9	983	26.1	26
Sand	120	0.09	2	16.7	1134	6.1	32

TI=Thawing Index (^{o}F-day)

Table A-28 Frost depth calculation for Brevort UP using Stefan equation

Material	γ_d	w	d	k	L	FI	∑FI
HMA	138	0.02	5.00	10.3	0	0.0	0
Gravel	130	0.075	12	17.9	1404	19.6	20
Sand	125	0.09	87	16.7	1620	1272.6	1292
γ_d = unit weight (pcf); w = water content (%); d = layer depth (in); k= thermal conductivity (Btu/(ft.hr.^{o} F/in); L= latent heat of fusion (Btu/^{3}ft); FI=freezing Index (^{o}F-day)							

Table A-29 Frost depth calculation for Brevort UP using Modified Berggren equation

Material	γ_d	w	d	C	k	L	Ĺ= ∑Ld/∑d	Ĉ= ∑Cd/∑d	μ= Ĉ / Ĺ *vs	λ	R	∑R	∑R+R/2	FI	∑FI
HMA	138	0.02	0.42	40	0.86	0	0	40	0.00	0	0.48	0.48	0.73	0	0
Gravel	130	0.075	1	30	1.5	1404	991	33	0.32	0.85	0.67	0.48	0.82	66	66
Sand	125	0.09	4.3	42	1.4	1620	1464	40	0.26	0.80	3.07	1.15	2.69	1219	1285
d = layer depth (ft); C= volumetric heat capacity(Btu/ft^3); k= thermal conductivity (Btu/(ft.hr.^{o} F); μ= fusion parameter; λ= correction factor; R= thermal diffusivity (hr °F/ Btu); FI=freezing Index (^{o}F-day)															
v_0= Annual Temp $_{average}$-32				6.7			**vs= n(CFI)/t**			9.6	**FI**	1280	**α=v0/vs**		0.7

Table A-30 Thaw depth calculation for Brevort UP using Nixon and McRoberts equation

Material	γ_d	w	d	k	L	TI	∑TI
HMA	138	0	5.00	10.3	0	0	0
Gravel	130	0.075	12	17.9	945	32.3	32
Sand	125	0.09	2	16.7	1089	5.5	38
TI=Thawing Index (^{o}F-day)							

Table A-31 Frost depth calculation for Cooks UP using Stefan equation

Material	γ_d	w	d	k	L	FI	∑FI
HMA	138	0.02	5.00	10.3	0	0.0	0
Gravel	130	0.075	12	17.9	1404	19.6	20
Sand	125	0.09	75	16.7	1620	945.8	965
γ_d = unit weight (pcf); w = water content (%); d = layer depth (in); k= thermal conductivity (Btu/(ft.hr.^{o} F/in); L= latent heat of fusion (Btu/^{3}ft); FI=freezing Index (^{o}F-day)							

Table A-32 Frost depth calculation for Cooks UP using Modified Berggren equation

Material	γ_d	w	d	C	k	L	Ĺ= ∑Ld/∑d	Ĉ= ∑Cd/∑d	μ= Ĉ / Ĺ *vs	λ	R	∑R	∑R+R/2	FI	∑FI
HMA	138	0.02	0.42	40	0.86	0	0	40	0.00	0	0.48	0.48	0.73	0	0
Gravel	130	0.075	1	30	1.5	1350	953	33	0.23	0.79	0.67	0.48	0.82	75	75
Sand	125	0.09	3.5	42	1.4	1555	1382	38	0.19	0.79	2.50	1.15	2.40	873	947
d = layer depth (ft); C= volumetric heat capacity(Btu/ft^3); k= thermal conductivity (Btu/(ft.hr.^{o} F); μ= fusion parameter; λ= correction factor; R= thermal diffusivity (hr °F/ Btu); FI=freezing Index (^{o}F-day)															
v_0= Annual Temp $_{average}$-32				6.8		**vs= n(CFI)/t**			6.7	**FI**		961	**α=v0/vs**		1.03

Table A-33 Thaw depth calculation for Cooks UP using Nixon and McRoberts equation

Material	γ_d	w	d	k	L	TI	∑TI
HMA	138	0	5.00	10.3	0	0	0
Gravel	130	0.075	12	17.9	983	33.6	34
Sand	125	0.09	3	16.7	1134	9.0	43
TI=Thawing Index (^{o}F-day)							

Table A-34 Frost depth calculation for Engadine UP using Stefan equation,

Material	γ_d	w	d	k	L	FI	∑FI
HMA	138	0.02	5.00	10.3	0	0.0	0
Gravel	130	0.075	12	17.9	1404	19.6	20
Sand	125	0.09	24	16.7	1620	104.3	124
Silty Clay	115	0.165	57	13.1	2732	992.3	1116

γ_d = unit weight (pcf); w = water content (%); d = layer depth (in); k= thermal conductivity (Btu/(ft.hr.^{o} F/in); L= latent heat of fusion (Btu/^{3}ft); FI=freezing Index (^{o}F-day)

Table A-35 Frost depth calculation for Engadine UP using Modified Berggren equation

Material	γ_d	w	d	C	k	L	Ĺ= ∑Ld/∑d	Ĉ= ∑Cd/∑d	μ= Ĉ / Ĺ *vs	λ	R	∑R	∑R+R/2	FI	∑FI
HMA	138	0.02	0.42	40	0.86	0	0	40	0.00	0	0.48	0.48	0.73	0	0
Gravel	130	0.075	1.42	30	1.5	1404	991	33	0.34	0.83	0.67	0.48	0.82	69	69
Sand	125	0.09	2.32	39	1.4	1620	1359	36	0.28	0.83	1.43	1.15	1.87	366	435
Silty Clay	115	0.165	3.62	42	1.1	2732	1882	40	0.22	0.84	1.62	1.15	1.96	664	1099

d = layer depth (ft); C= volumetric heat capacity(Btu/ft^3); k= thermal conductivity (Btu/(ft.hr.^{o} F); μ= fusion parameter; λ= correction factor; R= thermal diffusivity (hr °F/ Btu); FI=freezing Index (^{o}F-day)

v_0= Annual Temp $_{average}$-32	6.8	vs= n(CFI)/t	10.3	FI	1110	α=v0/vs	0.66

Table A-36 Thaw depth calculation for Engadine UP using Nixon and McRoberts equation

Material	γ_d	w	d	k	L	TI	∑TI
HMA	138	0	5.00	10.3	0	0	0
Gravel	130	0.075	12	17.9	983	33.6	34
Sand	125	0.09	2	16.7	1134	5.8	39

TI=Thawing Index (^{o}F-day)

Table A-37 Frost depth calculation for Golden Lake UP using Stefan equation

Material	γ_d	w	d	k	L	FI	∑FI
HMA	138	0.02	5.00	10.3	0	0.0	0
Gravel	130	0.075	12	17.9	1350	18.8	19
Sand	125	0.09	105	16.7	1555	1779.5	1798
γ_d = unit weight (pcf); w = water content (%); d = layer depth (in); k= thermal conductivity (Btu/(ft.hr.^{o} F/in); L= latent heat of fusion (Btu/^{3}ft); FI=freezing Index (^{o}F-day)							

Table A-38 Frost depth calculation for Golden Lake UP using Modified Berggren equation

Material	γ_d	w	d	C	k	L	Ĺ= ∑Ld/∑d	Ĉ= ∑Cd/∑d	μ= Ĉ / Ĺ *vs	λ	R	∑R	∑R+R/2	FI	∑FI
HMA	138	0.02	0.42	40	0.86	0	0	40	0.00	0	0.48	0.48	0.73	0	0
Gravel	130	0.075	1	30	1.5	1350	953	33	0.46	0.81	0.67	0.48	0.82	70	70
Sand	125	0.09	5.7	39	1.4	1555	1435	40	0.38	0.83	4.07	1.15	3.19	1709	1779
d = layer depth (ft); C= volumetric heat capacity(Btu/ft^3); k= thermal conductivity (Btu/(ft.hr.^{o} F); μ= fusion parameter; λ= correction factor; R= thermal diffusivity (hr °F/ Btu); FI=freezing Index (^{o}F-day)															
v_0= Annual Temp $_{average}$-32				5.2			**vs= n(CFI)/t**			13.4	**FI**	1804	**α=v0/vs**		0.39

Table A-39 Thaw depth calculation for Golden Lake UP using Nixon and McRoberts equation

Material	γ_d	w	d	k	L	TI	∑TI
HMA	138	0	5.00	10.3	0	0	0
Gravel	130	0.075	12	17.9	983	33.6	34
Sand	125	0.09	2	16.7	1134	5.8	39
TI=Thawing Index (^{o}F-day)							

Table A-40 Frost depth calculation for Harvey UP using Stefan equation

Material	γ_d	w	d	k	L	FI	∑FI
HMA	138	0	5.00	10.3	0	0.0	0
Gravel	130	0.075	12	17.9	1404	19.6	20
Sand with Gravel and Silt	120	0.09	24	16.7	1620	104.3	124
Sand	125	0.165	57	13.1	2732	992.3	1116

γ_d = unit weight (pcf); w = water content (%); d = layer depth (in); k= thermal conductivity (Btu/(ft.hr.^{o} F/in); L= latent heat of fusion (Btu/^{3}ft); FI=freezing Index (^{o}F-day)

Table A-41 Frost depth calculation for Harvey UP using Modified Berggren equation

Material	γ_d	w	d	C	k	L	Ĺ= ∑Ld/∑d	Ĉ= ∑Cd/∑d	μ= Ĉ / Ĺ *vs	λ	R	∑R	∑R+R/2	FI	∑FI
HMA	138	0	0.42	40	0.86	0	0	40	0.00	0	0.48	0.48	0.73	0	0
Gravel	130	0.075	1	30	1.5	1404	991	33	0.24	0.81	0.67	0.48	0.82	73	73
Sand with Silt	120	0.09	1.6	39	1.4	1555	1290	38	0.21	0.82	1.14	1.15	1.72	266	339
Sand	125	0.075	2.1	30	1.5	1350	1315	35	0.19	0.83	1.40	2.29	2.99	513	852

d = layer depth (ft); C= volumetric heat capacity(Btu/ft^3); k= thermal conductivity (Btu/(ft.hr.^{o} F); μ= fusion parameter; λ= correction factor; R= thermal diffusivity (hr °F/ Btu); FI=freezing Index (^{o}F-day)

v_0= Annual Temp $_{average}$-32	5.3	vs= n(CFI)/t	7.2	FI	855	α=v0/vs	0.73

Table A-42 Thaw depth calculation for Harvey UP using Nixon and McRoberts equation

Material	γ_d	w	d	k	L	TI	∑TI
HMA	138	0	5.00	10.3	0	0	0
Gravel	130	0.075	12	17.9	1089	12.9	13
Sand with Silt	120	0.09	2	16.7	945	5.1	18

TI=Thawing Index (^{o}F-day)

Table A-43 Frost depth calculation for Michigamme UP using Stefan equation

Material	γ_d	w	d	k	L	FI	∑FI
HMA	138	0	5.00	10.3	0	0.0	0
Gravel	130	0.075	12	17.9	1404	19.6	20
Sand	125	0.09	24	16.7	1620	96.8	116
Clayey Sand	120	0.09	89	13.1	1555	1627.2	1744

γ_d = unit weight (pcf); w = water content (%); d = layer depth (in); k= thermal conductivity (Btu/(ft.hr.^{o} F/in); L= latent heat of fusion (Btu/^{3}ft); FI=freezing Index (^{o}F-day)

Table A-44 Frost depth calculation for Michigamme UP using Modified Berggren equation

Material	γ_d	w	d	C	k	L	Ĺ= ∑Ld/∑d	Ĉ= ∑Cd/∑d	μ= Ĉ / Ĺ *vs	λ	R	∑R	∑R+R/2	FI	∑FI
HMA	138	0	0.42	40	0.86	0	0	40	0.00	0.00	0.48	0.48	0.73	0	0
Gravel	130	0.075	1	30	1.5	1404	991	33	0.39	0.81	0.67	0.48	0.82	73	73
Sand	125	0.09	2	39	1.4	1620	1359	38	0.33	0.81	1.43	1.15	1.87	384	457
Clayey Sand	120	0.09	4.2	30	1.1	1555	1467	34	0.27	0.82	3.82	1.15	3.06	1254	1711

d = layer depth (ft); C= volumetric heat capacity(Btu/ft^3); k= thermal conductivity (Btu/(ft.hr.^{o} F); μ= fusion parameter; λ= correction factor; R= thermal diffusivity (hr °F/ Btu); FI=freezing Index (^{o}F-day)

v_0= Annual Temp $_{average}$-32	5.8	vs= n(CFI)/t	11.7	FI	1735	α=v0/vs	0.5

Table A-45 Thaw depth calculation for Michigamme UP using Nixon and McRoberts equation

Material	γ_d	w	d	k	L	TI	∑TI
HMA	138	0	5.00	10.3	0	0	0
Gravel	130	0.075	12	17.9	945	16.3	16
Sand	125	0.09	2	16.7	1089	5.9	22

TI=Thawing Index (^{o}F-day)

Table A-46 Frost depth calculation for Seney UP using Stefan equation

Material	γ_d	w	d	k	L	FI	∑FI
HMA	138	0.02	5.00	10.3	0	0.0	0
Gravel	130	0.075	12	17.9	1404	19.6	20
Sand	125	0.09	81	16.7	1620	1122.5	1115
γ_d = unit weight (pcf); w = water content (%); d = layer depth (in); k= thermal conductivity (Btu/(ft.hr.^{o} F/in); L= latent heat of fusion (Btu/^{3}ft); FI=freezing Index (^{o}F-day)							

Table A-47 Frost depth calculation for Seney UP using Modified Berggren equation

Material	γ_d	w	d	C	k	L	Ĺ= ∑Ld/∑d	Ĉ= ∑Cd/∑d	μ= Ĉ / Ĺ *vs	λ	R	∑R	∑R+R/2	FI	∑FI
HMA	138	0.02	0.42	40	0.86	0	0	40	0.00	0.00	0.48	0.48	0.73	0	0
Gravel	130	0.075	1	30	1.5	1404	991	33	0.31	0.76	0.67	0.48	0.82	83	83
Sand	125	0.09	3.8	42	1.4	1620	1449	40	0.26	0.78	2.70	1.15	2.50	1053	1136
d = layer depth (ft); C= volumetric heat capacity(Btu/ft^3); k= thermal conductivity (Btu/(ft.hr.^{o} F); μ= fusion parameter; λ= correction factor; R= thermal diffusivity (hr °F/ Btu); FI=freezing Index (^{o}F-day)															
v_0= Annual Temp $_{average}$-32				7.3			**vs= n(CFI)/t**			9.4	**FI**	1113	**α=v0/vs**		0.78

Table A-48 Thaw depth calculation for Seney UP using Nixon and McRoberts equation

Material	γ_d	w	d	k	L	TI	∑TI
HMA	138	0	5.00	10.3	0	0	0
Gravel	130	0.075	12	17.9	983	16.3	16
Sand	125	0.09	6	16.7	1134	20.0	36
TI=Thawing Index (^{o}F-day)							

Table A-49 Frost depth calculation for St. Ignace UP using Stefan equation

Material	γ_d	w	d	k	L	FI	∑FI
HMA	138	0	5.00	10.3	0	0	0
Gravel	130	0.075	12	17.9	1404	19.6	20
Sand	125	0.09	24	16.7	1620	96.8	116
Silty Clayey Sand	115	0.165	52	13.1	2732	975.9	1092

γ_d = unit weight (pcf); w = water content (%); d = layer depth (in); k= thermal conductivity (Btu/(ft.hr.^{o} F/in); L= latent heat of fusion (Btu/^{3}ft); FI=freezing Index (^{o}F-day)

Table A-50 Frost depth calculation for St. Ignace UP using Modified Berggren equation

Material	γ_d	w	d	C	k	L	Ĺ= ∑Ld/∑d	Ĉ= ∑Cd/∑d	μ= Ĉ / Ĺ *vs	λ	R	∑R	∑R+R/2	FI	∑FI
HMA	138	0	0.42	40	0.86	0	397	40	0.00	0.00	0.48	0.48	0.73	0	0
Gravel	130	0.075	1	30	1.5	1404	1108	33	0.33	0.85	0.67	0.48	0.82	66	66
Sand	125	0.09	2	39	1.4	1620	1408	36	0.26	0.86	1.43	1.15	1.87	341	407
Silty Clayey Sand	115	0.165	2.1	48	1.1	2732	1912	41	0.21	0.88	1.91	1.15	2.11	650	1057

d = layer depth (ft); C= volumetric heat capacity(Btu/ft^3); k= thermal conductivity (Btu/(ft.hr.^{o} F); μ= fusion parameter; λ= correction factor; R= thermal diffusivity (hr °F/ Btu); FI=freezing Index (^{o}F-day)

v_0= Annual Temp $_{average}$-32	3.9	vs= n(CFI)/t	9.3	FI	1081	α=v0/vs	0.4

Table A-51 Thaw depth calculation for St. Ignace UP using Nixon and McRoberts equation

Material	γ_d	w	d	k	L	TI	∑TI
HMA	138	0	5.00	10.3	0	0	0
Gravel	130	0.075	12	17.9	945	16.3	16
Sand	125	0.09	2	16.7	1134	5.7	22

TI=Thawing Index (^{o}F-day)

Table A-52 Frost depth calculation for Twin Lakes UP using Stefan equation

Material	γ_d	w	d	k	L	FI	∑FI
HMA	138	0.00	5.00	10.3	0	0	0
Gravel	130	0.075	12	17.9	1404	19.6	20
Sand	125	0.09	24	16.7	1620	96.8	116
Silty Clayey Sand	115	0.165	63	13.1	2732	1432.5	1549

γ_d = unit weight (pcf); w = water content (%); d = layer depth (in); k= thermal conductivity (Btu/(ft.hr.^{o} F/in); L= latent heat of fusion (Btu/^{3}ft); FI=freezing Index (^{o}F-day)

Table A-53 Frost depth calculation for Twin Lakes UP using Modified Berggren equation

Material	γ_d	w	d	C	k	L	Ĺ= ∑Ld/∑d	Ĉ= ∑Cd/∑d	μ= Ĉ / Ĺ *vs	λ	R	∑R	∑R+R/2	FI	∑FI
HMA	138	0	0.42	40	0.86	0	0	40	0.00	0.00	0.48	0.48	0.73	0	0
Gravel	130	0.075	1	30	1.5	1404	991	33	0.38	0.85	0.67	0.48	0.82	66	66
Sand	125	0.09	2	39	1.4	1620	1359	36	0.31	0.85	1.43	1.15	1.87	349	415
Silty Clayey Sand	115	0.165	2.9	48	1.1	2732	1990	42	0.24	0.86	2.64	1.15	2.47	1102	1517

d = layer depth (ft); C= volumetric heat capacity(Btu/ft^3); k= thermal conductivity (Btu/(ft.hr.^{o} F); μ= fusion parameter; λ= correction factor; R= thermal diffusivity (hr °F/ Btu); FI=freezing Index (^{o}F-day)

v_0= Annual Temp $_{average}$-32	5.7	vs= n(CFI)/t	11.4	FI	587	α=v0/vs	0.5

Table A-54 Thaw depth calculation for Twin Lakes UP using Nixon and McRoberts equation

Material	γ_d	w	d	k	L	TI	∑TI
HMA	138	0	5.00	10.3	0	0	0
Gravel	130	0.075	12	17.9	945	16.3	16
Sand	125	0.09	2	16.7	1134	5.7	22

TI=Thawing Index (^{o}F-day)

Appendix B

Soil and Air Temperature Data

Appendix B

Soil and Air Temperature Data in Different RWIS Stations

This appendix houses the measured frost depth propagation and the calculated cumulative freezing degree day (CFDD) data for different RWIS stations in Michigan. The data were used in developing the statistical models.

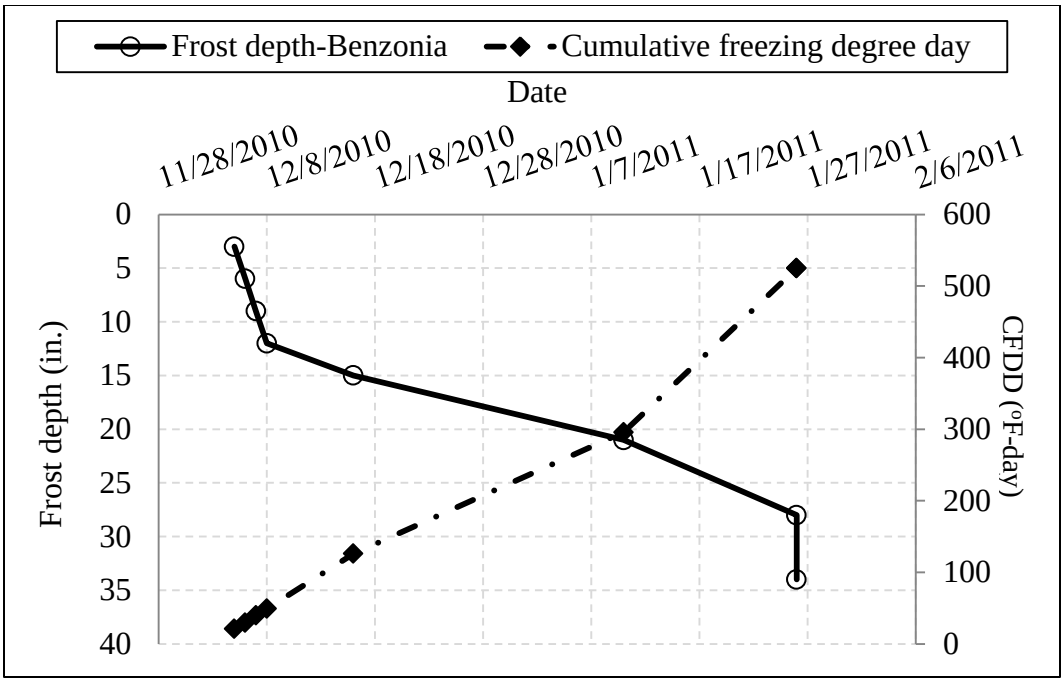

Figure B-1 Frost depth propagation and corresponding CFDD, Benzonia, LP

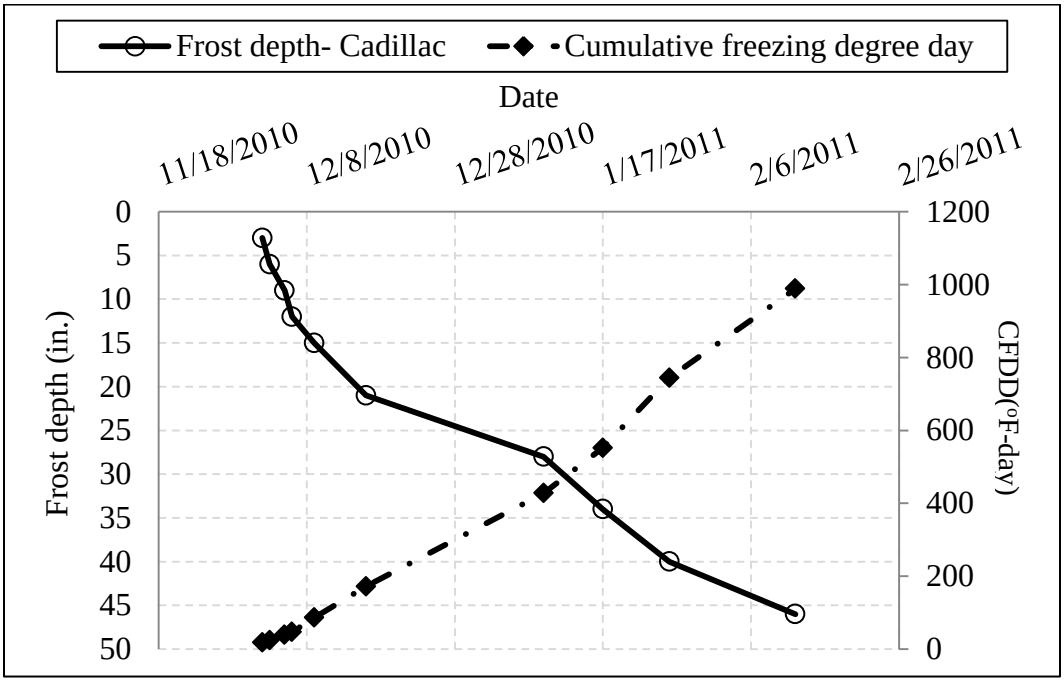

Figure B-2 Frost depth propagation and corresponding CFDD, Cadillac, LP

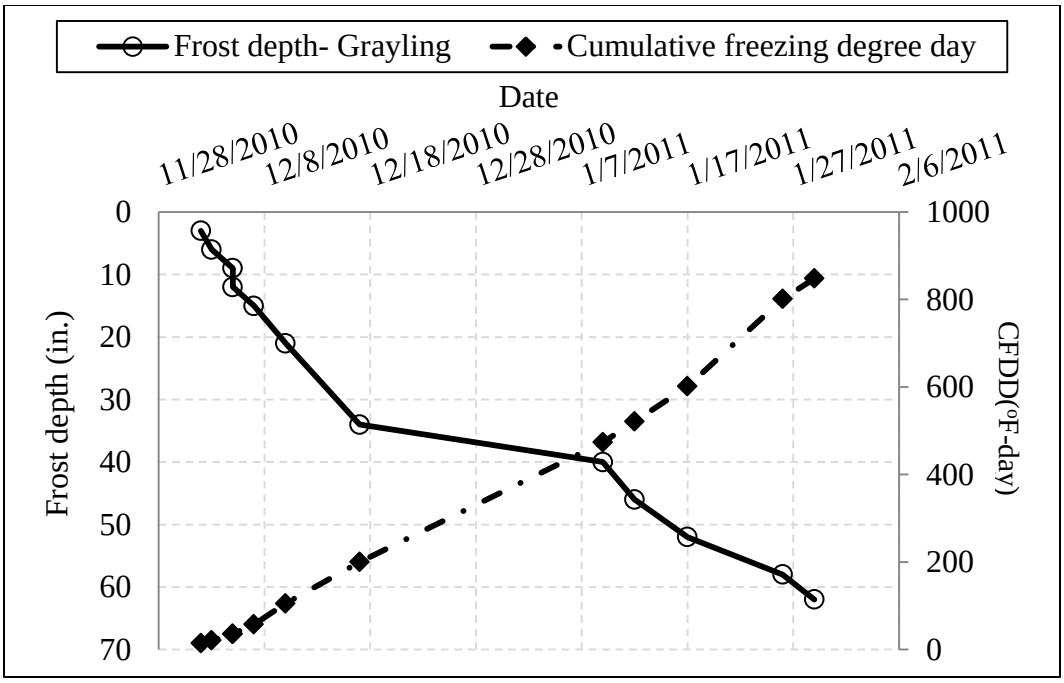

Figure B-3 Frost depth propagation and corresponding CFDD, Grayling, LP

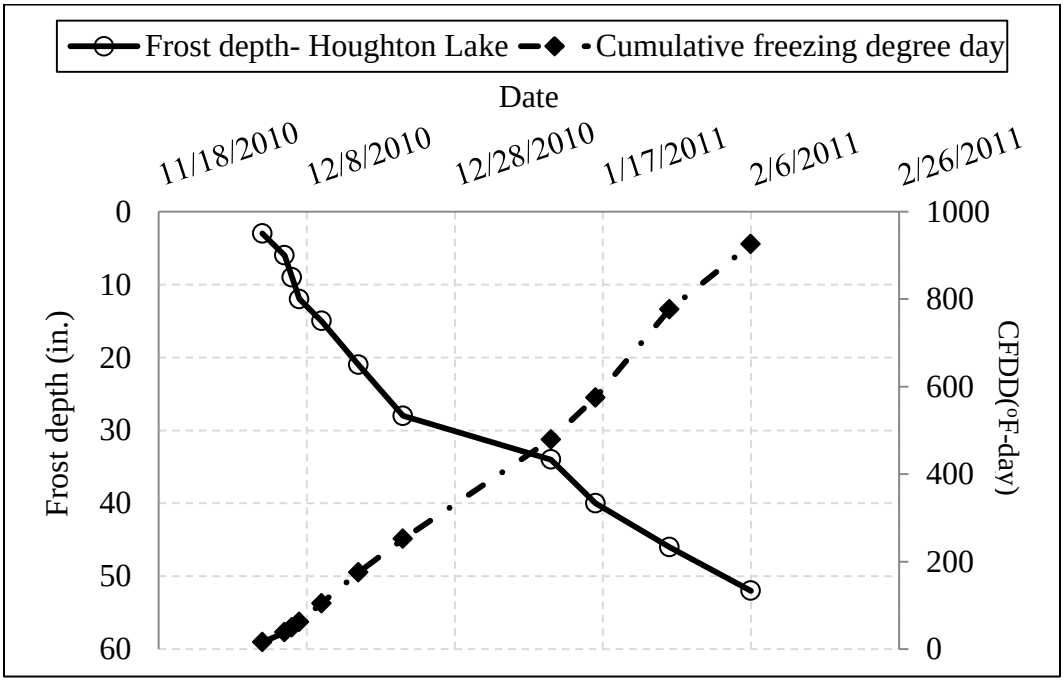

Figure B-4 Frost depth propagation and corresponding CFDD, Houghton Lake, LP

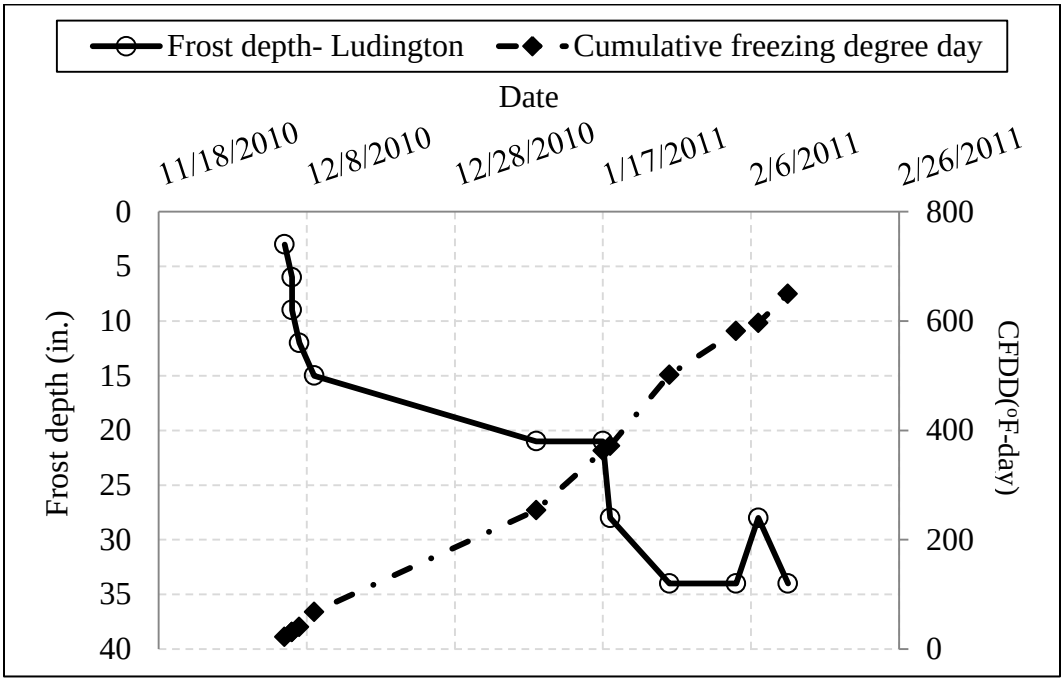

Figure B-5 Frost depth propagation and corresponding CFDD, Ludington, LP

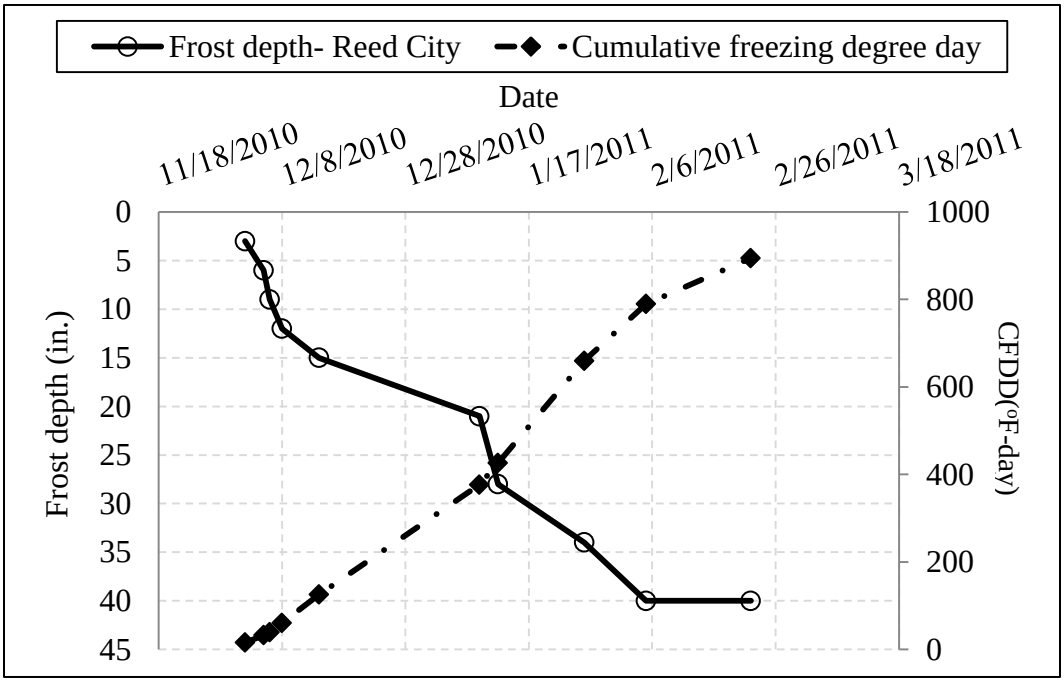

Figure B-6 Frost depth propagation and corresponding CFDD, Reed City, LP

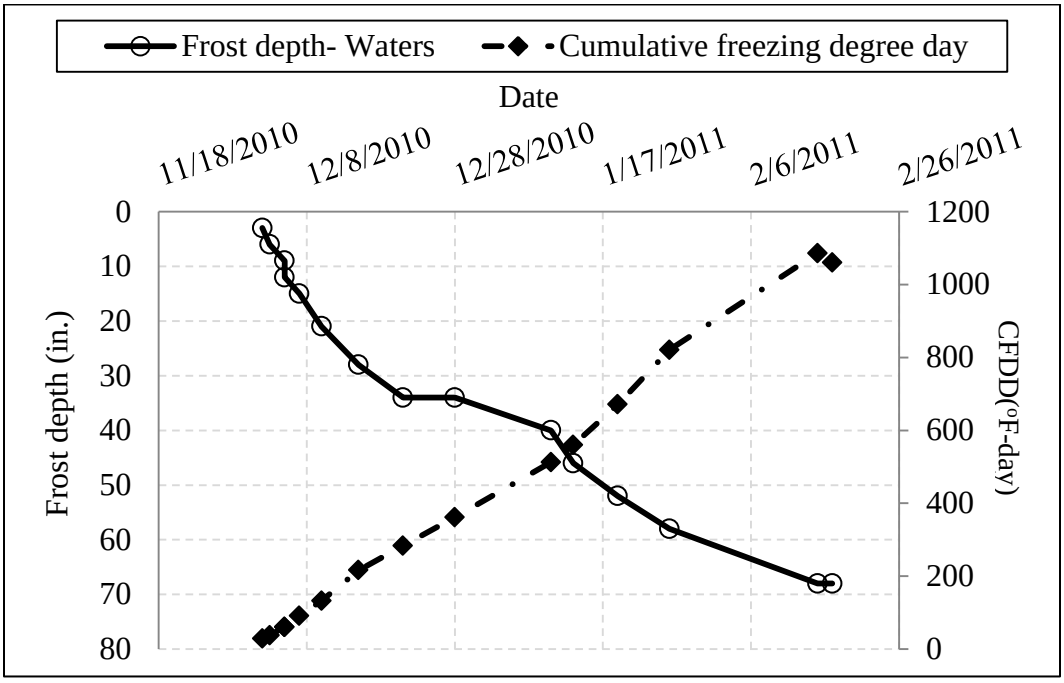

Figure B-7 Frost depth propagation and corresponding CFDD, Waters, LP

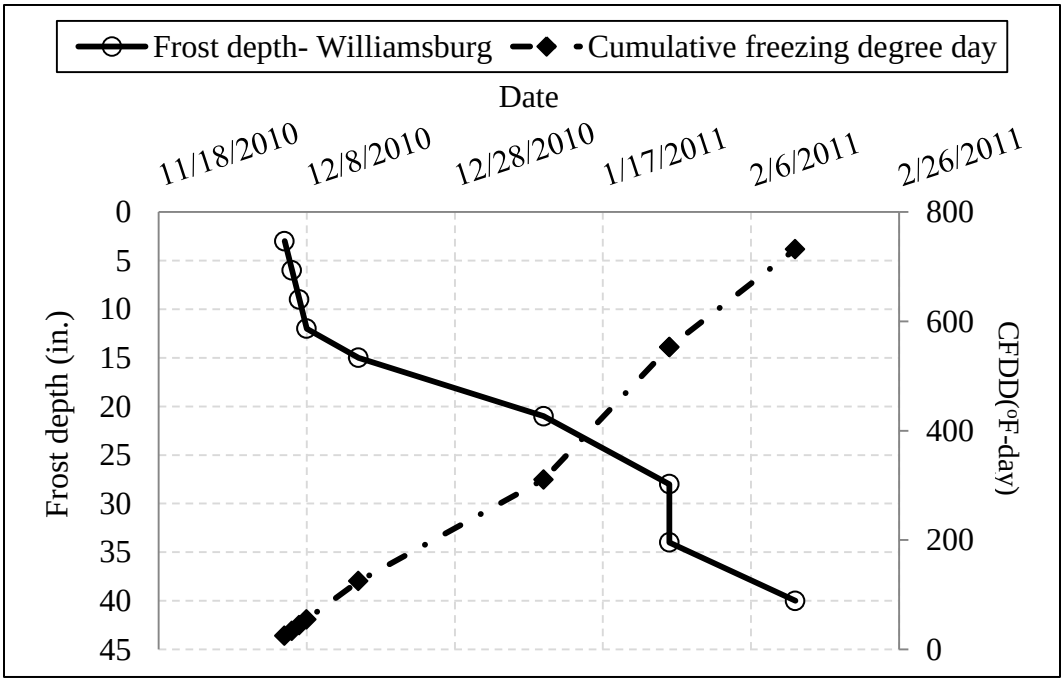

Figure B-8 Frost depth propagation and corresponding CFDD, Williamsburg, LP

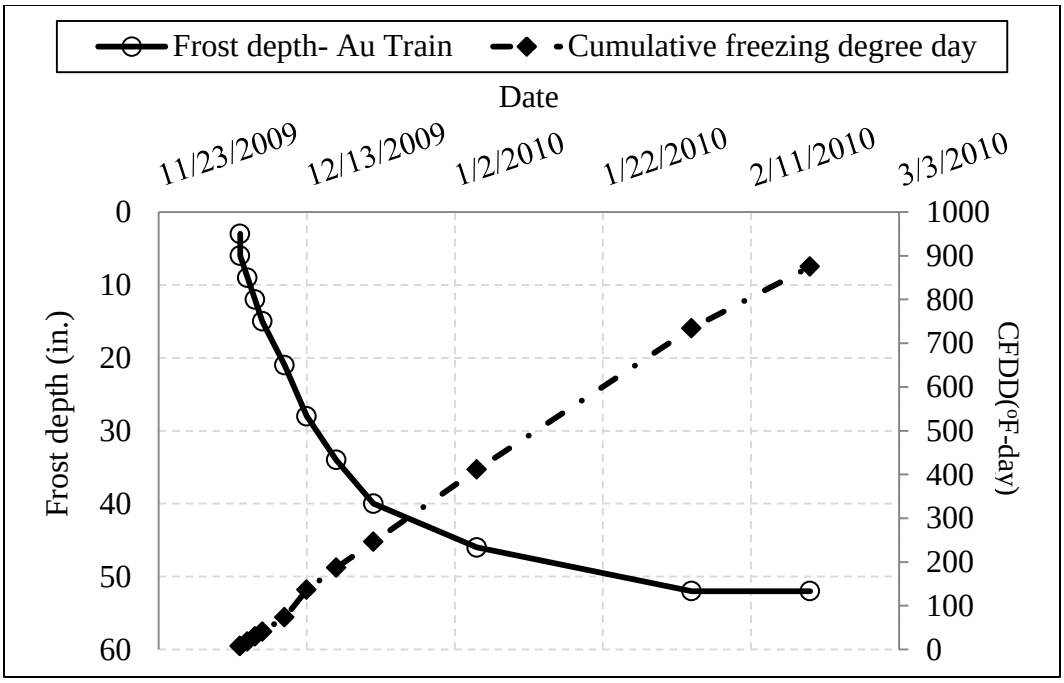

Figure B-9 Frost depth propagation and corresponding CFDD, Au Train-2009, LP

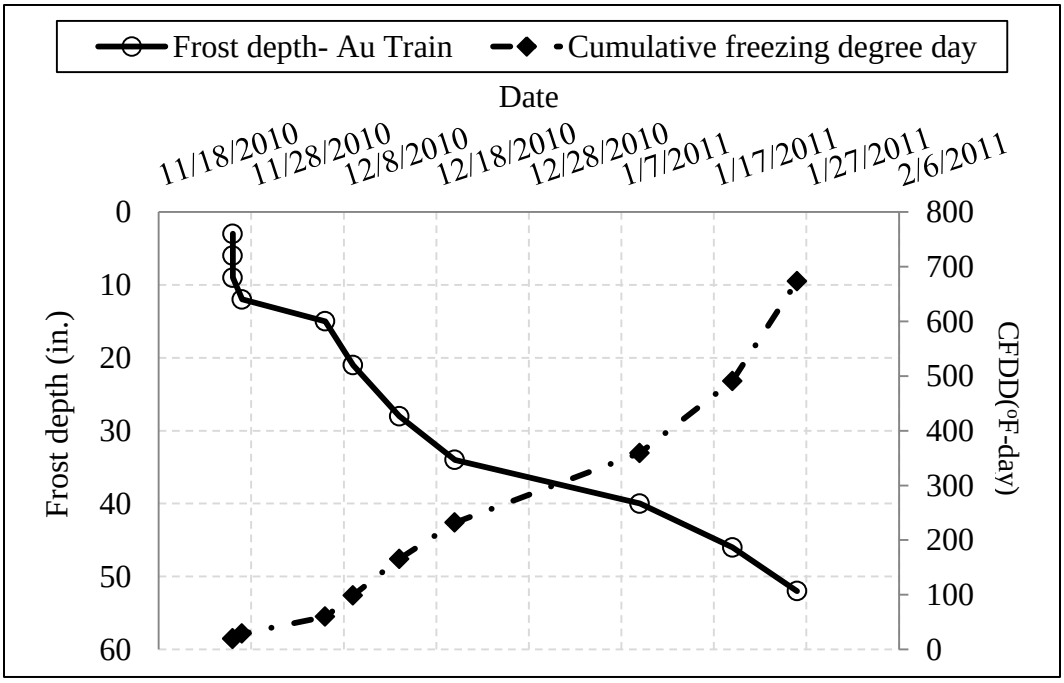

Figure B-10 Frost depth propagation and corresponding CFDD, Au Train-2010, LP

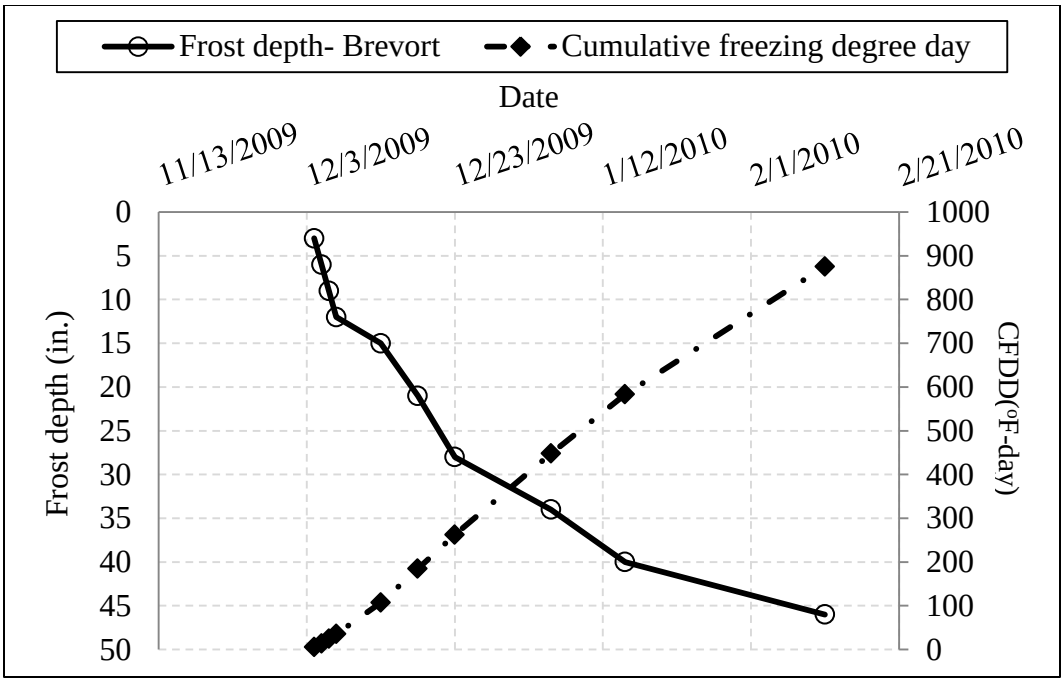

Figure B-11 Frost depth propagation and corresponding CFDD, Brevort-2009, LP

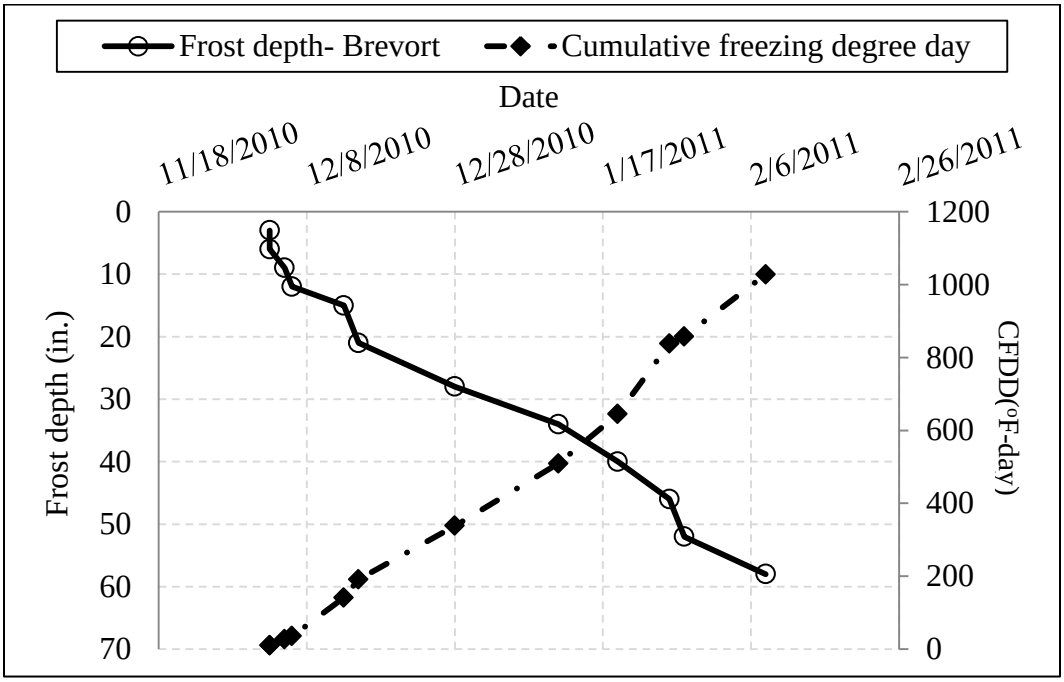

Figure B-12 Frost depth propagation and corresponding CFDD, Brevort-2010, LP

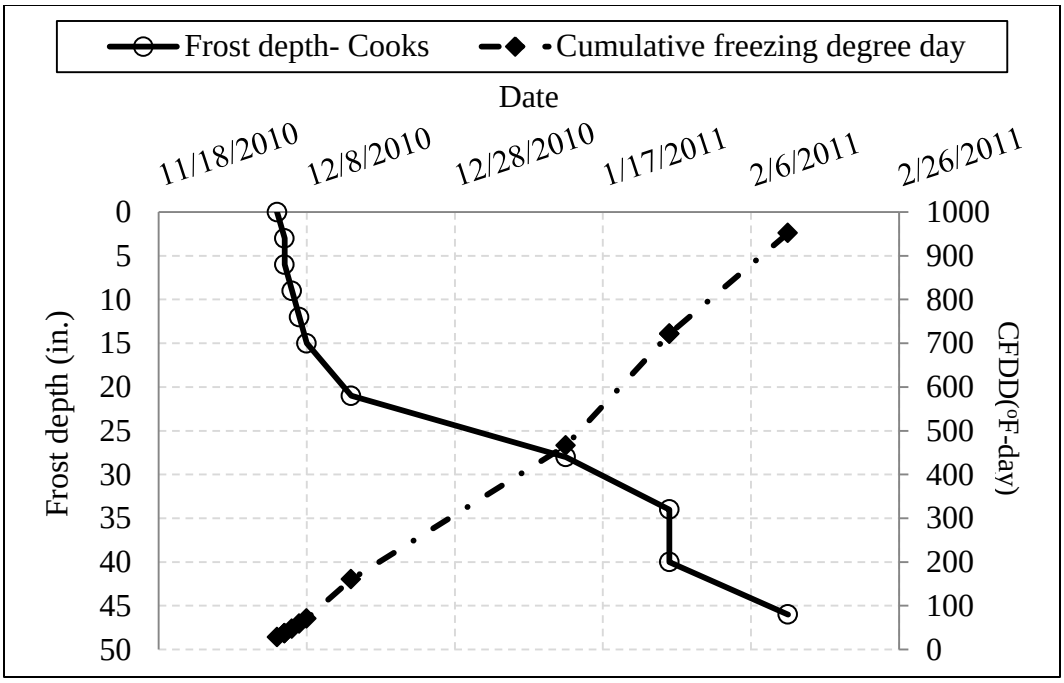

Figure B-13 Frost depth propagation and corresponding CFDD, Cooks, LP

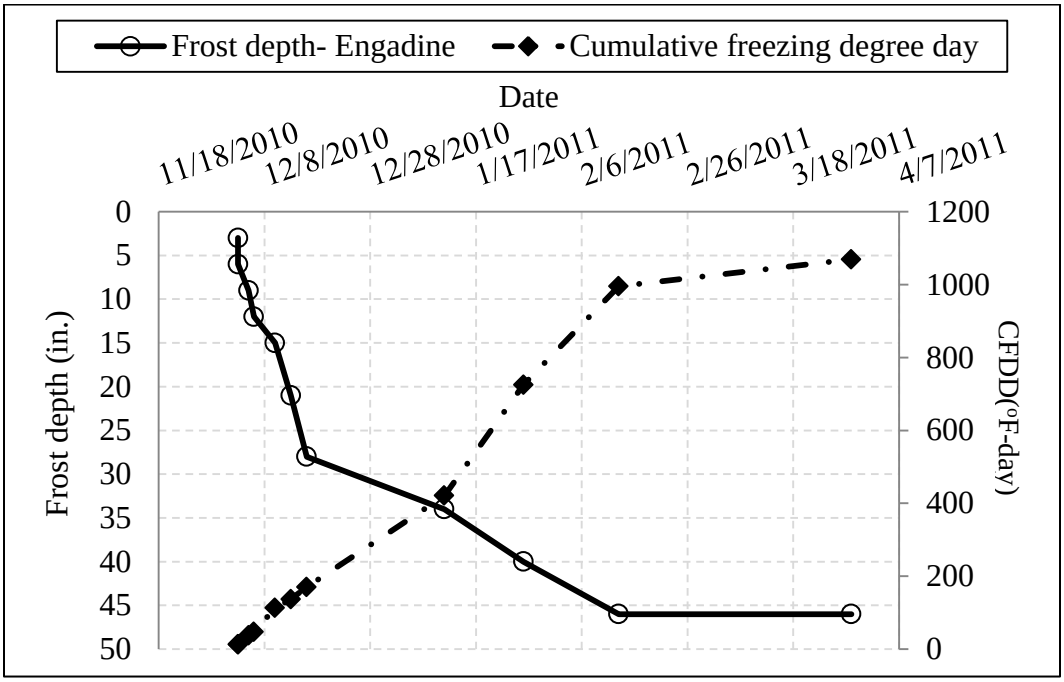

Figure B-14 Frost depth propagation and corresponding CFDD, Engadine, UP

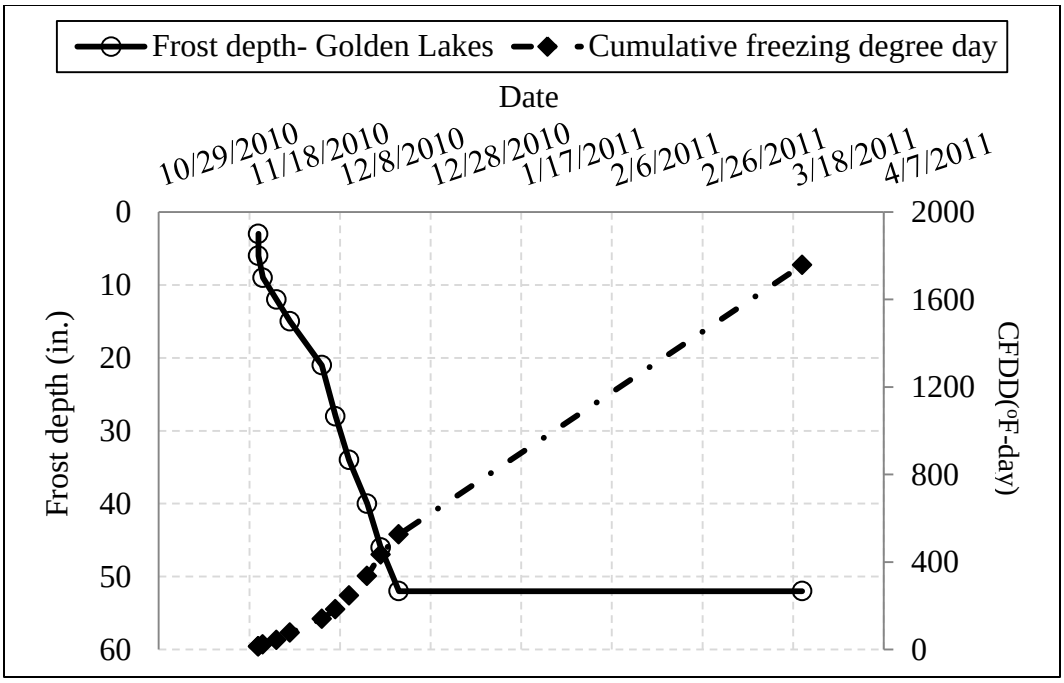

Figure B-15 Frost depth propagation and corresponding CFDD, Golden Lake, UP

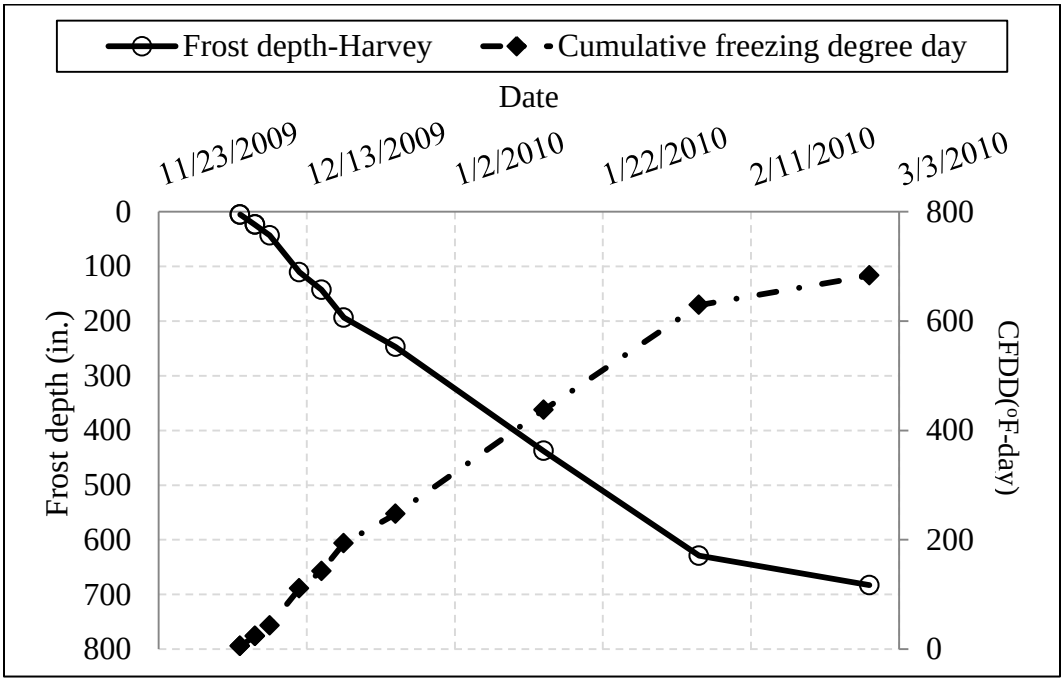

Figure B-16 Frost depth propagation and corresponding CFDD, Harvey- 2009, UP

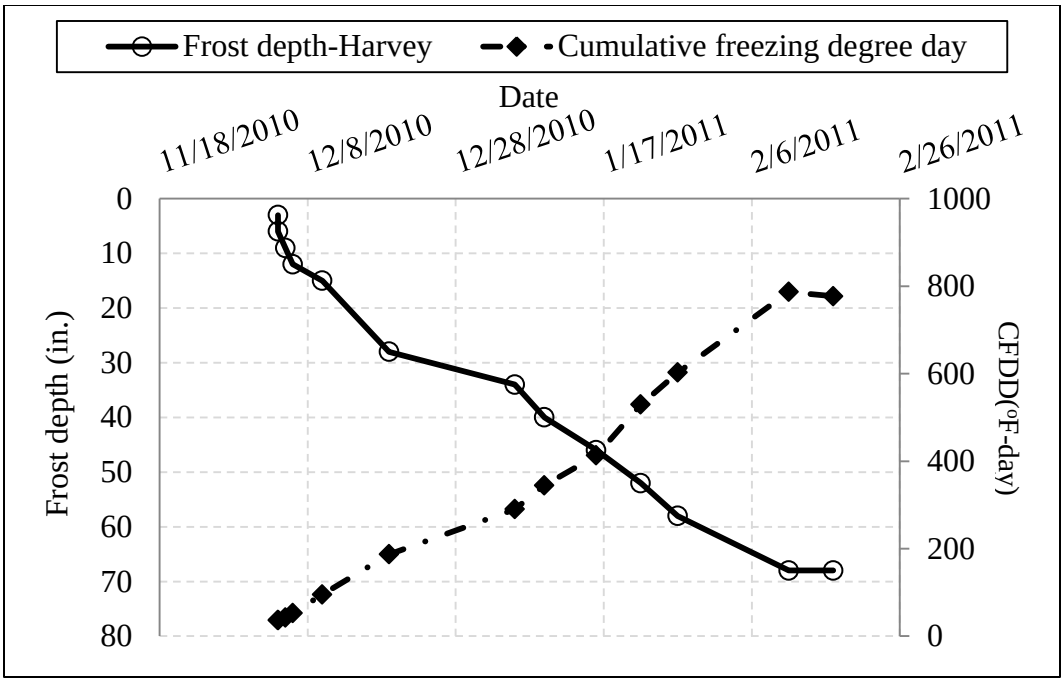

Figure B-17 Frost depth propagation and corresponding CFDD, Harvey- 2010, UP

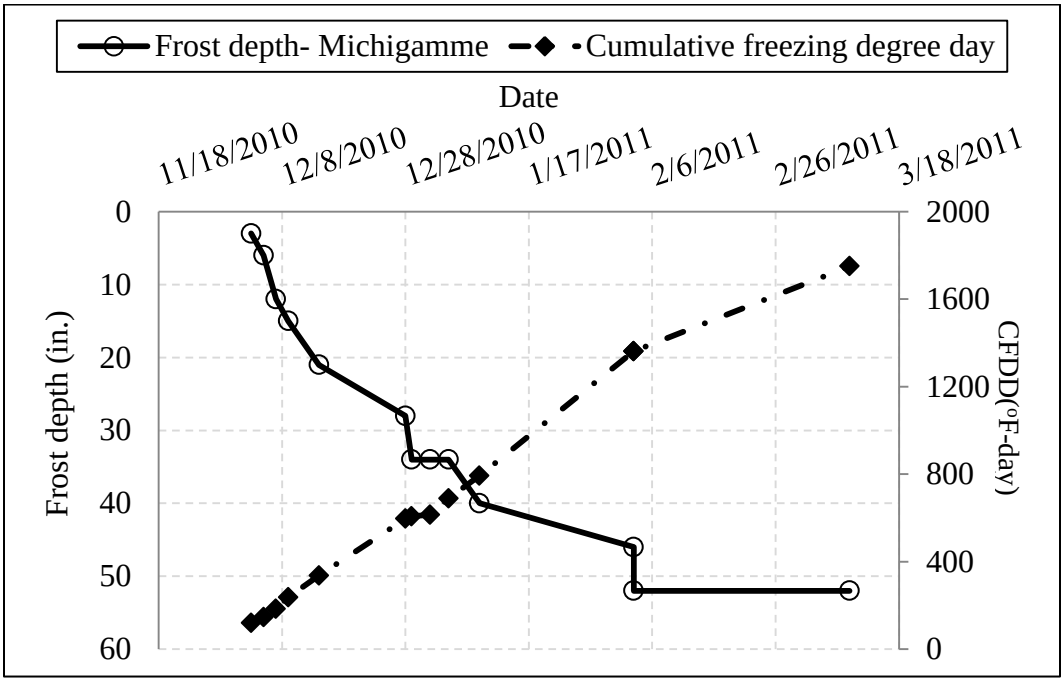

Figure B-18 Frost depth propagation and corresponding CFDD, Michigamme, UP

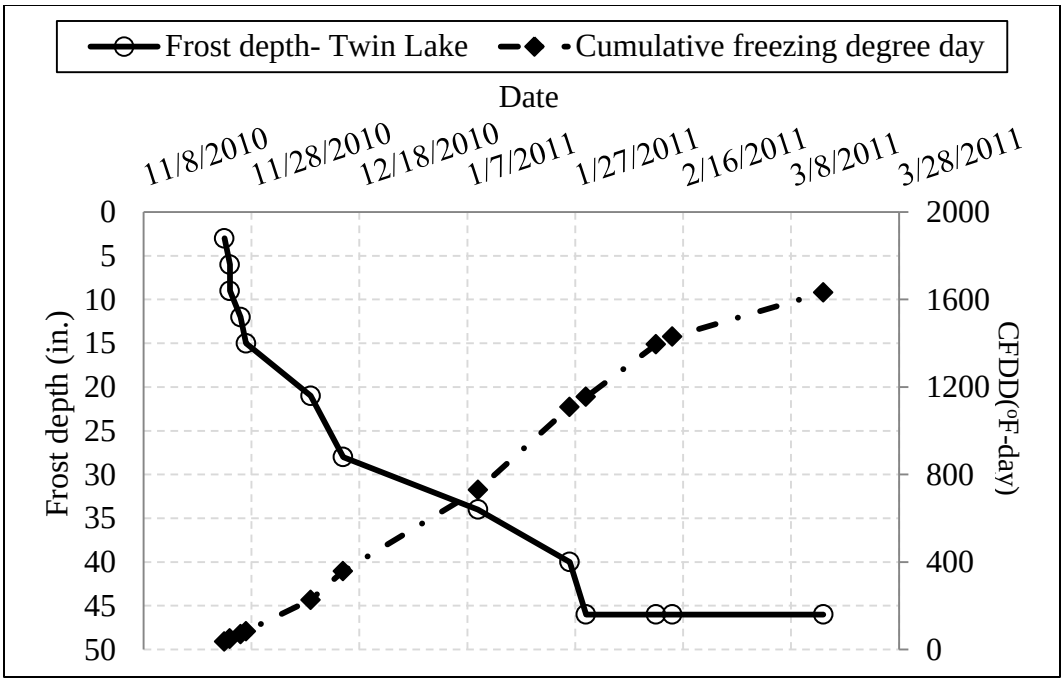

Figure B-19 Frost depth propagation and corresponding CFDD, Twin Lakes, UP

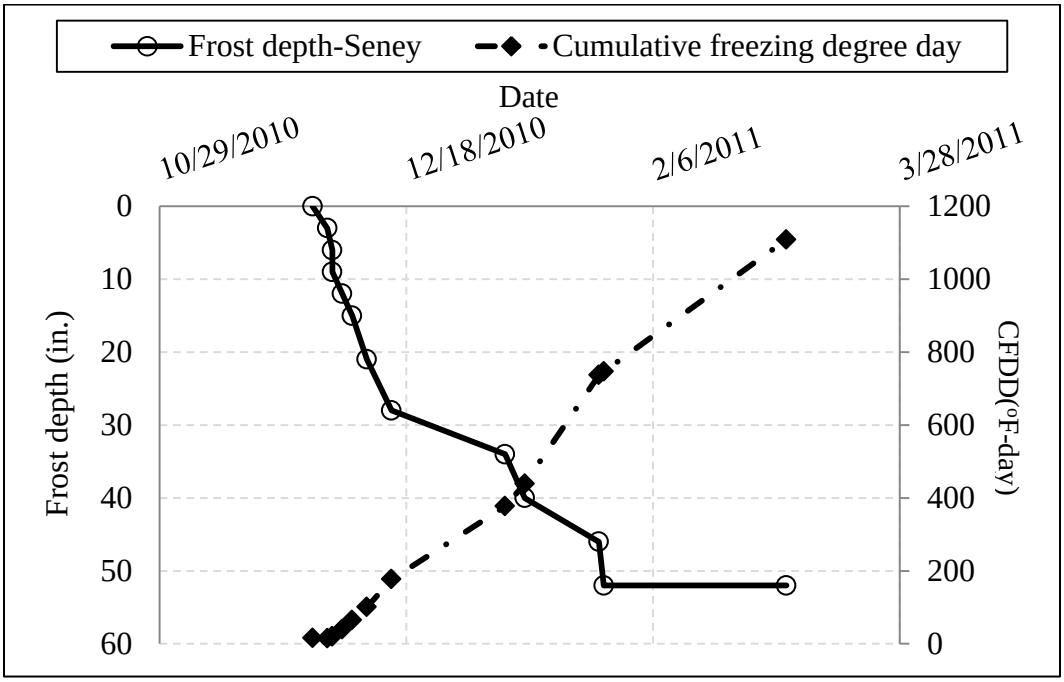

Figure B-20 Frost depth propagation and corresponding CFDD, Seney, UP

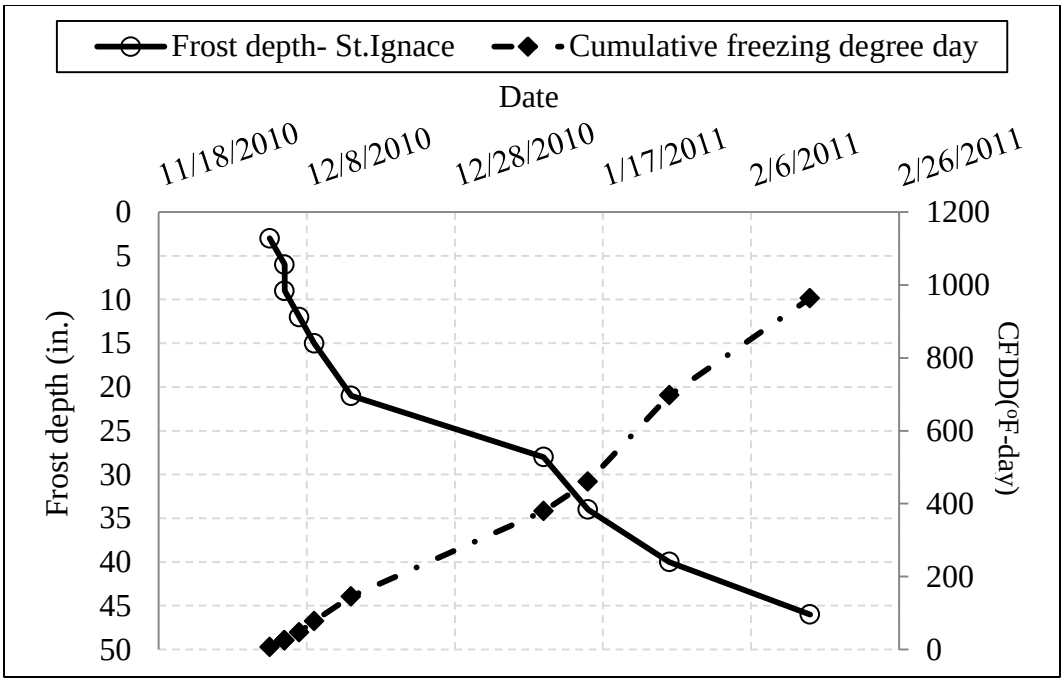

Figure B-21 Frost depth propagation and corresponding CFDD, St. Ignace, UP

Appendix C

Frost Heave Station Profiles

Appendix C

Frost Heave Stations Profile

This appendix houses the details pavement profiles of frost heave measured under the shoulders and pavements at five stations in Michigan. In the figures both the measured frost heave and frost depths were shown for each station (Novak, 1968).

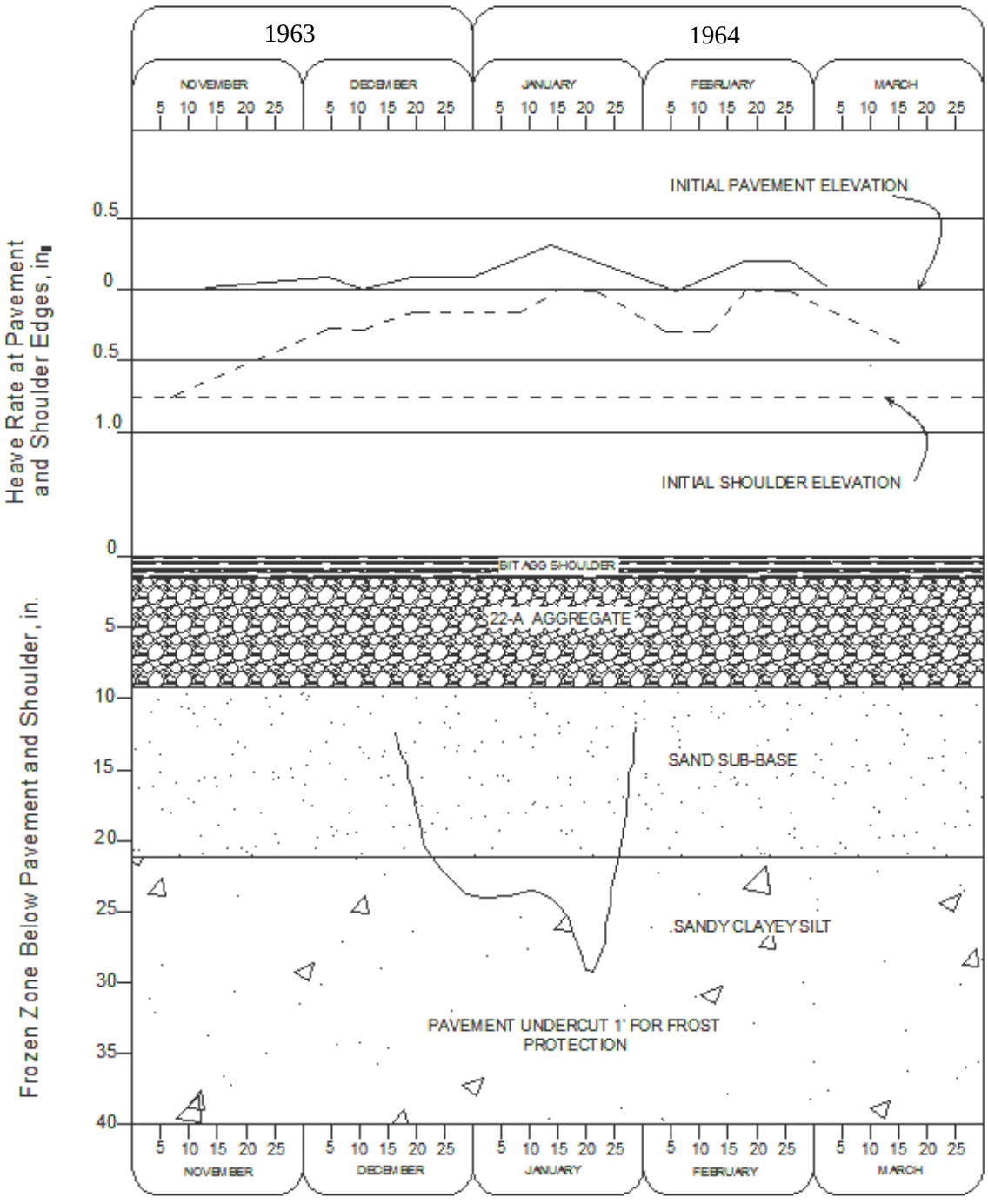

Figure C-1 Frost depth and corresponding frost heave, shoulder and pavement, Sta. 528+88

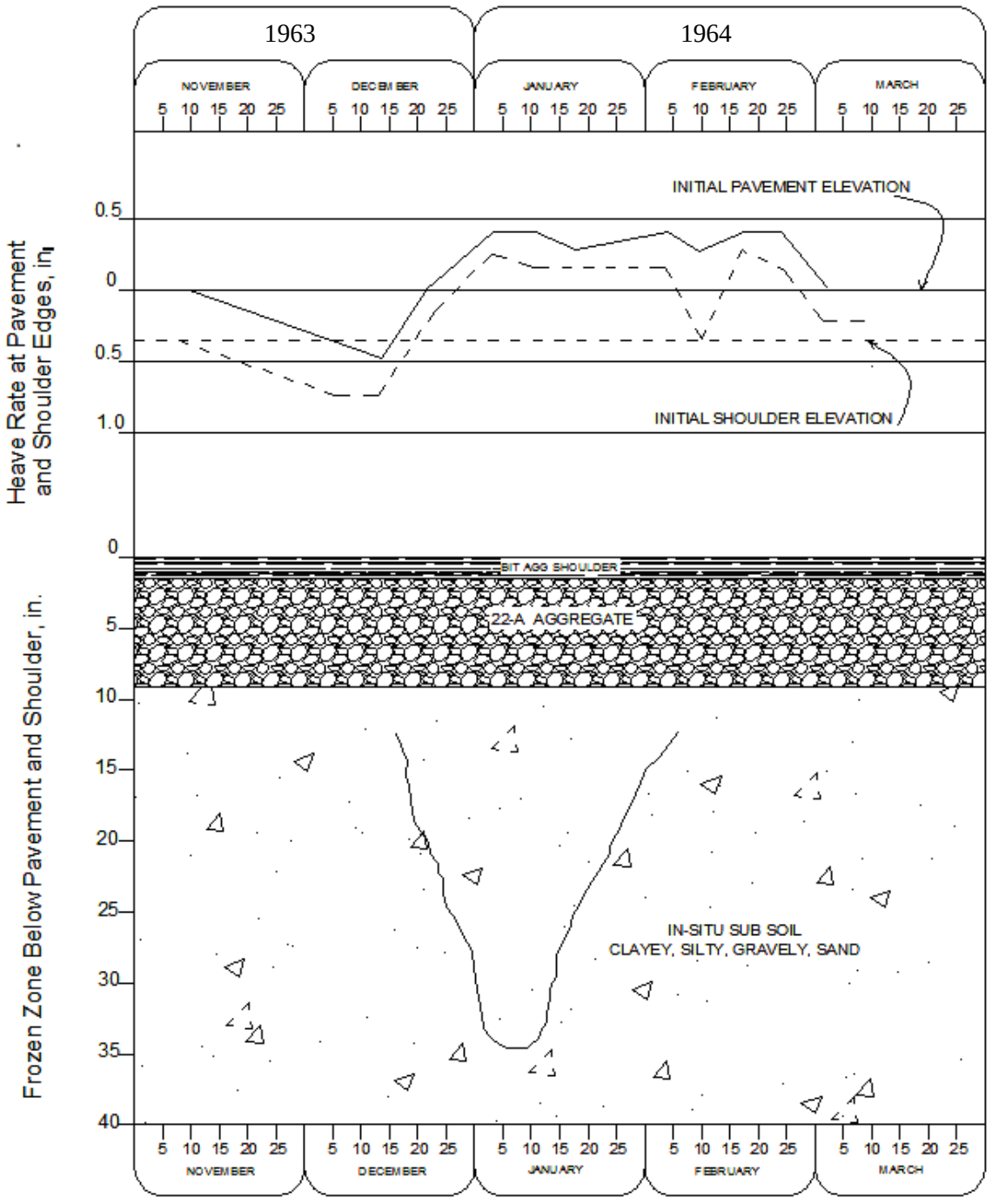

Figure C-2 Frost depth and corresponding frost heave, shoulder and pavement, Sta. 652+00

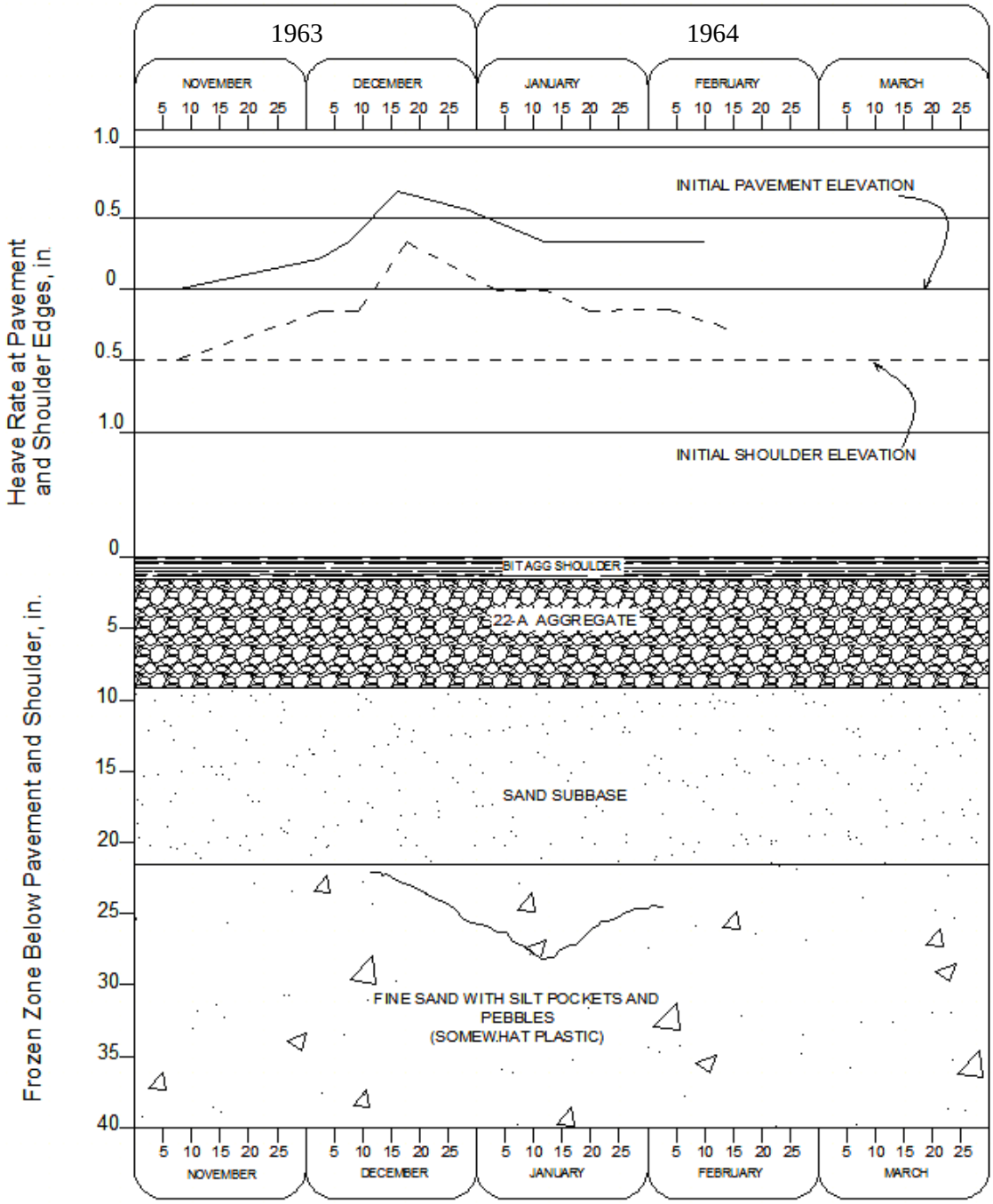

Figure C-3 Frost depth and corresponding frost heave, shoulder and pavement, Sta. 719+00

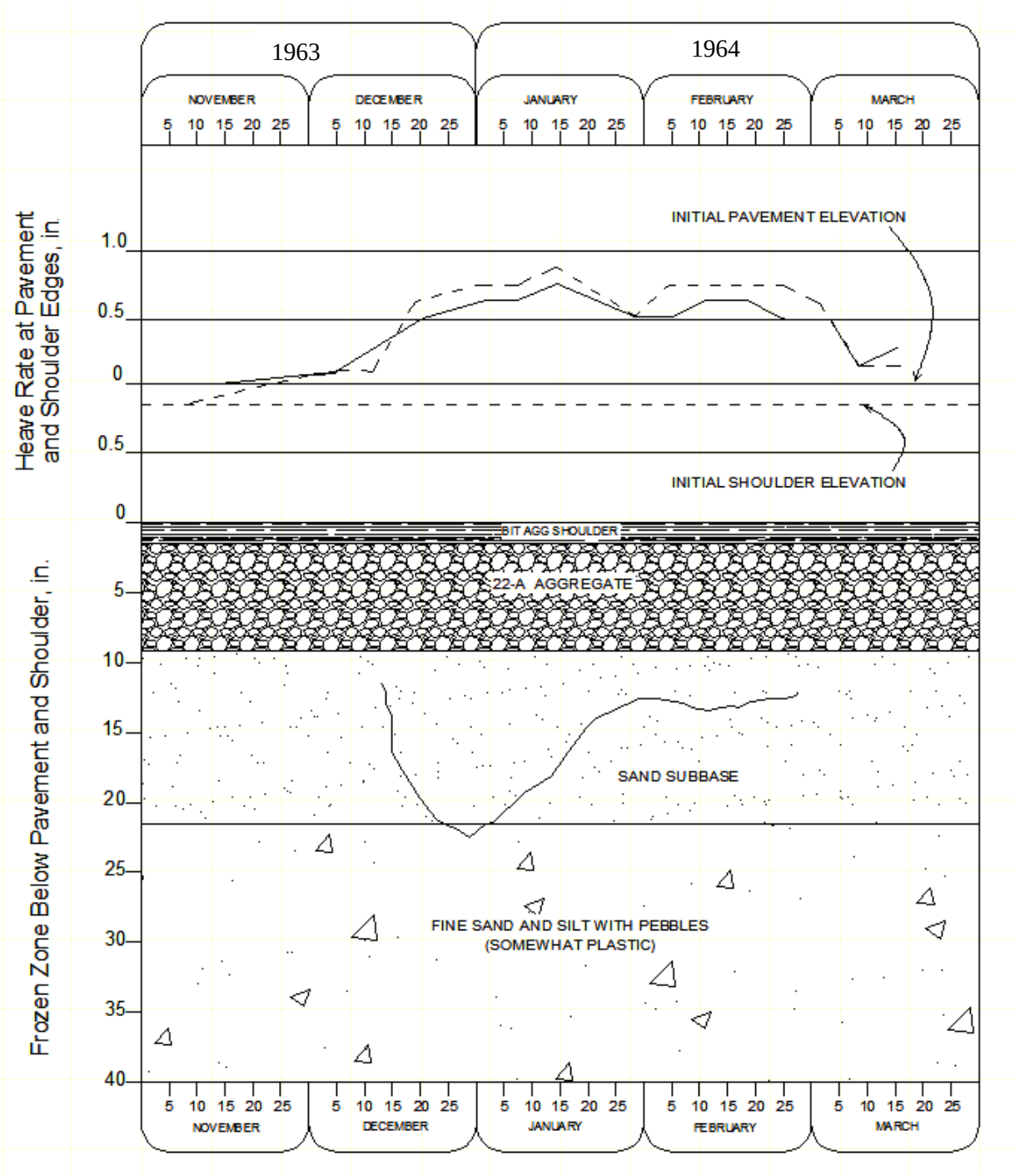

Figure C-4 Frost depth and corresponding frost heave, shoulder and pavement, Sta. 724+00

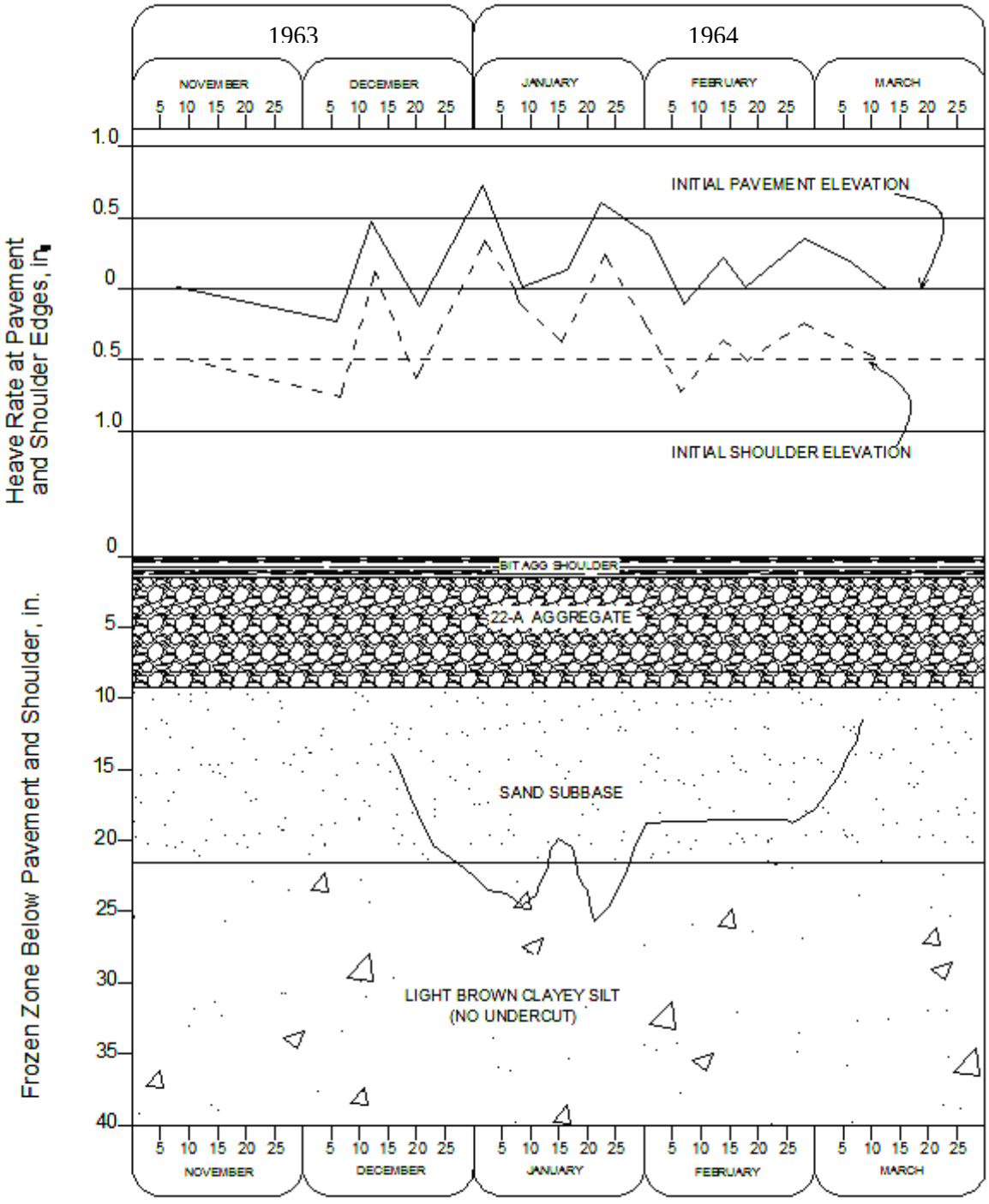

Figure C-5 Frost depth and corresponding frost heave, shoulder and pavement, Sta. 474+00

Appendix D

Unit Conversion

Unit Conversion

SI to English

1 m = 39.73 in = 3.281 ft

1 Pa = $1.45*10^{-4}$ psi = $2.09*10^{-2}$ psf

1 J = $9.48*10^{-3}$ Btu

1 W = 2.42 Btu/h

1 kg = $6.9*10^{-2}$ slug

1 N (kg. m/s^2) = $2.25*10^{-1}$ lb (slug.ft/s^2)

$9/5*(^oC+32) = ^oF$

English to SI

1 ft = 12 in = $3.048*10^{-1}$ m

1 psf = 144 psi = 47.88 Pa

1 Btu = 1055.06 J

1 Btu/h = $2.93*10^{-1}$ W

1 slug = 14.59 kg

1 lb = 4.45 N

$(^oF -32)*5/9 = ^oC$